THERMAL STABILITY OF DISTILLATE HYDROCARBON FUELS

by

Kishenkumar Tadisina Reddy

Submitted is partial fulfillment of the requirements for the degree of

Doctor of Philosophy

Approved by Nicholas P. Cernansky

Dr. Nicholas P. Cernansky
Principal Investigator

Research Sponsored by the NASA Lewis Research Center under
Grant No. NAG 3-183 and by Drexel University

Department of Mechanical Engineering and Mechanics
Drexel University, Philadelphia, PA 19104

October 1987

ABSTRACT

Thermal stability of fuels is expected to become a severe problem in the future due to the anticipated use of broadened specification and alternative fuels. Future fuels will have higher contents of heteroatomic species which are reactive constituents and are known to infuence fuel degradation.

One approach for studying the thermal degradation problem is to understand the detailed behavior of a prototypical distillate fuel component, i.e., a large n-alkane, and then extend the study to include binary and tenary fuel component combinations, etc. To study the degradation chemistry of selected model fuels, n-dodecane and n-dodecane plus heteroatoms were aerated by bubbling air through the fuels and stressed on a modified Jet Fuel Thermal Oxidation Tester facility operating at heater tube temperatures between 200-400°C. The resulting samples were fractionated to concentrate the soluble products and then analyzed using gas chromatographic and mass spectrometric techniques to quantify and identify the stable reaction intermediate and product species.

The soluble products consisted mainly of <C12 n-alkanes and 1-alkenes, <C12 aldehydes, tetrahydrofurans, C12 alcohol and ketone isomers, dodecylhydroperoxides (hypothesized), and C24 alkane isomers. Comparison of relative amounts and shifts in the distribution of these species with dopant addition led to inferences about the reaction mechanisms. The data from the present neat n-dodecane experiments agreed with the work of Hazlett et al., thereby verifying both sets of data. Also, new products were identified leading to a modification of the existing n-dodecane/oxygen reaction mechanism.

The modified n-dodecane oxidation mechanism requires that alkylperoxy radical reactions dominate in the autoxidation temperature regime ($T \leq 300°C$), while alkyl radical reactions are important in the intermediate temperature regime ($300 \leq T \leq 400°C$).

Heteroatom addition showed that the major soluble products were always the same, with and without heteroatoms, but their distributions varied considerably. 3,4-dimercaptotoluene and dibutylsulfide heteroatoms, individually added to n-dodecane, interfere with the hydrocarbon oxidation chain at the alkylperoxy radical and the alkylhydroperoxide link, respectively. 2,5-dimethylpyrrole heteratom, on the other hand, introduces cooxidation reactions involving heteroatom and oxygen and, consequently, inhibits ROOH formation. Pyridine, pyrrole and dibenzothiophene individually added to n-dodecane showed few significant effects.

THERMAL STABILITY OF DISTILLATE HYDROCARBON FUELS

A Thesis

Submitted to the Faculty

of

Drexel University

by

Kishenkumar Tadisina Reddy

in partial fulfillment of the

requirements for the degree

of

Doctor of Philosophy

October 1987

ACKNOWLEDGEMENTS

I would like to thank my advisors, Professors Nicholas P. Cernansky and Richard S. Cohen for their guidance, support and co-operation during the past few years of my doctoral research program. I acknowledge my thesis advisory committee members, Professors Irwin H. (Mel) Suffet, David L. Miller, Franklin A. Davis, and Dr. Robert N. Hazlett from Naval Research Laboratory whose helpful suggestions and comments contributed to the quality of this work.

My sincere thanks are extended to Patricia A. Partridge for guiding me through the intricacies and finer points of analytical and organic chemistry. Right now, I am capable of calling myself a chemist with a rich and varied experience in gas chromatography and mass spectrometry. I appreciate the co-operation of Dr. Hamid Sarv for helping me with the initial stages of the chromatography data analysis. I would like to thank Dr. Richard D. Wilk for helpful discussions on aspects of hydrocarbon reaction chemistry.

The financial support provided by the NASA Lewis Research Center (Grant No. NAG 3-183) for the early phase of this work is gratefully acknowledged. Also, the ongoing support from Drexel University, which permitted completion of the work, is appreciated.

Finally, I would like to thank my family for their patience, support and encouragement during the course of the work. Besides academia, the experience of a new culture has been personally enriching.

TABLE OF CONTENTS

Page

LIST OF TABLES

LIST OF ILLUSTRATIONS

Figure Page

ABSTRACT

THERMAL STABILITY OF DISTILLATE HYDROCARBON FUELS

KISHENKUMAR TADISINA REDDY

NICHOLAS P. CERNANSKY

RICHARD S. COHEN

Thermal stability of fuels is expected to become a severe problem in the future due to the anticipated use of broadened specification and alternative fuels and to increased demands on air and ground transportation engine performance. Future fuels will be derived from coal liquids, shale oil, and tar sands and will have higher contents of heteroatomic species (organic compounds containing nitrogen, sulfur and oxygen atoms) which are reactive constituents and are known to influence fuel degradation. As the composition of present fuels is very complex and the degradation products are numerous, detailed thermal degradation mechanisms for in-use distillate fuels are not available; the addition of reactive heteroatoms only complicates a difficult problem. A detailed description of the mechanisms occurring during fuel thermal degradation is desired, since suitable fuel additives then can be added to control the fuel instability problem.

One approach for studying the thermal degradation problem is to understand the detailed behavior of a prototypical distillate fuel component, i.e., a large n-alkane, and then extend the study to include binary and ternary fuel component combinations, etc. Following this method, the study of a single component model fuel, n-dodecane, was undertaken, motivated largely by the simplifications in degradation chemistry inherent in such systems. To study the degradation chemistry of selected model fuels, n-dodecane and n-dodecane plus dopants, were aerated by bubbling air through the fuels and stressed on a modified Jet Fuel Thermal Oxidation Tester facility operating at heater tube temperatures between 200-400C. The resulting samples were fractionated to concentrate the soluble products and then analyzed using gas chromatography and mass spectrometry techniques to quantify and identify the stable reaction intermediate and product species.

The soluble products consisted mainly of <C12 n-alkanes and 1-alkenes, <C12 aldehydes, tetrahydrofuran derivatives, C12 alcohol and ketone isomers, dodecyl-hydroperoxide (ROOH) decomposition products, and C24 alkane isomers. Comparison of relative amounts and shifts in the distribution of these species with dopant addition led to inferences about the reaction mechanisms. The data from the present neat n-dodecane experiments agreed with the work of Hazlett *et al*. thereby verifying both sets of data. Also, new products were detected and identified, leading to

a modification of the existing n-dodecane/oxygen reaction mechanism.

The modified n-dodecane oxidation mechanism indicates that alkylperoxyl radical reactions probably dominate in the autoxidation temperature regime ($T \leq 300C$). The dominant path is considered to be for the alkylperoxyl radical, RO_2*, to react bimolecularly with fuel to yield primarily alkyl-hydroperoxides. The RO_2* can undergo self termination and unimolecular isomerization and decomposition reactions, to yield smaller amounts of C12 alcohol plus ketone products and tetrahydrofuran derivatives, respectively. Thus, alcohol and ketone formation in this temperature regime implies that the main termination step is via RO_2* self termination reactions, which refutes an earlier hypothesis that alkyl radical termination reactions (giving C24 hydrocarbon isomers) are important.

In the intermediate temperature regime ($300 \leq T \leq 400C$), the alkyl radical, R* reactions dominate the RO_2* reactions, since the R* radical products such as n-alkanes and 1-alkenes form in greater concentrations than the RO_2* products such as ROOH's, C12 alcohols, C12 ketones and tetrahydrofurans. The R* radicals form mainly via two sources: (i) ROOH decomposition reactions which yield stable reaction products such as C12 alcohols, C12 ketones, <C12 aldehydes and a pool of R* radicals; and (ii) direct fuel pyrolysis. The R* radicals thus formed have two major reaction pathways; B-scission forming n-alkanes and

1-alkenes constitutes the dominant path, while R* radical dimerization reactions forming C24 alkane isomers makes up the minor reaction path. Small amounts of tetrahydrofuran products can be explained by RO_2* isomerization and decomposition reactions.

Dopant addition showed that the major soluble products were always the same, with and without dopants, but their distributions varied considerably. 3,4-dimercaptotoluene and dibutylsulfide dopants, individually added to n-dodecane, interfere with the hydrocarbon oxidation chain at the alkylperoxy radical and the alkylhydroperoxide link, respectively. 2,5-dimethylpyrrole dopant, on the other hand, introduces cooxidation reactions involving dopant and oxygen and, consequently, inhibits ROOH formation. Pyridine, pyrrole and dibenzothiophene, individually added to n-dodecane showed few significant effects.

CHAPTER 1

INTRODUCTION AND OVERVIEW OF THE PRESENT WORK

1.1 INTRODUCTION

Fuel stability, or more correctly fuel instability, is a measure of the general chemical reactivity of a fuel; it is specifically the gum, sediment and/or deposit forming tendency associated with exposure of the fuel either to long term storage at ambient temperatures (commonly referred to as storage instability) or to short term stress at higher temperatures (commonly referred to as thermal instability). Both storage and thermal instability form degradation products that manifest themselves as harmful deposits in storage tanks, distribution systems, fuel tanks, and combustion systems, ultimately leading to fuel system malfunctions and/or operating difficulties.

The overall mechanism of sediment and deposit formation is believed to start with fuel reacting with oxygen forming hydroperoxides, proceeding through a series of reaction steps forming soluble and insoluble oxidation products, and culminating with formation of surface deposits and/or sediments. In general, higher temperatures accelerate the processes. It should be noted that the sediments and surface deposits usually represent only a small fraction of the oxidation products formed during fuel degradation and also of the total fuel in use in the affected equipment. The

chemical analysis of the fuel deposits found in aircraft systems and engines, and sediments found in fuel storage tanks and fuel distribution systems, indicate that oxygen, nitrogen and sulfur atoms are highly concentrated in the deposits and sediments, strongly supporting the importance of those trace inorganic elements in the deposit/sediment formation process.

Fuel stability problems are likely to become more severe in the future. There is a tendency towards increased utilization of broadened specification petroleum based fuels and alternate fuels from tar sands, coal liquids, and/or shale oil. Further, the availability of distillate fuels is being expanded by blending cracked stocks from coking, visbreaking and catalytic cracking with straight-run or nonprocessed stocks. All of these fuels tend to have higher amounts of trace metals and lower hydrogen contents, i.e, contain relatively higher content of olefins, aromatics and heteroatomic compounds. (The heteroatoms include nitrogen, sulfur and oxygen atoms incorporated in organic compounds). The presence of these reactive constituents contribute to a decrease in the stability of the fuel.

Storage instability can be a significant problem even with distillate fuels such as diesel fuels, No. 2 fuel oils, and some other distillate fuels, e.g. in strategic reserves primarily for military purposes and for standby and emergency type applications (Nixon, 1962; Goetzinger et al., 1983). Consequently, these fuels also must resist

degradation. During long term storage, fuels can degrade producing sediments and/or suspended matter which can cause aircraft and/or storage site problems. For example, filter blockage by sediments and deposits can result in failure of engines to start, loss of power in flight, and reduced refueling rates. Furthermore, chemical degradation products can remain in the fuel and lead to other problems in air and ground transportation fuel systems. For example, peroxides formed in the fuel can severely attack some fuel system elastomers, causing them to harden, become brittle and crack. This type of elastomer failure can result in system malfunction or complete failure to operate.

Thermal instability is a particular problem in high performance gas turbines which employ commercial and military aviation fuels, and other applications in which the fuel is recirculated and used for injector and component cooling, i.e., diesel and aviation fuel recirculating systems. In these applications, fuel temperatures can be elevated for extended periods of time, thereby accelerating the deterioration process. Thermal instability was first recognized as a problem in aviation turbine engines in the 1950's. During the 1960's, supersonic aircraft operation exacerbated the thermal instability problem since the fuel served as the heat sink for cooling the aerodynamically heated wing surfaces. Moreover, the continuing trend toward more severe engine operation (i.e., higher pressures and temperatures) may increase the thermal stress on fuels.

Deposition of solids within the fuel systems of aircraft/diesel engines may lead to fouled heat exchangers, plugged fuel nozzles, and/or jammed fuel valves. This could result in excessive oil temperatures and non-uniform fuel spray patterns, causing distorted turbine/engine inlet temperatures and leading to a reduction in turbine/diesel engine life times (Brinkman et al., 1979; CRC, 1979; Peat, 1982).

Although considerable research effort has been devoted to elucidation and solution of the fuel degradation problem (mostly by the black box approach), knowledge of the detailed chemistry is lacking. Previous work, emphasizing research on jet fuels, diesel fuels, No. 2 fuel oils, model fuels (including specific alkanes, olefins, naphthenes, aromatics, etc.), and deposits (CRC, 1979; Taylor, 1979; Daniel, 1983; Goetzinger et al., 1983; Marteney et al., 1982; Wong and Bittker, 1983; Li and Li, 1985; Mayo and Lan, 1986), has yielded unclear and, at times, contradictory information regarding the effects of particular species on fuel degradation. Also, the chemical interpretation of the fuel stability data is very difficult, since the fuel composition is very complex and the fuel deterioration products are many. Clearly there is a need for the testing of fuels to monitor their degradation, and to test for their sediment and deposit forming tendencies. In the longer run, however, an understanding of the mechanism(s) leading to sediment and deposit formation must be developed so that

future fuels and engines can be designed to minimize these problems.

Degradation mechanisms for multicomponent distillate fuels have been postulated based only on the testing of the single component fuel n-dodecane (Hazlett et al., 1977). Therefore, detailed reaction mechanism data in relation to other components and dopants are lacking. In-use fuels contain many substances including olefins, aromatics, and naphthenes, all of which are more reactive than alkanes. These fuels contain traces of reactive nitrogen, oxygen and sulfur containing heteroatoms as well.

As noted, the heteroatoms concentrate in the fuel deposits, indicating that it is important to determine their effects during the fuel deterioration process. Previous low temperature (<300C) reaction mechanism studies involving pure hydrocarbon and heteroatom mixtures has shown that reactive sulfur, nitrogen and oxygen compounds can cause changes in the hydrocarbon oxidation chemistry by introducing additional cooxidation reactions, radical forming/scavenging reactions, etc., (Reich and Stivala, 1969). During thermal instability conditions, the fuel is exposed to temperatures between ambient and 550C and oxidation can occur. Therefore, the study of the reactions involving trace heteroatom interactions with major distillate fuel components is of consider interest as it leads to heteroatom plus hydrocarbon oxidation chemistry. The studies can then be extended to more complex mixtures.

In order to develop a more general understanding of fuel degradation mechanisms, the present Ph.D. thesis work was undertaken with the following specific objectives: (1) to determine the relationships between fuel components and contaminants and the thermal stability of the fuel; and (2) to determine the mechanism(s) of deterioration and to further understand the complex reactions occurring before, during and after the deterioration process.

The basic approach was to study model distillate fuels singly and in combination with deleterious trace component species. Effects to be tested included the influence of oxygen in and above the fuel and the influence of organically bound nitrogen and sulfur containing compounds in the model fuel. Specifically, n-dodecane was chosen as the model fuel since it is a prototypical component of distillate fuels and, additionally, its degradation chemistry was well studied by Hazlett et al. (1977). The fuels, n-dodecane and n-dodecane plus heteroatomic species, were aerated by bubbling air through the fuel and then were stressed using a modified Jet Fuel Thermal Oxidation tester (JFTOT) operating at temperatures up to 400C. The control and stressed fuel samples were examined by gas chromatographic (GC) and gas chromatography/mass spectrometric (GCMS) techniques to determine the concentrations and identities of stable reaction intermediates and end product species. Analysis of these data led to inferences about the mechanisms.

Chapter 2 gives additional background information about the general characteristics of distillate fuel stability, and presents a review of the pertinent literature in the areas of liquid phase hydrocarbon oxidation chemistry with and without contaminating organic heteroatoms. The experimental facility, system protocols and identities of the n-dodecane derived reaction products are described in Chapter 3. Neat n-dodecane system verification results and modified mechanisms are discussed in Chapter 4, while Chapter 5 presents the results and mechanisms of n-dodecane spiked with small amounts of sulfur and nitrogen containing compounds. Finally, the conclusions of the present work and recommendations for future work are discussed in Chapter 6.

1.2 OVERVIEW OF THE PRESENT WORK

A standard Jet Fuel Thermal Oxidation Tester (JFTOT) apparatus primarily monitors the coking and surface deposition tendency of aviation fuels. For the present work, the JFTOT was modified to study the formation of soluble degradation products in model fuels over a temperature range of ambient to 400C, so that several individual samples could be collected with a single filling of the reservoir. The control (ambient) and stressed fuel samples collected at heater tube temperatures of 200, 250, 300, 350 and 400C were examined by GC and GCMS techniques to determine the concentrations and identities of stable reaction

intermediates and end product species. Analysis of these data led to inferences about the mechanisms.

As noted, n-dodecane was chosen as the model fuel, since it is a prototypical component of distillate fuels and, additionally, its degradation chemistry was studied by Hazlett et al. (1977). Preliminary results showed that 99% purity, as-received grade n-dodecane contained many impurities and required additional purification; thus a vacuum distillation apparatus was developed to further purify the fuels. n-Dodecane with 99.8% purity (percent peak area basis during GC analysis) could be obtained from the distillation process. Tetralin, a second fuel desired for two-component experiments, also had unacceptable levels of impurities as-received and required cleanup. However, the tetralin oxidized during distillation and acceptably clean tetralin could not be produced. Hence, all experimentation was only with distilled n-dodecane.

No visible deposition was observed on the JFTOT heater tubes for all the experiments performed. However, analytical protocols were developed to separate the control and stressed fuel samples into several fractions, based on a polarity separation, and into several reaction product groups (Groups I-V), based on gas chromatographic analysis. The reaction products consisted mainly of C5-C10 n-alkanes and 1-alkenes (Group I-nonpolar), C7-C10 aldehydes (Group I-polar), tetrahydrofuran derivatives (Group II), dodecanol and dodecanone isomers (Group III), dodecylhydroperoxide

(ROOH) decomposition products (Group IV), and C24 alkane isomers (Group V). Positive peak identifications for Groups I, II, III and V were done using standard compounds, retention time matching and GCMS techniques. The Group IV assignment as hydroperoxides was based upon ROOH synthesis experiments followed by retention time matching. It is noted that the total amount of soluble products formed increased with JFTOT temperature over the range of temperatures tested.

During GC analysis, the parent n-dodecane elutes as a broad peak in the middle of the chromatogram, masking possible products, and also overloading the GC capillary column. Therefore, in order to obviate n-dodecane interference, a sample preparation and fractionation scheme using Silica Sep-pak cartridges was developed. This scheme separates unreacted n-dodecane and non-polar reaction product constituents into the non-polar fractions (NP) using cyclohexane washes, while polar constituents are fractionated into the polar fractions (P) using 2-propanol washes. Group I-NP and Group V, including the unreacted n-dodecane, are non-polar in nature and consequently elute in the first non-polar fraction (NP1 fraction). Group I-P and Group II-IV are polar in nature and elute in the first polar fraction (P1 fraction). Further non-polar washes removed residual dodecane while further polar washes showed that the P1 wash contained virtually all of the polar products. Thus, the Sep-pak fractionation scheme not only removes the

n-dodecane interference, but also separates the reaction products into its non-polar and polar constituents.

Sample analysis was done using both split injection and on-column injection, OCI, techniques. The P1 fraction analysis revealed the presence of thermally labile compounds (Group IV products) during split injection analysis. Since the OCI injection technique employs low injection temperatures (50C versus 280C), the P1 fractions were analyzed using this OCI technique, thereby minimizing Group IV product break down.

Using the protocols noted above, the analysis of the control and stressed fuel samples resulted in reasonable reproducibility of the Group I-V product concentrations. In general, the overall reproducibility including sampling and GC analysis is a function of individual product groups (Groups I-V) and JFTOT temperature. At low temperatures ($T \leq$ 250C), product reproducibility is poor due to very low concentrations, but it improves considerably at higher temperatures ($T \geq$ 300C). Also, one chromatographically well-resolved character impact peak, CIP, from each of the I-V Groups were chosen to represent the Group based on their low data scatter; i.e., the error bars using CIP's are lower than those using total Groups, thereby simplifying data interpretation. The details of the Group and CIP I-V reproducibility at various temperatures can be found in Chapter 3.

Once the reproducibility of the neat n-dodecane product data was confirmed, the detailed n-dodecane/oxygen reaction mechanism proposed by Hazlett et al. (1977) was used as a starting point in explaining the present results. The presence of autoxidation ($T \leq 300C$) and intermediate temperature ($300 \leq T \leq 500C$) regimes was confirmed, but several additional products such as Group II tetrahydrofurans, Group I-P aldehydes and Group V C24 alkane isomers were also detected as a result of our better analytical sensitivity. Consequently, the available n-dodecane/oxygen reaction mechanism was modified to include these products. The details of the modified n-dodecane reaction scheme can be found in Chapter 4.

After the detailed degradation behavior of a single component distillate fuel (neat n-dodecane work) was done, the study was extended to examine the effects of dopants. Specifically, n-dodecane was doped with sulfur and nitrogen containing heteroatomic species selected based on their reported deposition tendencies, and the mixtures were tested on the modified JFTOT apparatus. A typical dopant sequence involved baseline, 10 ppm, 100 ppm, and 1000 ppm (molar ratios) JFTOT experiments; a 150 cc distilled dodecane flush; followed by a second baseline JFTOT experiment. Also, prior to the second baseline experiment, the last portion of the flush was analyzed on the GC and checked for dopant carry over. If dopant was detected in trace quantities,

additional flushes were carried out until no dopant was detected.

Subsequently, the control and stressed samples were analyzed for the major soluble oxidation products using GC and GCMS techniques. The major soluble products were the neat n-dodecane oxidation products (Groups I-V), but with significant changes in their distributions. No dopant related products were detected, however, due either to very low concentrations (ppb levels) or to a polarity mismatch between the solvents and the dopant oxygenates during Sep-pak fractionation. Hence, all dopant mechanism inferences are based on changes in n-dodecane derived Group I-V product distributions alone.

During n-dodecane plus heteroatom compound experiments, it was found that the data from the pre-10 ppm and post-1000 ppm 3,4-dimercaptotoluene (DMT) baseline tests were not reproducible, indicating possible carry-over and contamination problems. Further, this irreproducibility cast doubt on all the baseline and dopant experimental data obtained up to that time. Consequently, the baseline n-dodecane reproducibility was reexamined, and the DMT dopant sequence was duplicated to check and verify the reproducibility of the dopant data and associated trends. First, eight baseline n-dodecane JFTOT experiments were performed in series to establish reproducibility of the neat n-dodecane Group I-V product concentrations, and the applicability of the analytical protocols that had been

developed and were being used up to this point. Comparison of the two sets of DMT data showed that the major data trends were identical, indicating that the dominant dopant effects are reproducible. For example, the Group IV products were progressively inhibited with increasing dopant concentration in both test sequences. On the other hand, the minor data trends were not always the same. For example, the previous 10 and 1000 ppm DMT derived Group II product curves were slightly inhibited relative to the baseline in the 300-400C range, while the corresponding recent data showed no such inhibition. In any case, since definitive dopant mechanistic inferences cannot be made with minor data trends, they do not affect the overall reaction mechanism conclusions. Hence, based on the agreement in the major data trends, the mechanism inferences for the dopant data are not affected.

Finally, based on the changes in the Group I-V product distributions with fuel compositional changes, extended fuel degradation mechanisms were developed. The details of the n-dodecane plus minor component reaction mechanisms can be found in Chapter 5.

CHAPTER 2

BACKGROUND AND LITERATURE SURVEY

The complex chemical and physical processes involved in the degradation of fuels have been studied extensively (Nixon, 1962; CRC, 1979; Taylor, 1979; Peat, 1982; Goetzinger et al., 1983). The literature cited here is primarily concerned with the deterioration of distillate fuels during thermal stressing. However, as noted, the degradation problems due to thermal stressing are similar to those following long-term storage. Therefore, in addition to a detailed discussion of thermal stability, aspects of storage stability will be discussed as well, and differences and similarities will be highlighted. Also, details of this literature are incorporated into the analyses and discussions in subsequent chapters.

2.1 DISTILLATE FUEL STABILITY

The wide variety of crude oil types and refinery techniques result in a multitude of compounds in any end product fuel and a very diverse nature of distillate hydrocarbon fuel characteristics. Further, there are variable thermal stresses imposed on the fuel both in storage and under high temperature conditions. As a result, the problem of determining the exact nature of the deposit mechanism(s) is extremely difficult. However, after many

years of investigation, a general theory as to what may occur has been proposed. Fig. 2.1 illustrates the series of processes which start with fuel oxidation and lead to sediments and deposits (Taylor and Frankenfeld, 1986).

2.1.1 General Characteristics

It is generally agreed that the reactions between fuel components and oxygen usually involve complex free radical autoxidative mechanisms (Scott, 1965; Emanuel et al., 1967; Mayo, 1968). The main features of all theories include an initiation reaction of fuel with oxygen to form free radicals. The free radical reaction rates and products formed during the free radical chain reactions are dependent on hydrocarbon structure, temperature, oxygen concentration, and the presence of catalysts or free radical initiators. Usually, these free radicals react with oxygen forming soluble organic hydroperoxides. The hydroperoxides can reach limiting concentrations and ultimately decompose to form radicals, which can participate in chain propagating reactions, and other products. The major hydroperoxide decomposition products are alcohols, ketones, aldehydes, esters, acids and hydroxyketones, depending on oxygen availability and initial fuel composition (CRC, 1979).

The detailed steps in the conversion of initial oxidation (soluble) products into insoluble products remains unclear. However, several hypotheses have been suggested for the evolution of insoluble products: (i) polymerization - soluble oxidation products can polymerize resulting in high

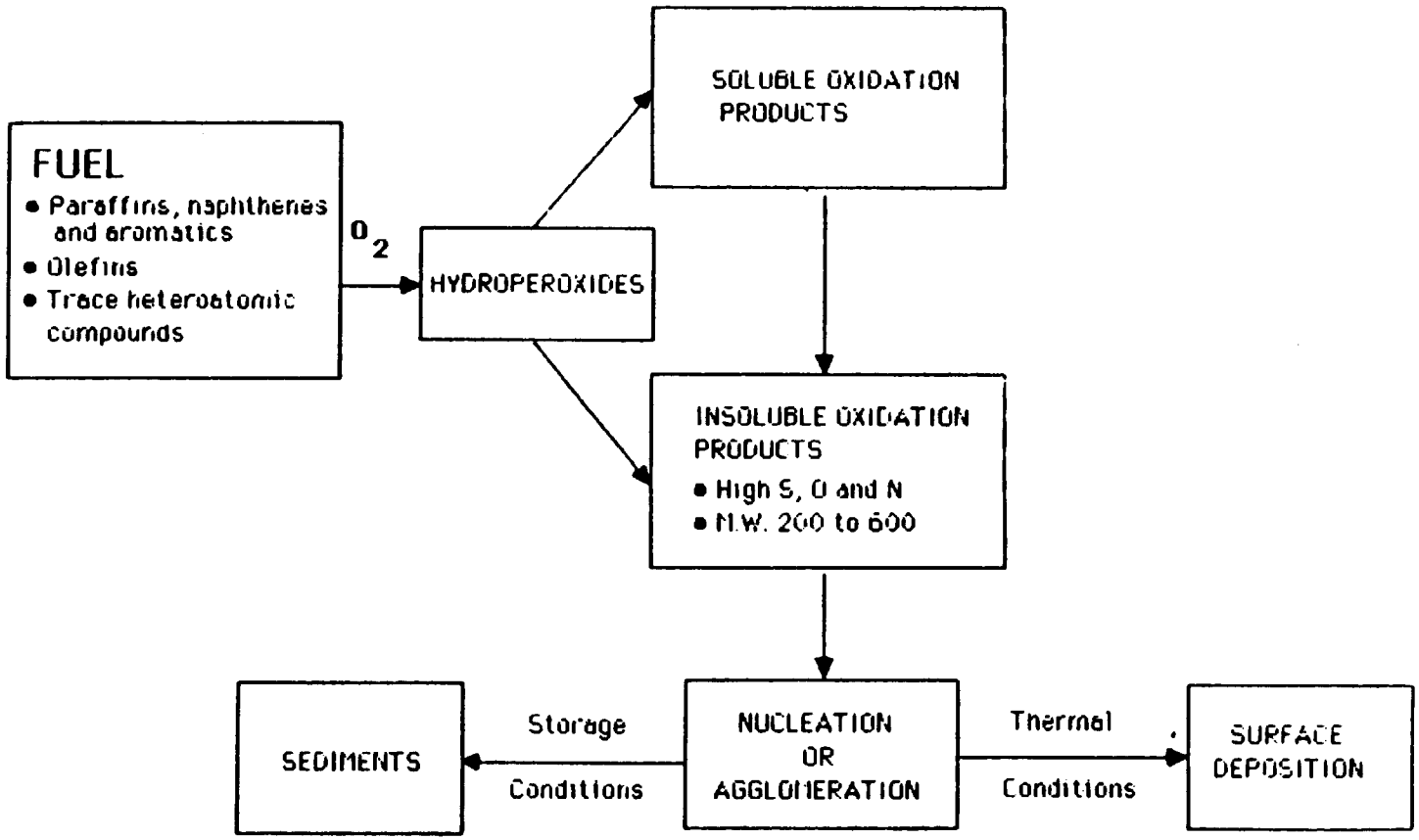

FIG. 2.1 Mechanism of Sediment/Deposit Formation (Taylor, 1986)

molecular weight compounds, although this may be limited to dimerization and trimerization (Mayo et al., 1975); (ii) increased polarity - reaction products become increasingly polar as oxidation progresses (supported by high concentrations of S, O, and N atoms in deposits; Hazlett, 1981); (iii) rearrangements and condensation reactions - studies of heating oil show that thiols can act as catalysts for oxidation and, after oxidation to sulfonic acids, can catalyze rearrangements and condensations (Sauer et al., 1958); and (iv) hydroperoxide thermolysis - studies on jet fuel show that the disappearance of hydroperoxides is followed by deposit formation (Taylor, 1979).

The composition of these sediments typically includes low, i.e., 400 to 600, molecular weight compounds rather than polymeric compounds, indicating that oxidized dimers and trimers are involved (Mayo and Lan, 1986). Studies have also shown that the quantity of sediments formed is less than the total quantity of oxidized fuel compounds, indicating that the solvent characteristics of the oxidized molecules play a critical role in stability processes. At storage conditions, insoluble oxidation products must nucleate and grow in order to form sediment particles large enough to be trapped by a filter. The evolution of this process has been followed by light scattering methods (Li and Li, 1985).

Examination of surface deposits, on the other hand, has shown the presence of microspherical particles,

typically measuring one to several thousand angstroms in diameter, which adhere to surfaces and ultimately form thin solid films (Schirmer, 1970). Metal surfaces are known to catalyze the deposit formation reaction (Taylor, 1968; Marteney et al., 1982). For example, Marteney et al. found that brass surfaces enhance the deposit formation rate relative to stainless steel and aluminum surfaces. Further, insoluble oxidized fuel molecules were found to produce particles whose density was not markedly greater than the base fuel itself, suggesting that these microspherical particles were formed in liquid phase at or near the metal surface, perhaps in the boundary layer. The ability of such particles to adhere to a surface under flowing fuel may also be a critical property for surface deposit formation (Taylor and Frankenfeld, 1986). Experimental evidence supports this hypothesis because with higher flow rates (i.e., lower bulk fuel temperatures and smaller boundary layer thicknesses), deposit formation is lower (Marteney et al., 1982). Thermal stability processes, therefore would be expected to be significantly influenced by fluid mechanics including heat and mass transfer effects. Further work is necessary to elucidate these effects.

Heterogenous catalysis (i.e., metal surfaces) would be expected to be more important in thermal stability than in storage stability because of higher temperatures and a greater surface to volume ratio. Homogenous catalysis (i.e., by dissolved metals) can be important in both storage and

thermal stability. Copper has been found to be the most deleterious metal to fuel stability, while iron, zinc, beryllium, cadmium, silver and cobalt are less harmful (Smith, 1967).

Fuel pressure is of significance as it determines whether liquid or vapor phases predominate at any temperature. Evidence supports the conclusion that deposits can form both in the liquid and vapor phases with the presence of both phases causing the greatest amount of deposits (Marteney et al., 1982).

During storage instability, color formation in fuel is often of concern to users, although, color per se is not a property which affects fuel performance in end-use equipment. Color is generally measured by light transmission so that the observed color is the complement of the light which is adsorbed in the fuel. Species in the fuel which adsorb in the visual region will thus produce color depending on their concentration and extinction coefficient (Nassan, 1983). Fuel molecules which adsorb strongly in the visual region tend to contain extended aromatic ring systems and heteroatoms (Nassan, 1983). Since autoxidation of distillate fuels often involves aromatic heteroatomic species which are converted to oxidized dimers and/or trimers to form extended ring systems, color formation is an expected result of autoxidation.

2.1.2 Effect of Fuel Composition

Hydrocarbon homologues (i.e., paraffins, naphthenes, aromatics, olefins, etc.) have been investigated for their storage and thermal instabilities. The only group which affected fuel thermal stability was the olefins, with variable magnitude of deposit formation depending on structure. The most deleterious unsaturates with respect to deposit formation included the acetylenes, di-olefins and mono-olefinic aromatics with conjugated side chains (CRC, 1979).

Extensive storage stability studies of all distillate fuels have been performed (Brinkman et al., 1980; Goetzinger et al., 1983). Early studies recognized that thermal or catalytically cracked stocks were more susceptible to sediment and color formation than straight run fractions. Olefins such as conjugated diolefins or aromatic olefins were identified as being contributors to instability (Nixon and Thorpe, 1956).

Heteroatoms were found to exert a strong influence on surface deposit/sediment formation. In general, heteroatoms are more easily oxidized than most other hydrocarbons found in distillate fuels. The ease of oxidation, however, does not parallel and is not necessarily a guide to the sediment/deposit formation rate. The addition of heteroatomic sulfur compounds of the type normally found in distillate fuels, i.e., thiols, sulfides, disulfides and condensed thiophene compounds, to straight run fuels such as

jet fuel did not increase sediment formation during storage stability testing (Frankenfeld et al., 1982). However, in the presence of cracked stocks, the addition of aromatic thiols causes an increase in sediment and color formation (Oswald and Noel, 1961). Other sulfur compounds such as disulfides and polysulfides also increase the rate of sediment formation in the presence of cracked stocks (Thompson et al., 1979). Although the role of sulfur compounds during storage stability testing are partially understood, thermal stability studies on sulfur compounds are lacking. Taylor and Wallace (1968) is the only reported study of sulfur compound effects during thermal stability testing of aerated jet fuels. They found that sulfides, disulfides and thiols accelerate surface deposit formation while condensed thiophenes had little effect.

Heteroatomic nitrogen compounds have been shown by a number of investigators to be deleterious to sediment and color formation at near ambient temperatures (Frankenfeld et al., 1982; Cooney et al., 1986). The nature of the fuel to which active nitrogen compounds were added influences the rate of sediment formation, with higher rates being obtained in diesel fuel than in jet fuel or n-dodecane (Frankenfeld et al., 1982). Significant differences in the reactivity of nitrogen compounds for sediment formation have been observed. In general, non-basic nitrogen heterocyclic compounds such as pyrrole and indoles have been found to be harmful for sediment formation whereas other nitrogen

compounds such as basic heterocycles of the quinoline type are not deleterious (Frankenfeld et al., 1982). Frankenfeld et al. also noted that the most deleterious species to fuel stability were alkylated heterocyclic nitrogen compounds, and the most reactive of those were compounds with two or more alkyl groups, at least one of which was on a carbon adjacent to the nitrogen. Sediments formed at high nitrogen levels (e.g., > 50 ppm N by weight) appear to consist entirely of oxidized dimers and trimers of the reactive nitrogen compound (Hazlett and Hall, 1981; Frankenfeld et al., 1982). As with sulfur compounds, thermal stability literature concerning nitrogen compound effects is also lacking. Taylor and Wallace (1968) and Reynold's (1977) work appears to be the only reported literature available. They report that thermal stability of jet fuels spiked with organic nitrogen compounds enhances the rate of surface deposit formation. Clearly, there is a need to understand the thermal instability behavior and chemical mechanisms of nitrogen compounds (added to other distillate fuels), since future fuels will likely have considerably higher contents of nitrogen relative to fuels in current use.

Heteroatomic oxygen compounds such as furans, carboxylic acids and phenols produced no measurable sediment formation when added by themselves to jet or diesel fuel. However, carboxylic acids interacted with nitrogen compounds to increase sediment formation in n-dodecane and jet fuel (Frankenfeld et al., 1982). Similar to the

situation with sulfur and nitrogen compound literature, there is a dearth of information regarding the effects of oxygen compounds during thermal stability testing. Since binary interactions of oxygen and nitrogen containing compounds increased sediment formation in model and jet fuels (Frankenfeld et al., 1982), it may be worthwhile studying fuel thermal instability using similar fuel and dopant combinations.

2.1.3 Effect of Temperature

Storage instability, involving hydroperoxide, color, or sediment formation at near ambient temperatures over an extended residence time, is dominated by low temperature (T < 300C) oxidative reactions. Thermal instability, involving surface deposition with exposure of fuel to much higher temperatures over much shorter residence times, is dominated by intermediate (300 $\leq$ T $\leq$ 500C) and high temperature (T > 500C) oxidation chemistry. Thus, the importance of various reactions change as the temperature rises, with pyrolysis reactions of the more unstable species (especially the free radicals) competing with oxidation reactions as the temperature is raised (Hazlett et al., 1977).

2.1.4 Effect of Deoxygenation

With the majority of fuels investigated, oxygen removal improves distillate fuel stability and decreases the amount of deposits produced in certain aircraft simulator experiments (Watt et al.,1968; Faith et al., 1971). However, several other thermal degradation processes can occur in the

absence of oxygen and these can result in fuel degradation and deposit formation in an oxygen free environment (e.g., Hazlett et al., 1977).

Studies made to determine the effects of fuel composition and environments on deoxygenated systems (Taylor, 1974, 1976a, 1976b) suggest that deposits are formed by chemical reactions and physical processes different from those of aerated systems. For example, the effects of adding specific sulfur compounds are complex. The addition of sulfides, disulfides, and thiols increased the rates of deposit formation in both deoxygenated and aerated fuel systems, while condensed thiophenes showed no effect with deoxygenation, the opposite effect to when fuel is aerated (Taylor and Wallace, 1968; Taylor, 1976a). These results suggest that the deposit formation rate is not always inhibited with fuel deoxygenation, but also depends on the type of trace sulfur compounds present in the fuel. Nitrogen compounds were studied (e.g., pyrroles, pyridines, amines, piperdines, amides and decahydroquinoline) and were found not to promote deposit formation, the opposite effect to when fuel is aerated (Taylor, 1976b). Oxygen containing compounds (e.g., hydroperoxides, carboxylic acids, phenols, furans, alcohols, ketones and esters) show a variety of effects, with peroxidic compounds shown to be highly deleterious, regardless of structure, even when added at quite low concentrations (Taylor, 1976b). Also, dissolved

metals were generally less deleterious with respect to deposit formation in deoxygenated fuels.

2.2 LIQUID PHASE OXIDATION OF HYDROCARBONS WITH AND WITHOUT HETEROATOMIC SPECIES

The study of organic compound reactions with oxygen are important since they produce energy that drives all life and most of the mechanical and heat energy used in technology. Over a wide temperature range, bounded roughly by enzyme-mediated oxidation at low temperatures and fast combustion reactions at higher temperatures, are a host of relatively slow oxidation processes involving free radicals. These free radical reactions are responsible for the conversion of hydrocarbons into useful industrial intermediates as well as for unwanted degradation in fuels, lipids and polymers, leading to the intensification of environmental pollution.

The fundamental oxidation reactions are typically long chain free radical reactions which include elementary stages involving chain initiation (the formation of primary free radicals), chain propagation leading to formation of hydroperoxides, followed by the molecular decomposition of the hydroperoxides, and finally chain termination in which the active free radicals are destroyed.

The current knowledge of the autoxidation of organic molecules has developed largely from the study of hydrocarbons, and the reaction schemes are concerned primarily with processes involving oxidative attack either

on carbon-hydrogen bonds or on olefinic double bonds. The liquid phase oxidation of hydrocarbons at low temperatures ($\leq$ 300C) have been reviewed extensively (Emanuel et al., 1967; Brown and Fish, 1969; Mayo, 1968; Mill and Hendry, 1980; Emanuel, 1981).

Interest in high temperature cracking of hydrocarbons ($\geq$ 500C) stems from the period during and following World War I when the rapidly increasing demands for gasoline and for gasoline of higher octane number led to the development of a variety of high temperature cracking processes in petroleum refineries. Scientific interest in hydrocarbon cracking (pyrolysis) was stimulated by the fact that hydrocarbon decomposition reactions involved free radicals as intermediates, and as such, required reaction mechanism elucidation. Free radical pyrolysis mechanisms were developed based on studies of low molecular weight hydrocarbons at atmospheric pressures by Kossiakoff and Rice (1943). Subsequently, the mechanisms were extended to include higher molecular weight hydrocarbons and higher pressures as well (Fabuss et al., 1964).

Even though the autoxidation and pyrolysis temperature regimes have been well studied, information regarding the intermediate temperature regime ($300 \leq T \leq 500$C) is lacking since the reactions are complex. At these temperatures, the primary oxygenated product, hydroperoxide, decomposes to form secondary oxygenated products, i.e., alcohols, ketones, acids, etc., which are subject to further conversion.

For intermediate temperatures, Hazlett et al.'s (1977) liquid phase n-alkane oxidation study appears to be the only one of its kind in the literature. Clearly there is a need to better understand the characteristics of hydrocarbon oxidation at these temperatures, since the rate of reaction increases and other secondary reactions become important at higher temperatures.

Distillate fuels in current use may be considered as pure hydrocarbon fuels because the heteroatom contents amount to only a few tenths of one percent. As noted in the introduction, these trace heteroatomic species exert significant deleterious effects on the stability of the liquid fuels by promoting deposit formation due to storage and exposure to elevated temperatures. Presently, the role of the heteroatoms influencing fuel instability is not well understood, since distillate fuels contain hundreds of components which complicate the analysis of the role of heteroatomic reaction chemistry. One basic approach is to study the effects of heteroatoms mixed in model fuel systems, and then possibly extend the understanding to in-use fuels. Available literature for model fuel plus heteroatom systems is restricted to a few selected cases, i.e., mercaptans and olefins (Oswald and Ruper, 1959), pyrroles and hydrocarbons (Oswald and Noel, 1961). The problem is compounded by the fact that the pertinent literature is concerned only with low temperatures. Information at intermediate and high temperatures, as

encountered in thermal stability situations, and the effects of other heteroatomic species particularly deleterious to fuel stability is lacking.

2.2.1 Oxidation of Hydrocarbons in the Liquid Phase

During the last quarter century, considerable research has been done on the kinetics and mechanisms of low temperature liquid phase oxidation by molecular oxygen of pure hydrocarbons typically found in distillate fuels (Emanuel et al., 1967; Brown and Fish, 1969; Mayo, 1968; Mill and Hendry, 1980; Emanuel, 1981).

In many instances, the oxidation takes place in the presence of various inhibitors and catalysts, so that the overall oxidation mechanism is complex. A typical reaction scheme is shown below:

Initiation

$RH \xrightarrow{SURFACE} R^* + (^*H)$ (Heterogenous) (1a)

$RH + O_2 \rightarrow R^* + HO_2^*$ (Homogenous) (1b)

$2RH + O_2 \rightarrow 2R^* + H_2O_2$ (Homogenous) (1c)

Propagation

$R^* + O_2 \rightarrow RO_2^*$ (Fast reaction) (2)

$RO_2^* + RH \rightarrow ROOH + R^*$ (Slow reaction) (3)

Decomposition of Peroxide

$ROOH \rightarrow RO^* + {}^*OH$ (4)

$2ROOH \rightarrow RO^* + RO_2^* + H_2O$ (5)

$RO^* + ROOH \rightarrow$ Products (6)

$RO_2^* + ROOH \rightarrow$ Products (7)

$ROOH \rightarrow$ Non-radical Products (8)

Induced Decomposition of Peroxide

X	+	ROOH	-->	Free radicals	(9)
Y	+	ROOH	-->	ROH + YO	(10)
Z	+	ROOH	-->	Inactive Products + Z	(11)
M	+	ROOH	-->	Free radicals	(12)

Self Termination

$2RO_2*$	-->	Inactive products	(13)

RH represents the hydrocarbon, RO_2* is the corresponding peroxy radical, and ROOH is the hydroperoxide. X, Y and Z are three different types of reactants which decompose organic peroxides, and M is a metal.

Initiation in liquid phase oxidation processes can occur by heterogenous (Reaction 1a) and homogenous routes (Reactions 1b and 1c) forming the alkyl radical. The alkyl radical, R*, reacts rapidly with oxygen forming the alkylperoxy radical, RO_2* (Reaction 2). The RO_2* radical abstracts a hydrogen from a C-H bond in the hydrocarbon molecule forming the hydroperoxide, ROOH, (Reaction 3). The peroxides can propogate the chain further by unimolecular/bimolecular decomposition reactions forming additional radicals and products (Reactions 4-8).

Metals and certain chemical compounds can accelerate the decomposition of peroxides at low temperatures, thereby changing the low temperature autoxidation significantly by increasing the initiation and the overall oxidation rate and also by accelerating secondary reactions (Reactions 9-12).

The free radicals chain terminate mainly by peroxy radical self termination (Reaction 13).

For a fixed initiation and termination rate, the rate of oxidation is controlled by the slow propagation step, Reaction 3, which reflects the strength of the weakest carbon-hydrogen bond in the hydrocarbon being attacked by a relatively unreactive and selective RO_2* radical. In general, paraffins and cycloparaffins containing relatively strong secondary- and tertiary- carbon-hydrogen, C-H, bonds will oxidize more slowly relative to aromatics with weak benzylic C-H bonds and olefins with weak allylic C-H bonds (Hendry et al., 1974). Also, olefins can undergo addition of peroxy radicals (Mayo et al., 1958) by Reaction 14:

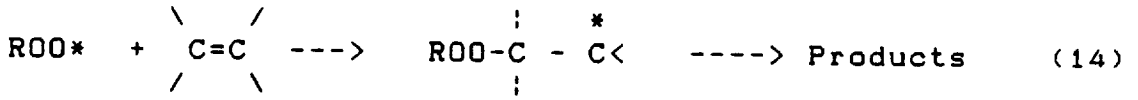

(14)

as well as intermolecular hydrogen transfer from an allylic position to a peroxy radical.

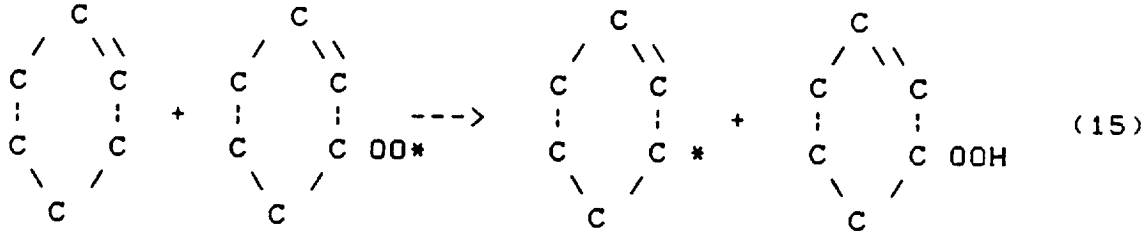

(15)

This peroxide formed in Reaction 15 is found to be the principal product (> 95%) under mild temperature conditions in neat cyclohexane (Mill and Hendry, 1980).

Inhibitors, commonly referred to as anti-oxidants, IH, have been used in a variety of commercial products to slow deterioration in air, rubber being among the first to

receive attention. Excellent reviews of the practical aspects of anti-oxidant development and use are available (Lundberg, 1962; Scott, 1965). Bolland and ten Haave (1947) proposed that inhibition resulted from chain-breaking by the faster reaction of RO_2* with IH than with the hydrocarbon to give a stable, comparatively unreactive radical, I*, which then terminates with RO_2* or I*, viz,

Chain-breaking Termination

$$RO_2* + IH \longrightarrow \text{Inactive products} \quad (16)$$

$$R* + IH \longrightarrow RH + I* \quad (17)$$

$$RO_2* + I* \longrightarrow ROOI \quad (18)$$

$$2I* \longrightarrow I\text{-}I \quad (19)$$

In many systems, the actual fate of I* depends on several factors, including the reactivity of I*, RH, ROOH, and the concentration of RO_2*. Thus, with simple hindered phenols, chain-transfer of I* with RH leads to propagation, although at a slower rate, by the reaction

$$I* + RH \longrightarrow IH + R* \quad (20)$$

Oxidation in mixtures of different hydrocarbons is much more complex (Russell, 1955; Benson, 1981). If binary mixtures of hydrocarbons R_1H and R_2H are considered, two types of radicals, R_1O_2* and R_2O_2*, are formed due to co-oxidation reactions, which can interact with both hydrocarbons involving both chain propagation and termination reactions. As a result, together with the chain propagation and termination reactions occurring in the

oxidation of pure hydrocarbons (R_1H and R_2H), chain propagation and termination cross-reactions also take place:

Cross-Propagation

$$R_1O_2* + R_2H \rightarrow R_1OOH + R_2* \quad (21)$$

$$R_2O_2* + R_1H \rightarrow R_2OOH + R_1* \quad (22)$$

Cross-Termination

$$R_1O_2* + R_2O_2* \rightarrow \text{Products} \quad (23)$$

The cross propagation rate coefficients do not vary significantly, but the rate of the two self-termination reactions can vary as much as a factor of 10^4. Thus, as the composition of the mixture is varied from 0-100% of the other hydrocarbon (R_2H), the importance of the various termination reactions changes accordingly (Russell, 1955).

Additionally, reactions involving alkyl radicals typically play a significant role in the oxidation of multicomponent mixtures at higher temperatures (Rafikova et al., 1971),

$$R_1* + R_2H \rightarrow R_1H + R_2* \quad (24)$$

$$R_2* + R_1H \rightarrow R_2H + R_1* \quad (25)$$

whereas at low temperatures the oxygen addition reaction ($R_1* + O_2 \rightarrow R_1O_2*$) dominates due to its low activation energy relative to Reactions 24 and 25.

As the temperature at which the oxidation occurs is increased from ambient levels, the rate of reaction increases and other secondary reactions become important. In particular, when peroxides begin to thermally decompose, they produce alkoxy and hydroxy radicals which are more

reactive and less selective compared to peroxy radicals and, therefore, lead to secondary reactions (Hazlett et al., 1977). During aircraft/diesel engine operation, the distillate fuels are exposed to relatively high temperatures (200-400C), making the fuels susceptible to secondary oxidations. These reactions are known to lead to surface deposits/sediments in close tolerance fuel system components, ultimately affecting engine performance. It is noted that relatively few studies dealing with liquid phase chemistry of large n-alkane hydrocarbons (> C8) at temperatures higher than those usually encountered during low temperature autoxidation reactions are reported in the literature.

As temperature increases, additional reaction paths become important. Above 180C, paraffins in the distillate fuel range can undergo intramolecular hydrogen abstraction, or radical isomerization, leading to rapid chain branching (Fish, 1964, 1968; Mill and Montorsi, 1973; Van Sickle et al., 1973; Jensen et al., 1979; Benson, 1981). These reactions usually become important only when the competing intermolecular process, notably hydrogen atom transfer and addition of oxygen, are slow.

The alkylperoxyl radicals abstract a hydrogen from within the molecule, forming hydroperoxyalkyl radicals, Reaction 26.

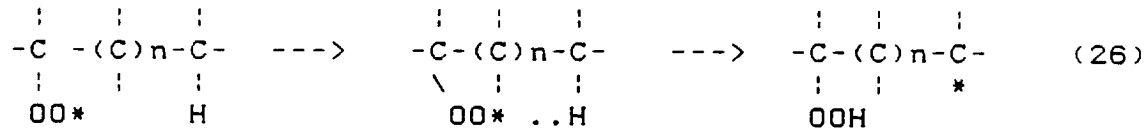

(26)

At low oxygen concentrations, the unpaired electron on the carbon atom of the hydroperoxyalkyl radical forms a bond with the oxygen atom, i.e., C-O bond closure, resulting in the formation of 'O' heterocyclic compounds and hydroxyl radicals, Reaction 27 (Boss et al., 1973; Van Sickle et al., 1973).

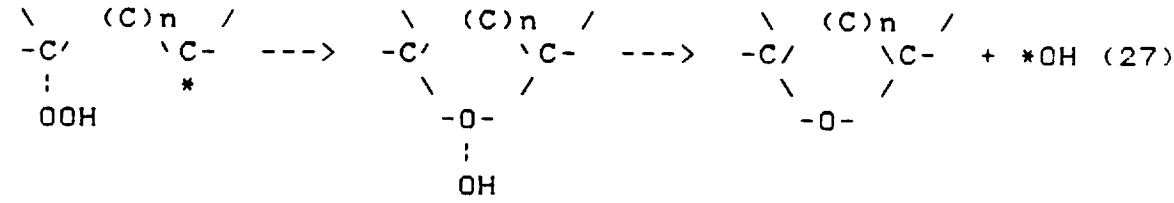

(27)

At higher oxygen concentrations, especially during dimethylalkane oxidation (Rust, 1957), the hydroperoxyalkyl radical can react further with oxygen to yield dihydroperoxides. Jensen et al. (1979) also reported various di- and tri- alkylhydroperoxides during n-alkane oxidation at 180C.

At higher temperatures, the thermochemistry of peroxy radical reactions have been evaluated for the gas phase (Benson, 1965). These data would be expected to be valid for the liquid phase also, since the intermolecular energies (1-3 kcal/mol) in relatively non-polar solvents such as n-alkanes are relatively weak in comparison to the energies of the covalent bonds (50-100 kcal/mol) (Benson, 1981). The fraction of the carbon radicals which would be oxygenated if

other loss mechanisms for the radicals were not important can be expressed as

$$[RO_2*] / [R*] = K_{eq} [O_2] \quad (28)$$

where [] refers to the radical and oxygen concentrations, while K_{eq} represents the equilibrium constant. Comparison of the K_{eq}'s and the bond energies for both alkyl and allyl/benzylic systems show that the formation of allyl/benzylic peroxy radicals (AO_2*) from a hydrogen abstracted allyl/benzylic C-H bond is reversible

$$A* + O_2 \; <===> \; AO_2* \quad (29)$$

whereas the formation of other alkyl peroxy radicals (RO_2*) is relatively irreversible at typical oxygen pressures (> 0.01 atmospheres) and at temperatures up to 227C (Benson, 1965; Maillard et al., 1983), viz

$$R* + O_2 \; ---> \; RO_2* \quad (2)$$

However, as temperature increases beyond 227C, the $[RO_2*]/[R*]$ ratio starts to decrease, and eventually reaches a value of unity at about 427C and at 0.01 atmospheres oxygen pressure. These values are considerably lower for the allyl and benzyl systems. For example, at 0.01 atmosphere oxygen pressure, the $[AO_2*]/[A*]$ ratio is 10 at 27C and 10^{-2} at 227C. Thus, the equilibrium constraint reduces the tendency of allylic/benzylic radical (A*) to chain propagate. The labile benzylic C-H bond enables aromatics to react relatively quickly with non-aromatic peroxy radicals (RO_2*) producing a relatively inert benzylic radical (A*) which then self-terminates to form inert products, viz

AO_2* ---> $A*$ + O_2 (29r)

AH + RO_2* ---> $ROOH$ + $A*$ (16)

$A*$ + $A*$ ---> $A-A$ (19)

The net result is that aromatics with allylic/benzylic C-H bonds can slow the rate of oxidation of more reactive species such as normal paraffins at higher temperatures. For example, toluene, p-xylene, ethylbenzene and cumene were found to inhibit the rate of oxidation of n-heptane at 350 to 540C, while benzene has no effect (Walling, 1968; Giammaria and Norris, 1962). These results indicate that, at temperatures typical of thermal stability conditions, aromatics with benzylic C-H bonds can function as weak inhibitors for the oxidation of compounds such as paraffins. This appears to explain the effect of aromatics on thermal stability surface deposit formation in pure blends (Taylor, 1969; Hazlett, 1979). Thus, hydrocarbon oxidation at thermal stability temperatures is much more complex than oxidation at ambient storage stability temperatures.

At very high temperatures, e.g., greater than 500C, fuel pyrolysis reactions become important (Kossiakoff and Rice, 1943; Fabuss et al., 1964). In essence, the first reaction of the chain is the abstraction of a hydrogen atom from the hydrocarbon molecule giving a new radical, Reaction 30. This is followed by the unimolecular decomposition of the new radical into particular fragments. Since C-C bonds are much weaker than C-H bonds, the splitting is always at a C-C bond (at the second C-C bond adjacent to the C-atom from

which the hydrogen is missing) and not at a C-H, or double or triple C bond, Reaction 31. Finally, a small free radical is formed that continues the chain, Reaction 32. An example of a one-step decomposition scheme (Fabuss et al., 1964; Hazlett et al., 1977) is depicted:

Radical Formation

$$R\text{-}H \quad \text{--->} \quad R^{*}\text{-}CH_2\text{-}{*}CH\text{-}CH_2\text{-}R^{1} + (*H) \qquad (30)$$

B-Scission

$$R^{*}\text{-}CH_2\text{-}{*}CH\text{-}CH_2\text{-}R^{1} \quad \text{--->} \quad R^{*}\text{-}CH_2\text{-}CH{=}CH_2 + R^{1}* \qquad (31)$$

Hydrogen Transfer

$$R^{1}* + R\text{-}H \quad \text{--->} \; R^{1}\text{-}H \text{ (smaller n-alkane)} + R* \qquad (32)$$

2.2.2 Co-oxidations of Hydrocarbons and Heteroatomic Compounds

As noted, our understanding of the autoxidation of organic molecules has developed largely from the studies of hydrocarbons; the resulting reaction schemes primarily involve oxidative attack either on C-H or on olefinic double bonds. Introducing heteroatoms into hydrocarbon molecules perturbs these processes and introduces the possibility of other reactions involving the heteroatom itself. The oxidation of heteroatom compounds has been less extensively studied than pure hydrocarbons (Walling, 1968; Trimm, 1980). Available co-oxidation literature is restricted to a few selected heteroatomic species, i.e., mercaptans and olefins (Oswald and Ruper, 1959); hydrocarbons and pyrroles (Oswald and Noel, 1961), and hydrocarbons plus nitrogen and sulfur compounds (Trimm, 1980). The problem is compounded by the

fact that the bulk of the available literature concentrates on the low temperature chemistry. Research at intermediate temperatures, as encountered in fuel thermal stability situations, including the effects of other particularly deleterious heteroatomic species, is lacking.

2.2.2.1 Effect of Heteroatoms on Neighboring C-H bonds:

In the familiar hydroperoxide chain mechanism for hydrocarbon autoxidation, with propagation steps

$$R* + O_2 \longrightarrow RO_2* \quad \text{(Fast Reaction)} \quad (2)$$

$$RO_2* + RH \longrightarrow ROOH + R* \quad \text{(Slow Reaction)} \quad (3)$$

Reaction 3 determines the point of oxidative attack on a molecule and, since it is slow and rate determining, it strongly influences the over-all rate. Even when they play no other role, heteroatoms should be expected to affect the reactivity of neighboring C-H bonds, either by resonanoe stabilization of the resulting radical or by altering the polar properties of the transition state. In practice, the latter is usually the dominant effect (Walling, 1968). Oxygen containing heteroatom compounds such as aldehydes and ethers undergo rapid low temperature autoxidation, presumably as a result of the heteroatom affecting the reactivity of the neighboring C-H bond (Walling, 1968). Autoxidation of sulfides is postulated to occur preferentially at the alpha-hydrogens (Trimm, 1980), although Mushrush et al. (1986) observed a different effect in that the sulfur molecule is attacked first, forming mainly sulfoxides.

2.2.2.2 Attack on Heteroatom-Hydrogen Bonds: The feasibility of reactions similar to Reaction 3, but involving attack on hydrogen bonded to an atom other than carbon, depends initially on the energetics of the process. Since D(ROO-H) seems to be ≈ 90 kcal/mol, regardless of R, a bond strength for hydrogen of this order or lower becomes a requirement for fast reaction. Table 2.1 lists some bond dissociation values for isoelectronic molecules (Walling, 1968).

In the second row elements of the periodic table, the D(N-H) and D(O-H) bond energies are large (actually greater than C-H), and since, as we have already noted, these atoms facilitate peroxy radical attack on neighboring carbon, it is not surprising that direct oxidation of amino and alcohol functions is not usually accomplished by molecular oxygen. Heteroatom-hydrogen bonds in aromatic compounds such as aromatic amines, thiols and phenols are relatively weak and lead to the formation of the corresponding radical.

$$AOH + ROO* \longrightarrow ROOH + AO* \qquad (33)$$

$$A_2NH + ROO* \longrightarrow ROOH + A_2N* \qquad (34)$$

However, such heteroatom radicals will not add oxygen to form a peroxy radical; thus, they will not chain propagate and their reactivity results in their being strong inhibitors of hydrocarbon oxidation. It is noteworthy that Reactions 33 and 34 are much faster than 3, even when the overall energetics appear comparable. Apparently reactions forming and breaking C-H bonds tend to be slower than iso-

TABLE 2.1

Bond Dissociation Energies (Kcal/mol)

Second Row Elements of the Periodic Table		
Alkane derivatives		
CH_3CH_2-H = 98	CH_3NH-H = 102	CH_3O-H = 102
Aromatic derivatives		
$C_6H_5CH_2$-H = 85	C_6H_5NH-H = 80	C_6H_5O-H = 88
Third Row Elements of the Periodic Table		
Alkane derivatives		
CH_3SiH_2-H = 83	CH_3P-H = 85	CH_3O-H = 88
Aromatic derivatives		
---	---	C_6H_5S-H = 80.5

energetic processes involving hydrogen bonds to most other elements of the periodic table, suggesting easier peroxy radical attack. However, examples of simple hydroperoxide chain processes are relatively few.

Autoxidation of mercaptans, RSH, gives rise to thiyl radicals (RS*), but these, like phenoxy radicals, are inert toward oxygen and normally dimerize to disulfides.

$$RS^* + RS^* \longrightarrow RS\text{-}SR \qquad (35)$$

In the presence of olefins, however, mercaptans participate in co-oxidative chain reactions in which the thiyl radicals add to the olefins to form a hydroperoxide (Kharasch et al., 1951).

$$RS^* + CH_2 = CHR' \longrightarrow RSCH_2\overset{*}{C}HR' \qquad (36)$$

$$RSCH_2\overset{*}{C}HR' + O_2 \longrightarrow RSCH_2\overset{OO^*}{\overset{|}{C}}HR' \qquad (37)$$

$$RSCH_2\overset{OO^*}{\overset{|}{C}}HR' + RSH \longrightarrow RSCH_2\overset{OOH}{\overset{|}{C}}HR' + RS^* \qquad (38)$$

It is generally found that the hydroperoxide initially formed undergoes further reaction. The co-oxidation reactions of thiols and olefins appear to be responsible for the deleterious effect of aromatic thiols on fuel storage stability (Oswald et al., 1962).

It is generally accepted that certain alkyl and aryl mono-, di-, and poly-sulfides act as anti-oxidants and prevent the free radical oxidation of hydrocarbons (Scott, 1965). The anti-oxidant mechanism of these compounds has been the focus of considerable research which has shown that

sulfides can act both as hydroperoxide decomposers (Koelewijn and Berger, 1974), and free radical scavengers (Koelewijn and Berger, 1972). The mechanism for hydroperoxide decomposition is not certain, but is generally accepted to be:

$$R_1SR_2 + ROOH \longrightarrow R_1SOR_2 + ROH \quad (39)$$

The sulfide R_1SR_2, reacts with ROOH, forming sulfoxide, R_1SOR_2, and an alcohol. Previous work has established that (i) the effect of the sulfide is catalytic, and (ii) the catalyst that decomposes the hydroperoxides is not the sulfide but a product that is formed from the sulfide. Circumstantial evidence has indicated that the catalyst is sulfur dioxide (Bridgewater and Sexton, 1978).

The sulfide will be a free radical scavenger if the sulfur-oxygen compound that is formed by oxidation can decompose to form a sulfenic acid. Thus, if the sulfoxide formed via Reaction 39 is active, it becomes the precursor to the real anti-oxidant, a sulfenic acid (R_1SOH), via Reactions 40-42.

$$R_1SOR_2 \longrightarrow R_1SOH + R_2\bullet \quad (40)$$

$$R_1SOH + ROO\bullet \longrightarrow ROOH + R_1SO\bullet \quad (41)$$

$$R_1SO\bullet \longrightarrow \text{Inert Products} \quad (42)$$

The anti-oxidant nature of sulfides at low temperatures appears to explain the negligible effect of sulfides on model fuel storage stability (Frankenfeld et al., 1982). These results are in sharp contrast to the results of thermal stability studies (Taylor and Wallace, 1968), in

which sulfide and disulfides were quite deleterious to jet fuel stability. The formation of deposits under high-temperature conditions apparently proceeds by reaction pathways different than in the ambient storage conditions.

Heterocyclic compounds containing a five-membered ring with one nitrogen atom such as pyrroles, indoles, and carbazoles in the form of alkylated derivatives are found in small quantities in petroleum products. The oxidation of these compounds is suggested to occur by molecular oxygen involving peroxidic intermediates (Oswald and Noel, 1961). Sediments resulting from co-oxidations of 2,5-dimethyl-pyrrole (DMP) and n-decane show that they are made of repeating units of oxidized DMP. This result suggests that DMP derived oxide radicals, DMPO*, are involved in self-condensation reactions (Frankenfeld et al., 1982), which supports the peroxidation theory postulated by earlier workers. The position of substituents on the nitrogen heteroatoms greatly influences their reactivity; alkylation adjacent to the nitrogen atom is the easiest to oxidize, while nitrogen-alkylation appeared to be relatively stable towards air oxidation. The reactivity of nitrogen heterocycles towards oxygen was suggested to parallel sediment formation in model fuels (Frankenfeld et al., 1982).

2.3 CLOSURE

In summary, the available literature shows that the autoxidation ($\leq$ 300C) and high temperature ($\geq$ 500C) liquid

phase oxidations of hydrocarbons have been studied extensively, while information regarding the intermediate temperature regime (300 $\leq$ T $\leq$ 500C) is lacking. This temperature regime needs to be investigated further, since distillate fuels are being exposed to such temperatures during air/ground transportation engine operation, causing sediment/deposit formation and adversely affecting engine operation. Previous work in this temperature regime has shown that the reactions are very complex. In particular, the primary oxygenated product, hydroperoxide, decomposes to form secondary oxygenated products, i.e., alcohols, ketones, acids, etc., which are subject to further conversion. In this regard, Hazlett et al.'s (1977) C12 n-alkane oxidation study appears to be one of the few cited works at intermediate temperatures. Clearly, there is a need to expand the current understanding of the fundamental hydrocarbon oxidation chemistry at the intermediate temperatures.

As noted in the introduction, heteroatomic trace species exert significant deleterious effects on the stability of the liquid fuels by promoting deposit formation due to storage and exposure to elevated temperatures. Presently, the role of the heteroatoms influencing fuel instability is not well understood, since in-use distillate fuels contain hundreds of components which complicate the understanding of the heteroatomic reaction chemistry.

Available literature for model fuel plus heteroatom systems is restricted to a few selected cases, i.e., mercapton and olefins, pyrroles and hydrocarbons, sulfides and hydrocarbons. The problem is compounded by the fact that the pertinent literature is concerned with only low temperatures. Information at intermediate and high temperatures, as encountered in thermal stability situations, and the effects of other heteroatomic species particularly deleterious to fuel stability is lacking. Thus, the current study of n-dodecane as a model fuel alone and in combination with harmful heteroatomic species, tested between 200-400C, was designed to fill in some of the gaps in the current knowledge.

CHAPTER 3

EXPERIMENTAL FACILITY AND ANALYTICAL METHOD DEVELOPMENT

The experimental facilities and analytical methods for enhancing and ensuring the detection of fuel derived soluble degradation products are discussed in this chapter. The modified Jet Fuel Thermal Oxidation Tester (JFTOT) facility and its operation is discussed in Section 3.1. Analytical methods such as Gas Chromatography (GC), chemical separation and Gas Chromatography/Mass Spectrometric (GCMS) techniques employed to isolate, detect and identify individual degradation products are dealt with in Sections 3.2 and 3.4. The sample handling techniques adopted for minimizing contamination of control and stressed fuel samples are discussed in Section 3.3. Finally, the short-term and long-term overall system reproducibility results are dealt with in Section 3.5.

3.1 JFTOT MODIFICATION AND OPERATION

The standard JFTOT apparatus is used to determine if an aviation turbine fuel meets the current thermal stability requirement as per ASTM method D-3241. For the present work, the JFTOT was not used to estimate the amount of deposits formed in a test, but was modified to study the formation of soluble degradation products in model fuels over ambient to 400C temperatures. Using the standard JFTOT procedures with sample collection from the stressed fuel reservoir, cross-contamination of fuel samples between runs was observed,

even with extensive cleaning of all the fuel lines and purging of dead volumes. Consequently, modification of the JFTOT and its operating procedures was required in order to eliminate this cross-contamination problem.

To accomplish this, a special sample collection tee was placed in the fuel return line after the heater tube but prior to any stagnant lines or dead volumes, Fig. 3.1. To ensure proper flushing of the tee and transfer lines before sample withdrawal, the sampling tap was kept cracked open throughout the experiment and several minutes were allowed before actual sample collection at each operating condition. This procedure increased the total instrument flow from 3 ml/minute to approximately 3.75 - 4.0 ml/minute; this higher flow rate is expected to result in slightly lower deposit formation (Vranos and Marteney, 1980) due to the shorter residence times and lower bulk fuel temperatures across the heater tube. In addition to providing clean samples, this modification permitted several samples to be collected in a single JFTOT run with one filling of the fuel reservoir. This was accomplished by changing the heater tube temperature in several increments (e.g., 200 to 400C in 50C steps) over the course of the run, with collection of valid samples at each temperature condition after system stabilization and adequate flushing of the sample line and tee with fresh sample (15 minutes combined time). Details of the modified JFTOT operating procedure are given in Appendix A.

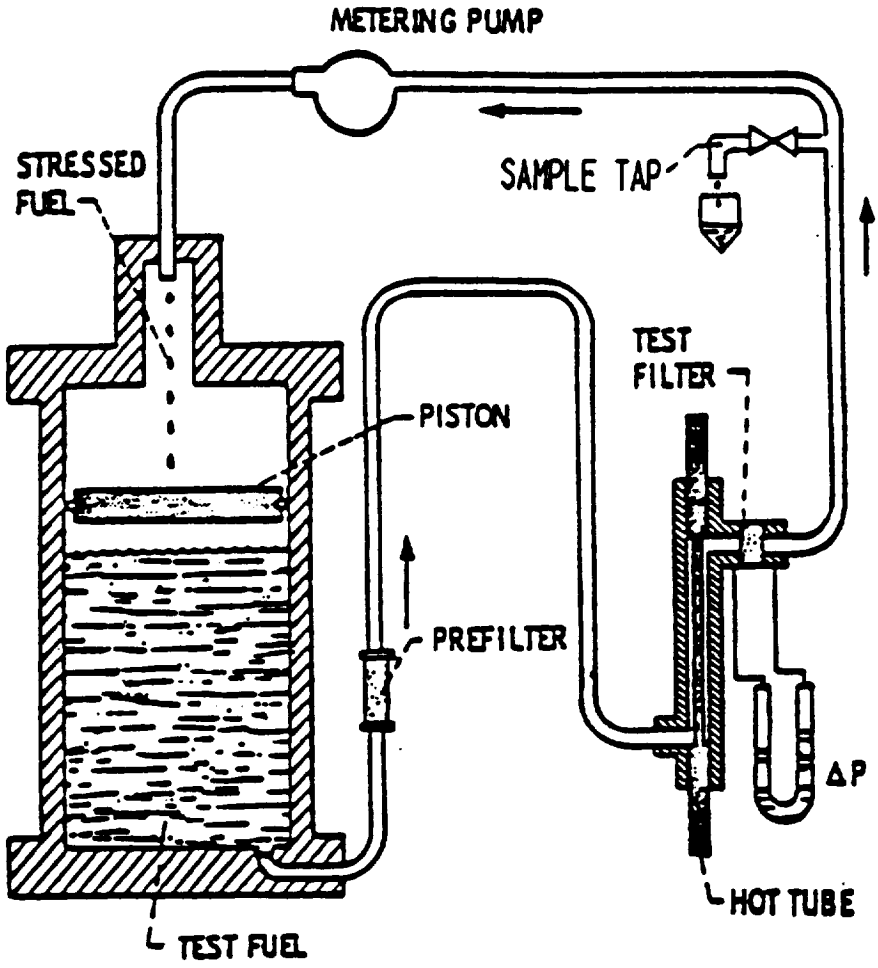

FIG. 3.1 Modified Jet Fuel Thermal Oxidation Tester (JFTOT) with Sample Withdrawal System

It is noted that the heater tube temperatures quoted in this thesis work are maximum wall temperatures attained at the center of the 2 3/8 inch aluminum tube over a 3 to 5 mm length. The fuel temperature at the location of the thermocouple (placed inside the heater tubes) is much less, perhaps 50-75C lower at that point. The bulk fuel temperature averaged over the entire span of the heater tube may be even lower, being approximately 100C less than the quoted heater tube temperatures.

3.2. CHROMATOGRAPHIC/SEPARATION METHODS

Attempts to analyze the JFTOT stressed samples were first made using liquid chromatographic (LC) techniques. UV detection at 220 and 254 nm was not successful in following the deposit precursors in the stressed samples, due to the low concentrations of detectable products. Subsequently, the JFTOT samples were analyzed on a Varian 3700 Gas Chromatograph (GC) equipped with both split and on-column injectors and flame ionization detection (FID). The analytical column was a fused silica DB1 (SE-30 type) bonded phase capillary column - 0.25 mm diameter x 30 meters long (J & W Scientific Co., California). During split injection analysis, breakdown products of thermally unstable species were detected; hence the cold on-column injection (OCI) technique was employed, wherever possible, to minimize sample breakdown. Additionally, since the soluble degradation products were at trace level concentrations, a

Sep-pak fractionation scheme, based on polarity separation, was employed to separate and enhance detection of the non-polar and polar constituents of interest.

3.2.1 GC Parameters

GC split injection techniques provided reasonable sensitivity for monitoring soluble product formation. However, sample volumes were restricted to 0.8-1.4 microliters (µl) due to capacity constraints on the capillary column. The GC split and on-column injector conditions employed throughout the work are given in Table 3.1.

3.2.2 Peak Profile Analysis Technique

Peak profiling is a technique for monitoring the compositional changes occurring in the fuel by graphing a number of sample chromatograms on a single plot. Figure 3.2 shows representative GC split injection results of samples collected in a single modified JFTOT run. Each rectangle is a replotted chromatogram which represents the fingerprint of the fuel at the noted JFTOT heater tube temperature. The x-axis gives the time of elution of the mixture components in minutes (linear scale), while the y-axis gives species concentrations in peak area counts (logarithmic scale). Each line in the rectangle represents a single compound or group of compounds with the height being proportional to the concentration. One can then monitor the changes occurring in the composition of the parent fuel as the stressing level is increased. Degradation product species can be easily

TABLE 3.1

GAS CHROMATOGRAPHIC CONFIGURATION AND OPERATING CONDITIONS

Gas Chromatograph	:Varian 3700
Analytical Column	:0.25 mm I.D.;30 meter DB1 (SE-30 type) bonded phase capillary column
Oven Temperature Program	:50C - 10 mins., 3C/min., and 275C - 15 mins.
Carrier Gas Flow Rate	:Hydrogen; 1 cc/min.
FID Temperature	:300C
FID Sensitivity	:1 x 10 E-12 amps/mV
FID Gas Flow Rates	:300/30 cc/min. (Air/Hydrogen)
Integrator	:Spectra Physics 4200
Integration Parameters	:Peak Threshold - 50; Peak Width - 3 secs.; Signal Attentuation - 4 Chart Speed - 1, 5 cm/min.
Split Injection	
Injector Temperature	:280C
Injector Split Ratio	:45:1
Sample Injection Volumes	:0.8 - 1.4 microliters (µl)
On-Column Injection	
Injector Temperature Program	:50C - 0 mins.; 100C/min.; 280C - 50 mins.
Injection Volume	:0.5 µl

Note: O_2, CO, CO_2, H_2 gases were not analyzed due to column and detector limitations.

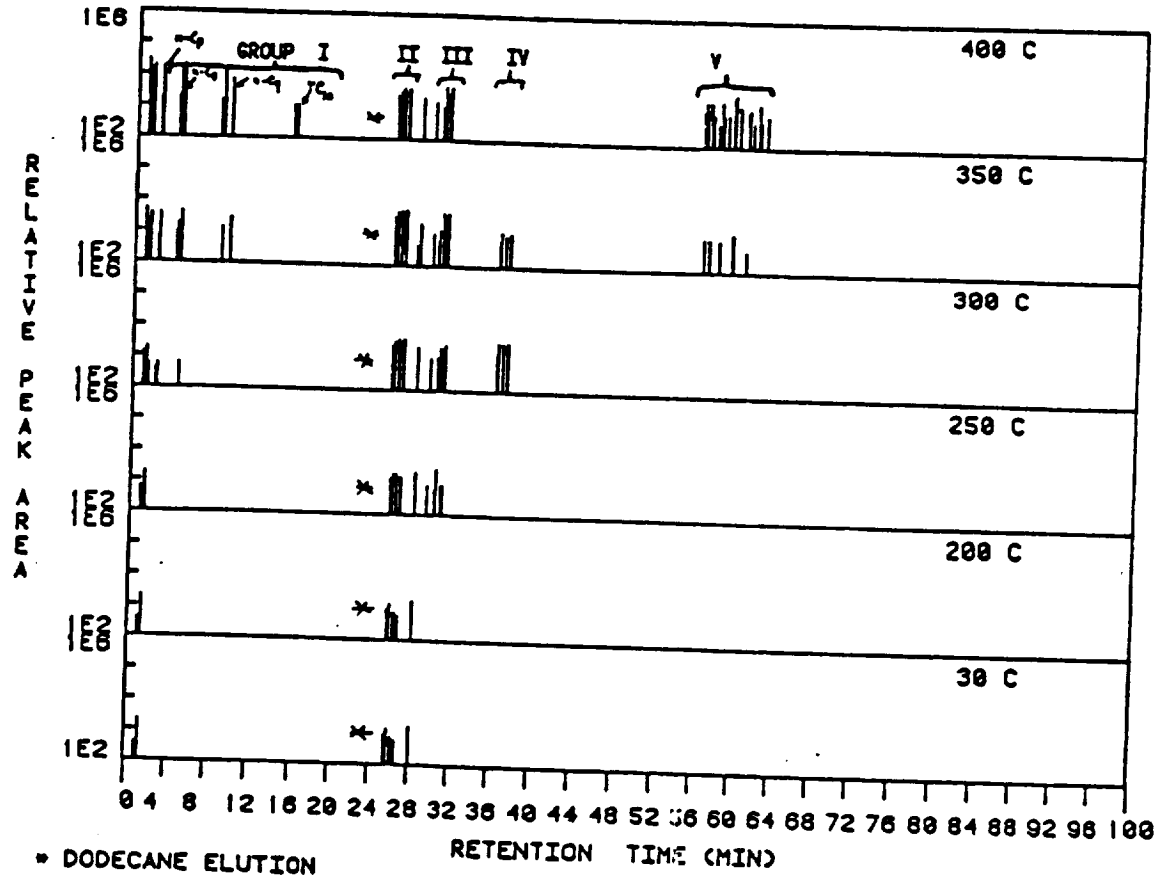

FIG. 3.2 GC Peak Profiles of JFTOT Stressed, Distilled n-Dodecane

observed, since the retention times of the new species will be different from that of the parent fuel (shown by the asterisk). Based on retention time bands, the major soluble products appear in five retention time ranges of the GC chromatogram and were designated as Groups I, II, III, IV and V, respectively, thus enabling simplification of data interpretation and analysis.

During split injection analysis, n-dodecane elutes as a large peak covering 7-10 minutes of all GC chromatograms, shown as asterisks in Fig. 3.2, thus overloading the capillary column and masking possible products in that time range. To overcome this n-dodecane interference, a sample preparation and fractionation scheme using Sep-pak cartridges (Waters Associates, Milford, Massachussetts) was developed.

3.2.3 Sep-pak Fractionation Scheme

The Sep-pak fractionation scheme is a technique for separating the non-polar and polar constituents based on species polarity. A procedure developed earlier (Shala, 1983) was modified for this study. One ml of the sample is adsorbed onto a silica Sep-pak cartridge and the non-polar and polar compounds are selectively stripped off by eluting using cyclohexane (NP1, NP2, NP3 fractions) and 2-propanol (NP/P, P1, P2, P3 fractions) respectively as solvents. In all, seven elutions are performed for a given sample; the details of the scheme are shown in Table 3.2.

TABLE 3.2

SEP-PAK FRACTIONATION SCHEME

1. 1 ml sample placed on Silica Sep-pak Cartridge

2. 2 ml cyclohexane elution - NP1 fraction
(contains primarily Group I-NP and Group V species plus most of the unreacted n-dodecane)

3. 2 ml cyclohexane elution - NP2 fraction
(contains residual n-dodecane)

4. 2 ml cyclohexane elution - NP3 fraction
(contains residual n-dodecane)

5. 1 ml 2-propanol elution - NP/P fraction
(removes cyclohexane)

6. 1 ml 2-propanol elution - P1 fraction
(contains primarily Groups I-P, II, III and IV species)

7. 1 ml 2-propanol elution - P2 fraction
(contains residual n-dodecane)

8. 1 ml 2-propanol elution - P3 fraction
(contains residual n-dodecane)

Using GC analysis on the fractions obtained in this way, it was found that Group V and a major part of Group I products (designated as Group I-NP), including the unreacted n-dodecane, elute in the NP1 fraction, while Groups II-IV and a minor part of Group I products (Group I-P) elute in the first polar fraction, P1, Fig. 3.3. The other fractions contained primarily residual n-dodecane and were of little interest.

Reproducibility of the Sep-pak procedure was checked by collecting a duplicate set of fractions from the same stressed JFTOT sample (84/7/400C sample) and comparing the two data sets, Figs. 3.3 and 3.4. The respective NP1, NP2, NP/P, P1, and P2 fraction profiles were identical, implying that the fractionation procedure was reproducible.

3.2.4 Development of GC/On-column Injection Technique

GC/FID results of the baseline P1 fractions performed using split injection analysis were not always good for quantification, since a number of degradation products were at the limits of FID detection under the prevailing sample size restrictions. Thus, on-column injection (OCI) was also employed to attain improved sensitivity and reproducibility. In this case, the peak areas of the degradation products were large enough to be integrated and reported with only a 0.5 μl sample size. Additionally, OCI was far superior to split injection in detecting thermally labile species, since the thermal breakdown of labile compounds (e.g., Group IV compounds) is minimized using OCI at 50C relative to

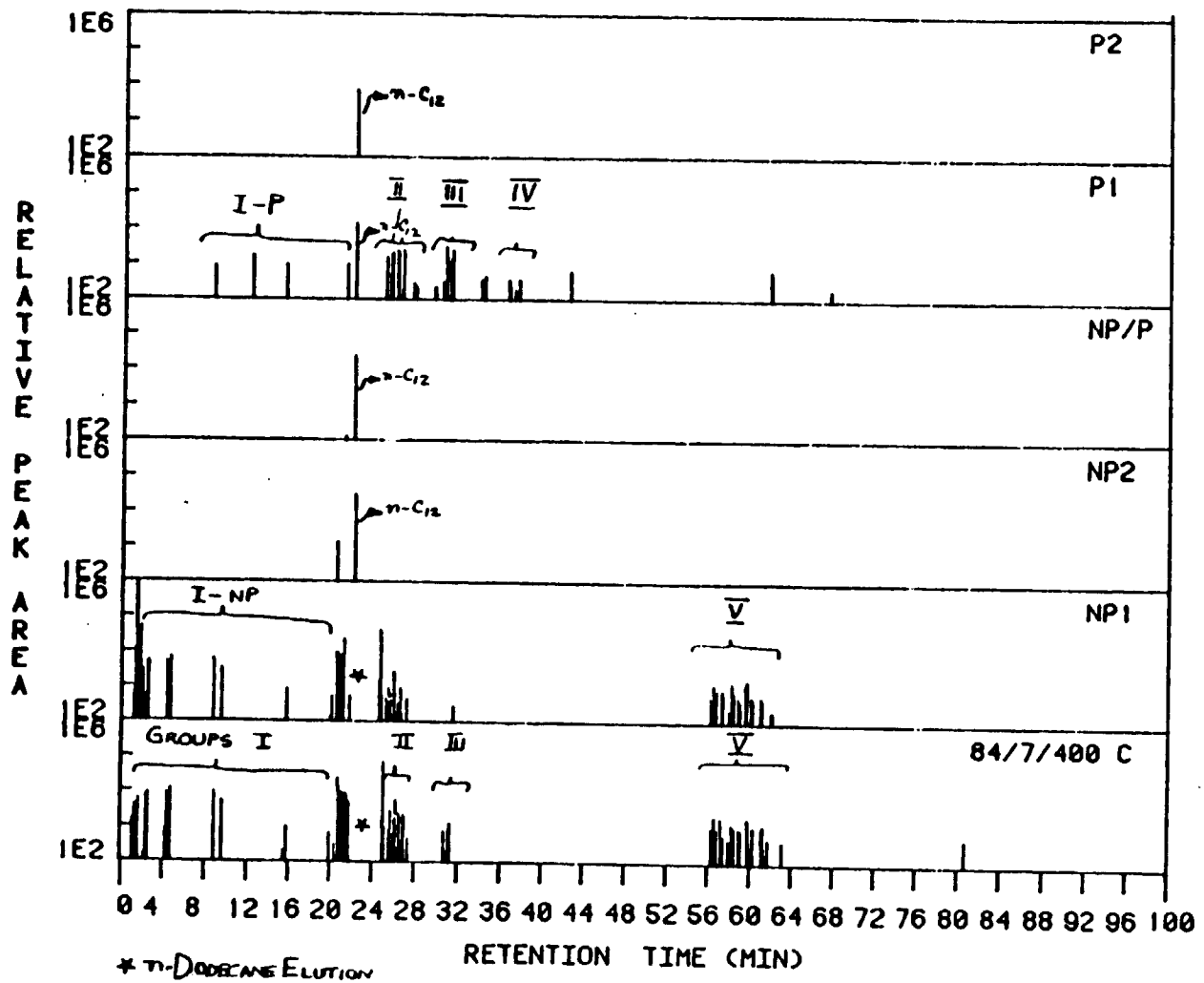

FIG. 3.3 GC Profiles of Sep-pak Fractions

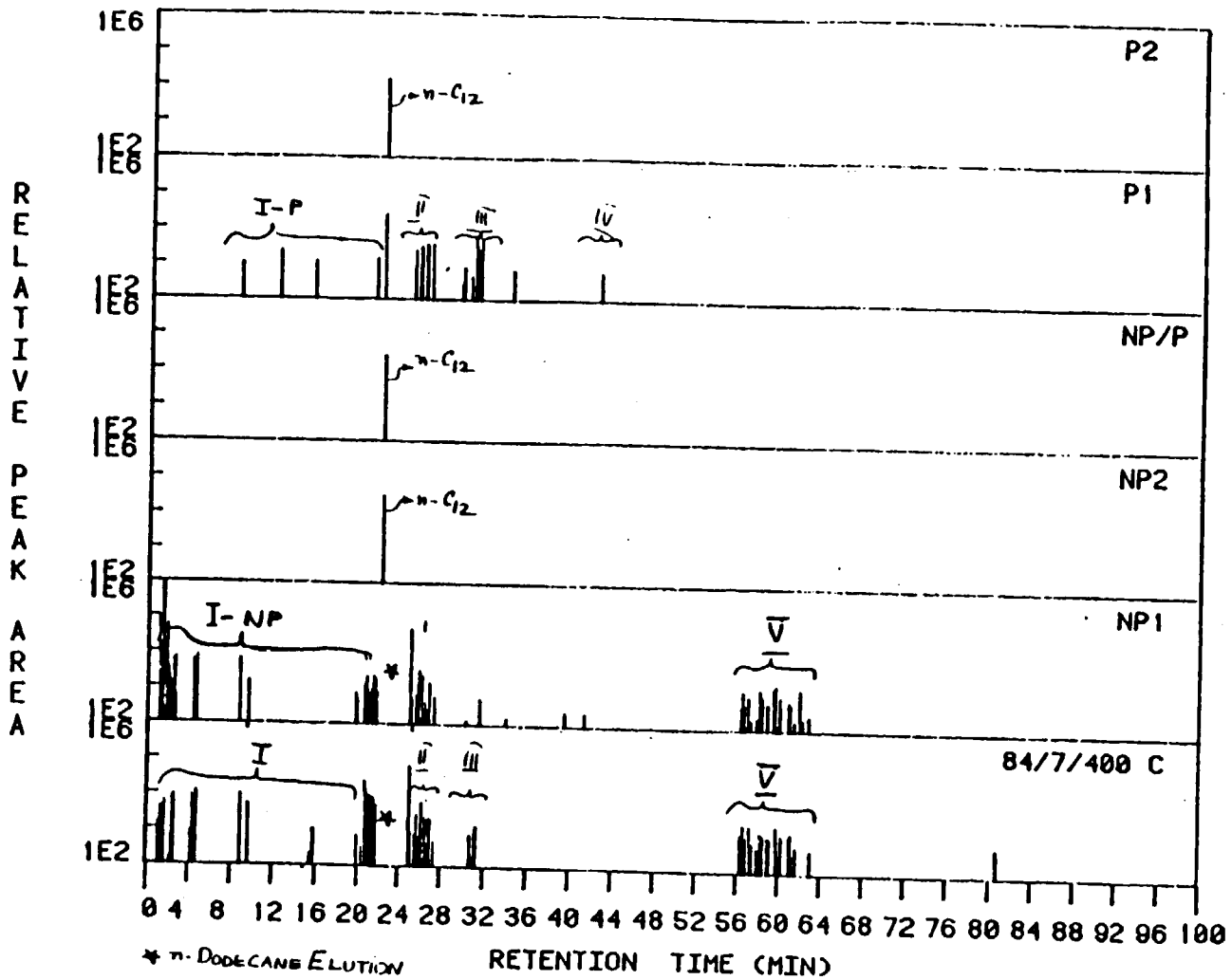

FIG. 3.4 Duplicate GC Profiles of Sep-pak Fractions

the split injection at 280C. This results in higher sensitivity and larger peaks appearing on the OCI generated chromatograms. Hence, all polar fraction analysis was done with the OCI technique only. Thus, the two techniques are complimentary and both were employed for monitoring the Group I-V products.

3.2.5 Character Impact Peak Representation

One chromatographically well-resolved character impact peak, CIP, was chosen from each of the Group I-P and Groups II-IV to represent that product Group based on the CIP's low data scatter (smaller error bars). It was found that the ratio of the CIP area to the total Group peak area remains constant over the 200-400C temperature range:

CIP I-P/Total I-P	=	0.3127± 0.044	(± 14.0%)
CIP II/Total II	=	0.1660± 0.015	(± 8.12%)
CIP III/Total III	=	0.1237± 0.017	(± 13.9%)
CIP IV/Total IV	=	0.2525± 0.021	(± 8.11%)

This implies that the baseline Group I-P and Groups II-IV data can be adequately represented by using only one peak, thereby simplifying data analysis and interpretation.

3.2.6 Limitations of the Sep-pak Fractionation Protocol

While the Sep-pak fractionation scheme is successful in separating the oxygenated compounds of interest, it did not concentrate the dopant compounds in the P1 fraction (the fraction of interest) due to their limited solubility in the cyclohexane and 2-propanol solvents (for example, 3,4-dimercaptotoluene is partially soluble in both

solvents). However, as the solubility characteristics and polarity differences between cyclohexane and 2-propanol works adequately in separating the major non-polar and polar type compounds in the baseline n-dodecane and n-dodecane plus dopant samples, the scheme was used for monitoring Group I-P, II, III and IV products. Sample isolation techniques employing other Sep-pak methodologies were not attempted since each dopant species would require a unique Sep-pak protocol due to different solubility characteristics.

3.3 SAMPLE HANDLING

Preliminary JFTOT stressing of n-dodecane resulted in very low to trace concentrations of soluble degradation products. It was noted that the concentrations of the soluble degradation products were comparable to those of the impurities present in the as-received n-dodecane. This led to the examination of the system protocol under use. The sample handling phases of the system protocol which contributed the most to variations and errors were identified as sample vial contamination and n-dodecane purity.

A GC peak profile plot of JFTOT stressed, as-received n-dodecane is shown in Fig. 3.5. The figure shows formation of new species in the 300 and 400C plots in the 0-20, 28-42, and 46-70 minute retention time ranges. This plot also shows the presence of impurities spread over a wide range of retention times in the unstressed fuel (control sample), indicating the need to purify the n-dodecane before use.

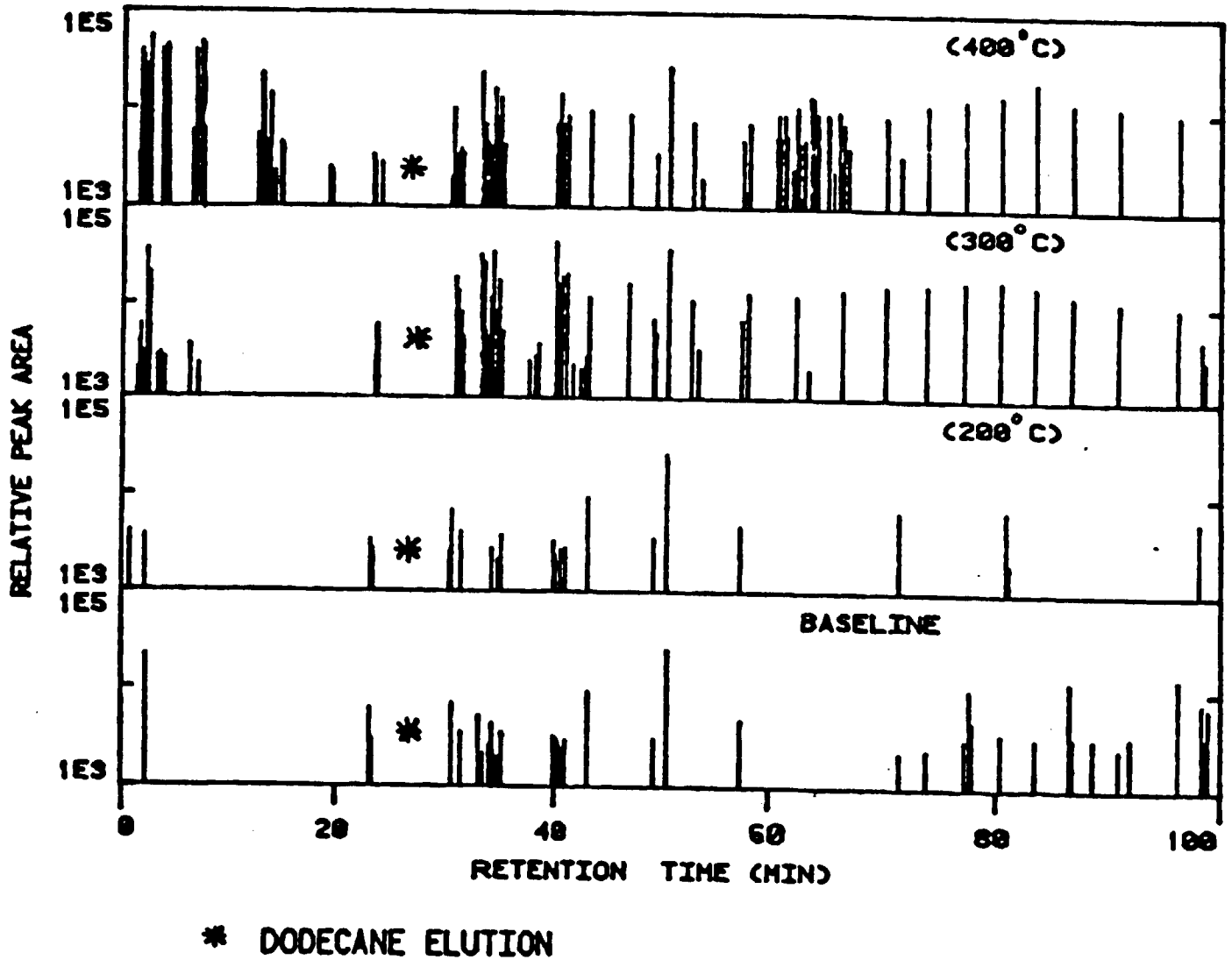

FIG. 3.5 GC Peak Profiles of JFTOT Stressed, As-Received n-Dodecane

This led to the development of a vacuum distillation apparatus, as described in the next section.

It was found that the set of lines spaced at equal intervals in the 60-100 minute retention time range observed in the 300 and 400C samples, Fig. 3.5, originate from vials used for sample collection and storage. Thereafter, the vials were cleaned by washing with soap and water, distilled water, 50/50 (volume percent) water/hydrochloric acid mixture, distilled water, methanol, and cyclohexane, followed by oven baking. The above procedures result in acceptable sample collection and handling techniques.

3.3.1 Vacuum Distillation System and Operation

Fuel purification requirements necessitated development of a vacuum distillation system. The system consists of a heating pot, distillation column packed with glass helices, distillation head, product receiver, vacuum system and heating element as shown in Fig. 3.6. The heating pot is a large glass globe located at the bottom of the column and contains the material to be distilled. The bowl shaped heating element is placed under the heating pot and the rate of heating is controlled manually through a rheostat. The column is a long glass tube packed with glass helices to provide increased surface to volume contact area. The distillation head is an intricate piece of glassware located at the top of the column which condenses the vapors and has the ability to send the condensate either back to the column or to a product receiver (erlenmeyer flask) via a thin tube.

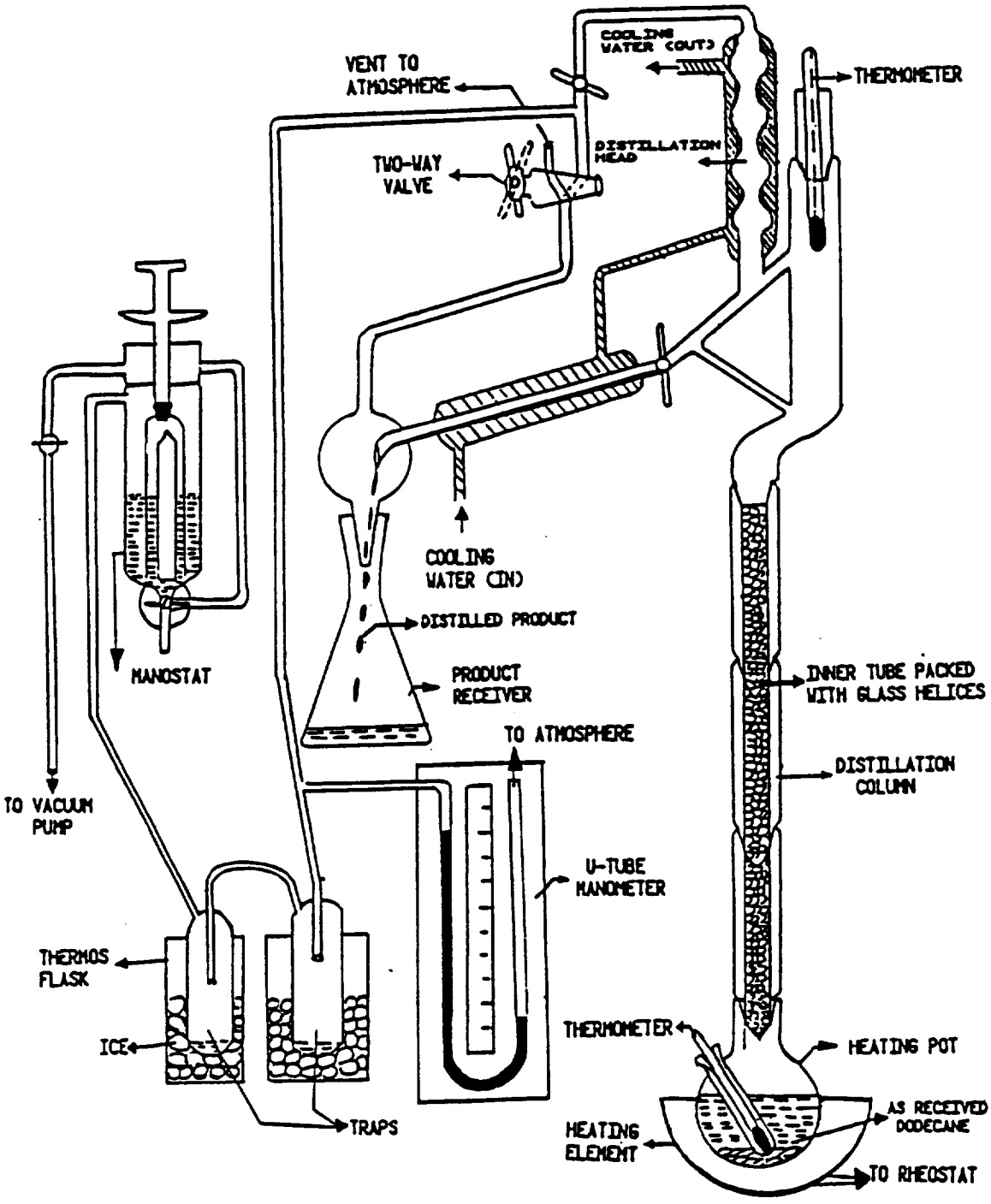

FIG. 3.6 Vacuum Distillation Apparatus

A two way valve permits isolation, evacuation and repressurization of the receiving section without affecting the column. Vacuum is also connected to the system via a port on the distillation head. Two ice cooled vapor traps in series prevent any heavy hydrocarbons from entering the pump. A cartesian manostat is also connected in this line to accurately control the pressure. The assembled apparatus is sealed using ground glass joints (tapered joints, size 24/40) to prevent air entering into the system. A standard procedure for n-dodecane distillation has been developed and may be found in Appendix B.

Distillation using the apparatus is successful in removing most of the impurities in n-dodecane. GC chromatograms of n-dodecane samples before and after distillation, Fig. 3.7, showed the removal of nearly all species in the 0-22 and 30-100 minute retention time range. The purity, as revealed by capillary GC, was 99.8% on a peak area percent basis. However, for sensitive detection of the JFTOT stressed soluble degradation products, large amounts of n-dodecane (0.8-1.4 ul at 45:1 injector split ratio) must be injected into the capillary column. This large injection of n-dodecane solvent overloads the capillary column and results in undetermined peaks appearing before and after the n-dodecane elution (20-27 minute retention time range). Nonetheless, the use of distilled n-dodecane and clean sample vials virtually eliminated all the spurious peaks in the 2-18 and 30-100 minute ranges, and enabled better

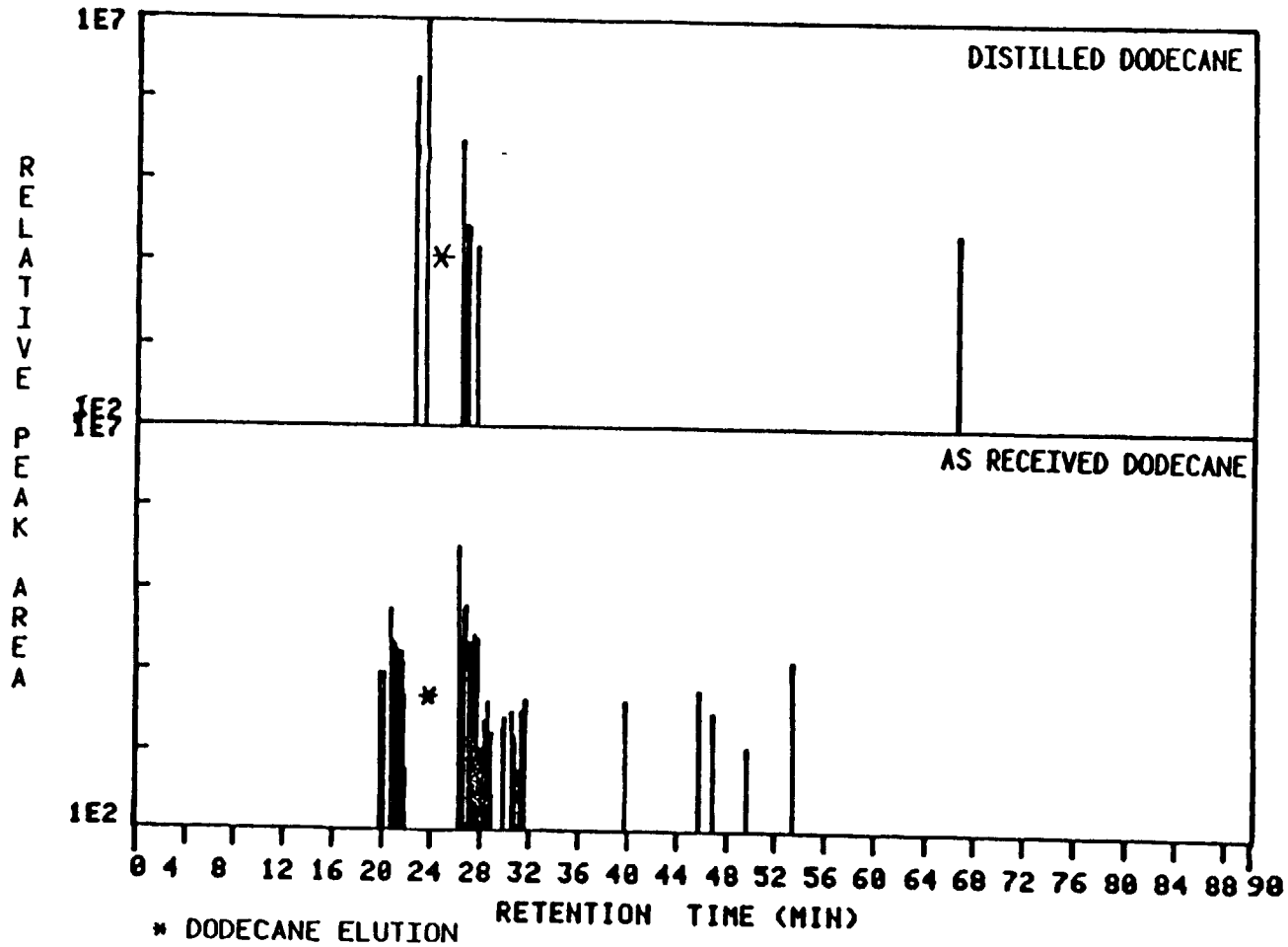

FIG. 3.7 GC Peak Profiles of As-Received and Distilled n-Dodecane

observation of the fuel derived degradation products as shown in Fig. 3.2. Thus, all subsequent n-dodecane and n-dodecane plus dopant experiments were performed with distilled n-dodecane.

Attempts to purify tetralin, a typical aromatic compound found in jet fuels and contemplated for two pure component mixture (n-dodecane/tetralin, 90/10 volume percent) experiments in this program, were not successful. After distillation, tetralin oxidizes very rapidly, forming a dark residue at the bottom of the product flask and showing impurities over a wide GC retention time range. Consequently, unless the distilled tetralin can be isolated from atmospheric air or otherwise stabilized, it cannot be used for JFTOT experiments.

3.4 IDENTIFICATION OF n-DODECANE DERIVED REACTION PRODUCTS

The GCMS instruments employed for identification purposes were Finnigan (Model # 4023) and Hewlett-Packard (Model # 5970) systems. The major products in each of the fractions and Product Groups were identified initially by matching the GCMS derived mass spectra with NBS spectra, and subsequently by positive peak identification using retention time matching with commercial standards.

Group I consists mainly of non-polar C5-C10 n-alkanes and 1-alkenes (I-NP), and polar C7-C10 aldehydes (I-P). Group II species were tentatively identified as tetrahydrofurans (THF's) with different alkyl substituent

groups such as methyl, propyl, and pentyl groups attached at the 2- and 5- positions. Standards necessary for positive identification of Group II species were not available, but the similarity of mass spectras obtained with that of 2,5-dimethyltetrahydrofuran lends support to the GCMS identification. Group III products were positively identified as 6-, 5-, 4-, 3-, 2- dodecanone and 5-, 4-, 3-, 2- dodecanols. Group V products are tentatively identified as tetracosane ($C_{24}H_{50}$) isomers with no oxygen present.

The Group IV products are thought to be the dodecylhydroperoxides, ROOH's, or their most probable decomposition and/or GC capillary column derivatization products. However, Group IV GCMS identity matches with the NBS data do not yield ROOH's, since no ROOH's higher than C7 are reported in the NBS mass spectral data base. Nevertheless, with concentrations two to three times greater than Group I-P, II and III products, the Group IV components appear to be primary oxidation products. Many literature sources cite ROOH's as the primary oxidation product formed during low temperature hydrocarbon autoxidation, with small concentrations of secondary oxidation products via ROOH decomposition, i.e., alcohols, ketones, esters, acids and hydroxyketones also possible, depending on the oxygen availability and initial fuel composition (CRC, 1979). Also, tentative GCMS identification of two Group IV products as trimethylnonanol (C12 alcohol) and 3-hydroxydodecanoic acid (C12 acid) are another indication that Group IV species

are ROOH's. Acid and alcohol species are known thermal decomposition products of ROOH.

Since positive identification of n-C12 ROOH's is not possible using the NBS mass spectra data base, the n-alkane hydroperoxides were synthesized using a modified tetralinhydroperoxide preparation technique (Knight and Swern, 1954). This synthesis involved placing 5-10 ml of distilled n-dodecane in a Kuderna-Danish (KD) flask and then putting the flask in a constant temperature bath at 90C. A stream of oxygen is passed through the n-dodecane for 2 hours ensuring that there is minimum contact with ambient air. The reaction temperature and time of 90C and 2 hours, respectively, were selected based on the detection of oxidation products from the synthesis. The procedure involves separating the polar, oxygenated species from the unreacted n-dodecane using the Sep-pak fractionation scheme and subsequently detecting them employing the GC/OCI analysis. The object was to synthesize and form only the primary oxidation products, i.e., ROOH's, by selecting the lowest possible reaction temperatures and times and thereby minimize the formation of secondary oxidation products such as alcohols and ketones, etc.

The effect of reaction time on n-dodecane + O_2 product synthesis using GC/OCI analysis of the P1 fractions is depicted in Fig. 3.8. This peak profile plot shows chromatograms of the baseline n-dodecane, two synthesized samples at reaction times of 2 hours and 3 hours

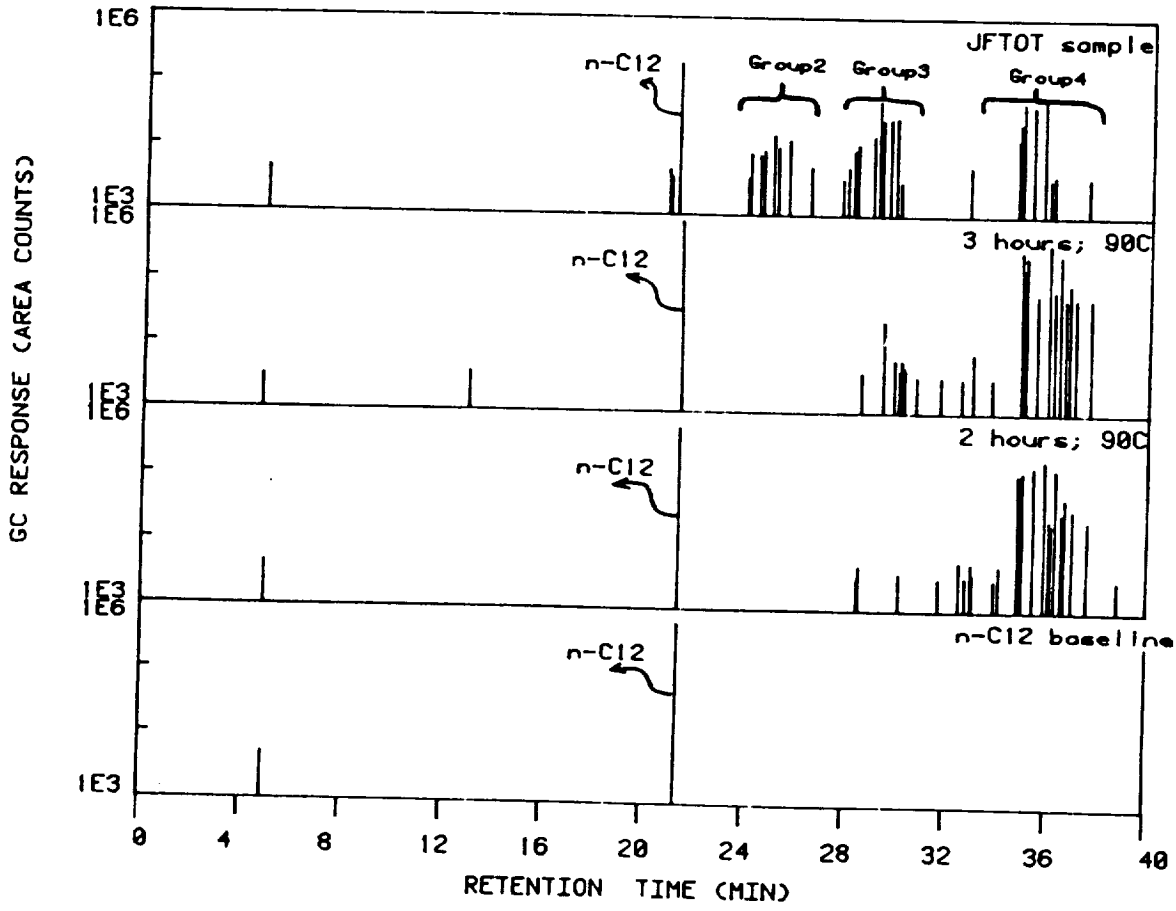

FIG. 3.8 Effect of Reaction Time on n-Dodecane + O_2 Synthesis Using GC/OCI Analysis of P1 Fractions

respectively, and a typical JFTOT stressed n-dodecane sample P1 fraction as a calibration standard. It can be observed that the retention times of the major products formed during the 2 hour (and 90C) synthesis match with the JFTOT derived Group IV products, indicating that Group IV products may be ROOH's. As the reaction time of the n-dodecane + O_2 synthesis is increased to 3 hours, the major products are again within the Group IV retention time band, but secondary oxidation products such as Group III alcohols and ketones also form in small quantities. Hence it appears that ROOH synthesis is best achieved at reaction temperatures and times of 90C and 2 hours.

Since ROOH's are thermally unstable and subject to decomposition, storage effects of the synthesized samples were also studied. Figure 3.9 plots peak profiles of the n-C12 + O_2, 2 hour synthesis sample P1 fraction analyzed after 0, 4 and 14 days of storage, respectively. The sample chromatograms after 4 and 14 days of storage show that a small quantity of Group IV products break down to form Group III alcohols and ketones, thereby skewing the original Group IV product distributions. Hence it is inferred that the synthesis and JFTOT stressed P1 fraction samples should be analyzed as soon as possible (between 0-4 days). Also, it is noted from Figs. 3.8 and 3.9 that Group II tetrahydrofurans were not detected during either the n-C12 + O_2 syntheses experiments or during the stressed sample storage stability experiments. This implies that the Group II products

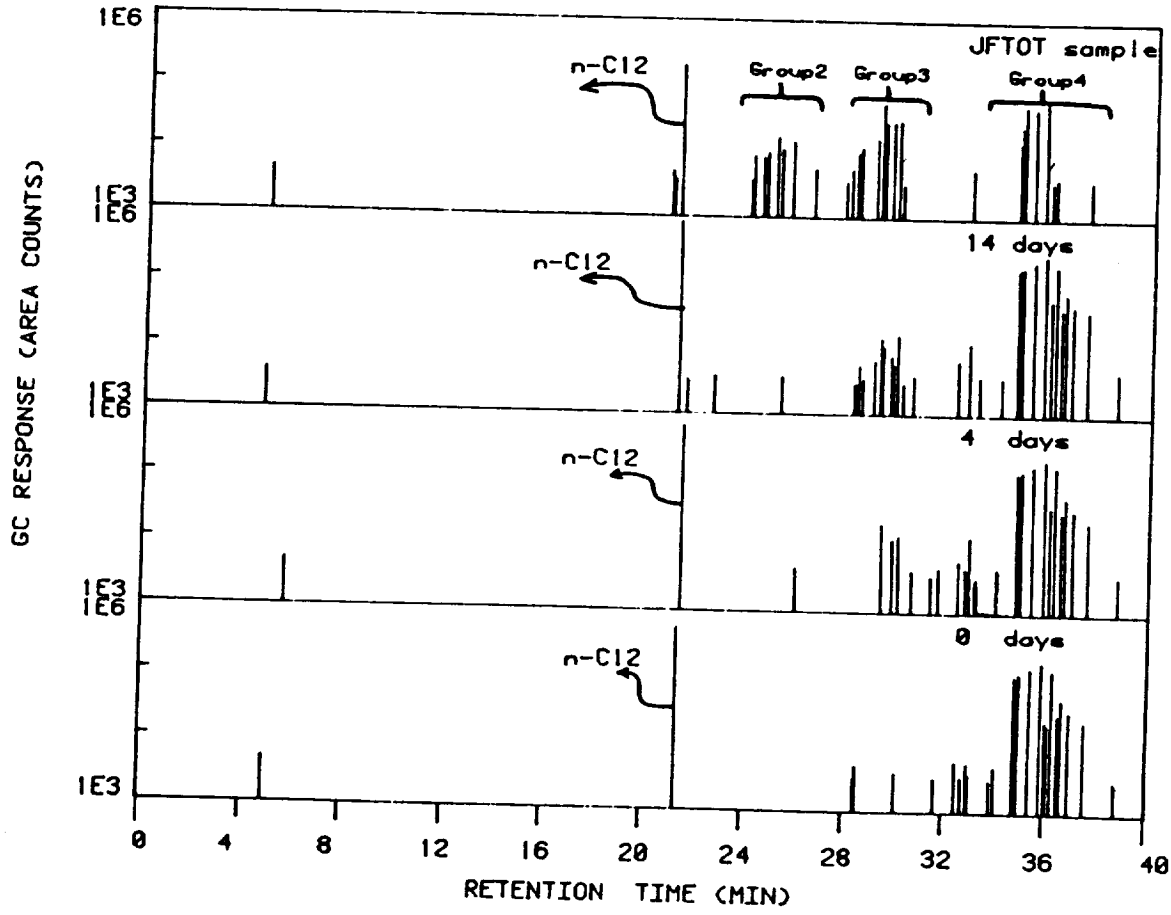

FIG. 3.9 Effect of Storage Time on n-Dodecane + O_2 Synthesis Samples Using GC/OCI Analysis of P1 Fractions

observed in the JFTOT samples probably form due to the JFTOT stressing conditions alone and are not artifacts arising from the Sep-pak fractionation and GC/OCI analysis protocols.

Since the JFTOT derived Group IV products are presumed to be ROOH's, based on identical GC retention times, the next step involved comparison of the GC/MS mass spectra for the synthesis and JFTOT stressed Group IV species. The tentative GC/MS identification of 3-hydroxydodecanoic acid for one of the synthesized Group IV species is identical with the corresponding JFTOT derived species, indicating a very good match. The library search results for the other four Group IV species were not the same, but a number of identical matches appeared on the list of top ten NBS library matches. For example, the other four Group IV species from the synthesized samples had 6, 1, 5 and 8 identities in common with the top ten NBS library matches identified for the corresponding JFTOT stressed species. A ten out of ten (10/10) is a good NBS library match even though the rankings are not identical, while 1/10 can be considered a poor match.

3.5 SYSTEM REPRODUCIBILITY

Optimization of the GC analytical parameters provided the added benefit of verifying the overall system reproducibility which includes modified JFTOT operation, sampling, sample storage, and GC analysis. The sampling reproducibility within a single JFTOT run (at a constant

temperature) is discussed in Section 3.5.1, while the reproducibility of multiple JFTOT runs, performed over the entire range of test temperatures (200 - 400C), is discussed in Section 3.5.2. Additionally, the long term JFTOT system reproducibility is discussed in Section 3.5.3.

3.5.1 Reproducibility Within a JFTOT Experiment

The reproducibility of the system at a given JFTOT temperature including sampling and GC analysis technique were checked by collecting 300C samples from one JFTOT run at six different times and comparing the peak profiles, Fig. 3.10. It is observed from the plot that similar products appear in all the chromatograms, and that the reproducibility for some of the products appearing below 1000 (1E3) relative peak area counts is poor, since the concentrations are near the limits of FID detection. The average percent relative standard deviation values (%RSD = standard deviation/mean value x 100) for GC retention time and product response (area counts) were 0.15% and 26%, respectively. When the above samples were Sep-pak fractionated and the resulting P1 fractions analyzed, the corresponding %RSD values were 0.7% and 16%, respectively, indicating that sample fractionation improves peak area reproducibility, but retention time reproducibility worsens somewhat. Also, at higher temperatures, the product peak area reproducibility improves; for example, a similar reproducibility analysis for a 400C sample yielded %RSD values of 6% (compared to 26 and 16%) due to higher product

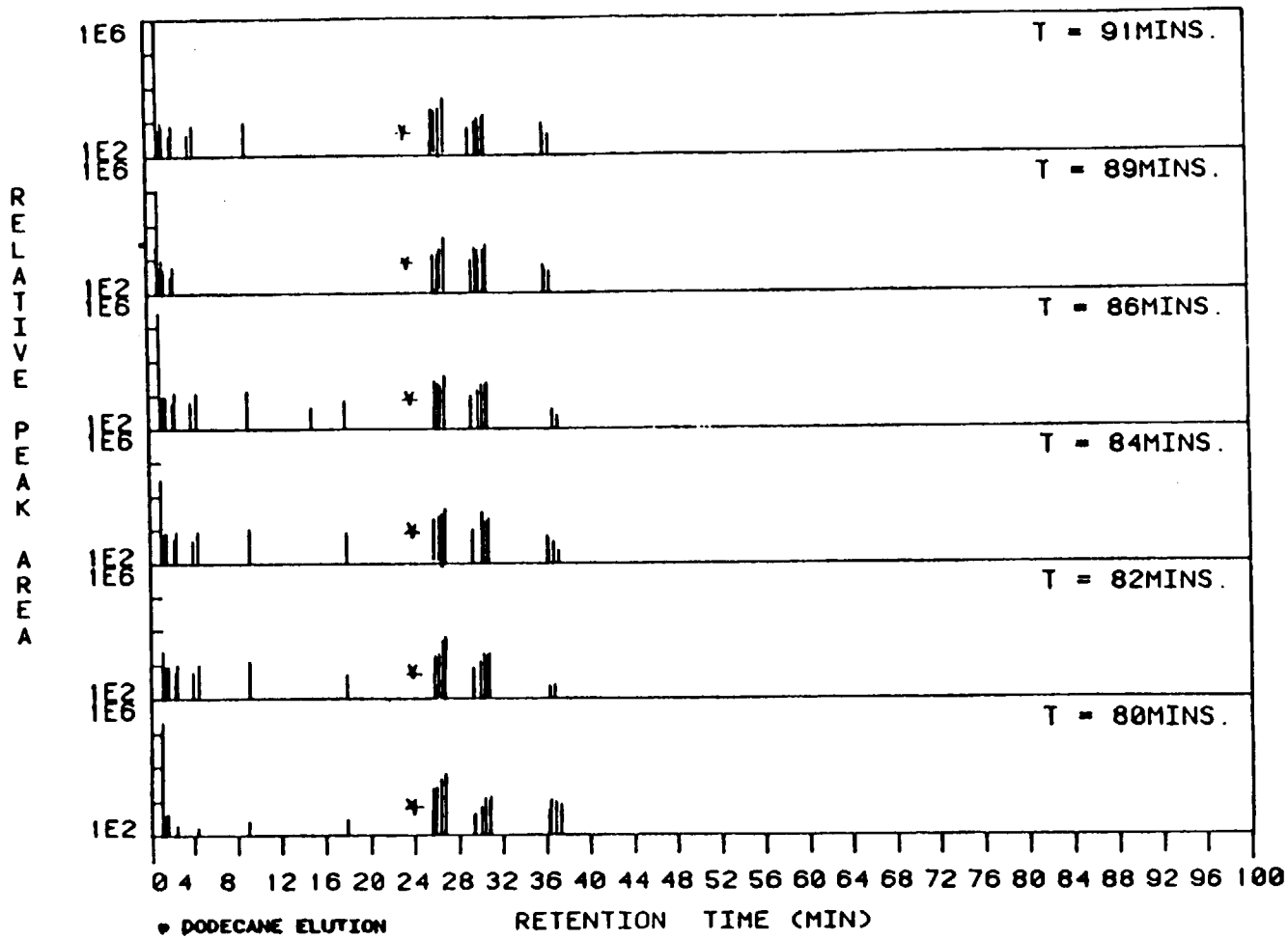

FIG. 3.10 GC Profiles of JFTOT Stressed n-Dodecane Samples Collected at Various Times During a Single JFTOT Run at 300C

concentrations, thereby enabling better detection of the products and lower data scatter.

3.5.2 Reproducibility of Multiple JFTOT Experiments

The JFTOT run-to-run reproducibility of n-dodecane baseline product data was determined by running six successive baseline experiments, performing GC analyses, and subsequently calculating the peak area means and standard deviations of the Group I-V data. The phases of the experimentation which could contribute the most to variations and errors were identified as follows: the batch to batch variability of commercially available n-dodecane, the filtration procedure, the distillation procedure, the modified JFTOT operation, the order of experimentation, sample handling, the Sep-pak fractionation procedure, and GC analytical techniques. In order to obtain reproducible baselines, certain experiments were designed to identify the sources of error and minimize them. The experimental program was as follows:

A. Distill n-dodecane in three 1000 cc lots, and run two JFTOT baseline experiments from each lot to verify lot to lot reproducibility.

B. Select and optimize a GC technique (split and/or OCI) for analyzing stressed n-dodecane samples.

C. Utilize the optimized GC parameters to obtain baseline data as product concentration profiles (versus JFTOT stress temperature) and lot number.

D. Mimic the last part of a typical dopant sequence and

verify if dopant cross-contamination affects the baseline. (Each set of dopant experiments was performed in the following sequence: n-dodecane baseline, n-dodecane + 10 ppm dopant, n-dodecane + 100 ppm dopant, n-dodecane + 1000 ppm dopant, a 150 cc n-dodecane flush followed by a n-dodecane baseline). The last part of the dopant sequence includes the n-dodecane + 1000 ppm dopant experiment, the 150 cc flush and the post dopant baseline experiment.

E. From the acquired baseline data, perform statistical analysis on product concentrations to get mean, standard deviation, %RSD, and 95% confidence intervals, and, based on probability theory and cumulative distribution function analysis, establish a criteria for accepting/rejecting a baseline n-dodecane experiment.

The results of the above experiments can be summarized as follows: initially, lot to lot reproducibility was assumed to be valid a priori, since optimization required statistical calculations (mean, standard deviation and %RSD values) from the baseline data. To verify lot to lot reproducibility, the n-dodecane stressed samples were analyzed by GC split injection techniques. The above results are summarized in Table 3.3 which shows that the %RSD values are high when product concentrations are low, near the detectability limits of the flame ionization detector (FID). For example, at 250C, the %RSD values for Group I-IV data are high due to low product concentrations. Similarly, at 350C, the %RSD values for Groups I-V are low, but a high

TABLE 3.3

Reproducibility of the GC Split Injection Analysis Technique for n-Dodecane Samples Collected at 250, 300, 350 and 400C

JFTOT Temperature	%RSD Values for Stressed Sample Product Groups I	II	III	IV	V
250C	56.0	27.4	43.6	23.5	---
300C	8.5	11.3	10.8	15.5	---
350C	11.8	9.0	12.0	24.2	45.4
400C	14.4	26.0	13.3	>100.0	14.3

Note: %RSD implies percent relative standard deviation

(%RSD = standard deviation/mean value x 100)

%RSD value is noted for Group V, which is attributed to its trace level concentrations. The poor reproducibility (high %RSD values) obtained for product Groups I-V, plus the fact that large amounts of samples could not be injected due to capillary column overloading (by n-dodecane), led to the conclusion that the split injection technique was not sensitive enough for entire sample analysis. As noted, the column overloading problem was resolved by employing the sample fractionation step (Shala, 1983), modified to separate the non-polar (mostly n-dodecane) and polar constituents of the entire sample into two distinct fractions. The polar fraction contains virtually all of the oxygenated products originating from the JFTOT stressing of n-dodecane. Subsequently, all GC analysis was performed on the polar fractions only.

Initially, for polar fraction analysis using split injection techniques, one 250C polar fraction was selected to optimize the split ratio and injector temperature parameters. The optimum split injection parameters, based on maximized Group II, III and IV peak area response, turned out to be a 45:1 split ratio and an injector temperature of 280C. Using the optimized parameters, a study was made of six 250C polar fraction samples to verify if the Sep-pak fractionation step (implying analysis of polar fractions) improves peak area reproducibility over the entire sample analysis. The results of the above experiments are summarized in Table 3.4. The data shows that the %RSD values

TABLE 3.4

Reproducibility of GC/OCI and GC/Split Injection Techniques, for n-Dodecane Samples Collected at 250C

%RSD Values for JFTOT Samples Collected at 250C

GC INJECTION TECHNIQUE	GROUPS II	III	IV
SPLIT INJECTION			
Entire Sample Analysis	27.0	43.6	23.5
Polar Fraction Analysis	22.8	21.9	26.0
ON-COLUMN INJECTION			
Polar Fraction Analysis	18.7	16.9	25.6

obtained from polar sample analysis were lower than those employing entire samples, indicating that Sep-pak fractionation involves negligible error and improves reproducibility.

Attention was turned next to OCI analysis to check if further lowering of %RSD values could be achieved, since it is widely reported in chromatography literature that OCI is more sensitive than the split injection techniques. The six 250C polar samples previously used for split injection studies were analyzed using GC/OCI techniques. The results from the OCI experiments are included in Table 3.4. The OCI analysis yielded lower %RSD values than split injection analysis, implying that the OCI technique is better suited for polar sample analysis.

Once the GC/OCI analysis technique was found to be better suited for polar fraction analysis, the reproducibility of the GC/OCI technique itself was evaluated. This was accomplished by analyzing one polar fraction sample six times. Repetitive analysis of the polar sample showed that the %RSD values for the total Group II, III and IV areas were $\pm$ 9.4%, $\pm$ 16.0%, and $\pm$ 6.0%, respectively. Selected, well-resolved character impact peaks from each of the product Groups further reduced the %RSD values to $\pm$ 2.0%, $\pm$ 8.0%, and $\pm$ 6.0% respectively, indicating that the character impact peak (CIP) representation introduces fewer integration errors than using the total Group area representation. The Group III

reproducibility (CIP and total area) is poor relative to Group II and IV data due to the presence of C12 alcohol and ketone isomers which have nearly identical boiling points and, hence, elute as fused peaks on a non-polar DB1 column, causing large integration errors. Thus, a part of the error arising during GC/OCI analysis was identified and minimized using the CIP representation.

An added reason for employing the GC/OCI analysis technique for polar fraction analysis was to aid the detection of thermally unstable compounds in the polar sample constituents. Since the OCI technique is a cold injection technique and employs low injector temperatures relative to split injectors, it is ideally suited for analysis of thermally unstable compounds. In the present work, thermally labile compounds were detected during analysis of an identical polar fraction sample using both split and OCI techniques and by noting changes in the normalized Group II-IV product distributions (The Group II, III and IV peak areas were normalized with respect to the internal standard peak area). The results of the above experiments are summarized in Table 3.5. Group IV products were inferred to be thermally labile compounds since the combined area for all peaks in the group using the OCI analysis was higher than that obtained by the split injection analysis by 0.46 (arbitrary units relative to the internal standard), indicating that they break down during split injection analysis. At the same time, the Group II

TABLE 3.5

Changes in Normalized Group II-IV Peak Areas with Injection Technique

INJECTION TECHNIQUE	-	GROUP II	GROUP III	GROUP IV	GROUP (II+III+IV)
SPLIT	-	1.144	0.764	1.340	3.248
OCI	-	0.703	0.825	1.800	3.328
(SPLIT-OCI)		+0.441	-0.061	-0.460	-0.080

Note: Group areas are normalized with respect to the internal standard peak area.

areas obtained by OCI were lower than those using split injection analysis by 0.441 arbitrary units, implying that the Group IV compounds that break down in the split injector form primarily Group II compounds. Normalized Group III product areas obtained by split injection analysis were 0.061 arbitrary units lower than those using the OCI analysis. The difference is due either to a small fraction of Group III products breaking down in the split injector forming Group II components, or to the difference in the Group (II+III+IV) normalized area = 0.080 units between the split and OCI injection techniques (column 4 in Table 3.5).

Even though the split injection technique was found to be unsuitable for polar fraction analysis due to the presence of thermally unstable compounds, it can still be employed for Group I and V analysis using entire samples. The %RSD values obtained with the above technique are comparable with those obtained by OCI analysis with polar fraction injection. On the other hand, Group I-P, II, III and IV polar fractions from the Sep-pak fractionation should always be analyzed using OCI.

Similar OCI analysis, performed on the polar fractions of the 300C, 350C and 400C samples, showed that the peak area reproducibility is a function of product Group and temperature. All %RSD values for OCI were lower than the corresponding values using split injection. The highest %RSD's occurred at 400C, where the Group IV %RSD values

were 66% and 100% for the OCI and split injection techniques, respectively.

The next step in identifying error was checking to see if small quantities of Group II products and if the order of experimentation affected baseline n-dodecane reproducibility. The former is important because small quantities of polar and reactive Group II products (at the ppm level) formed during room temperature storage of distilled n-dodecane might alter the n-dodecane oxidation reactions. Additionally, the order of experimentation is important since the post-1000 ppm dibenzothiophene baseline data (after 150 cc flush) looked similar to the 100 ppm dopant data and hinted at cross-contamination effects. For checking the above concerns, two baseline experiments, pre- and post-1000 ppm dopant JFTOT runs, were performed to examine for cross-contamination effects (by searching for differences in product concentration profiles with respect to the data obtained from the six baseline experiments) using refiltered n-dodecane containing no Group II impurities. Refiltered product was obtained by passing n-dodecane through a silica column packed with 100/200 mesh size silica gel.

The results from the above experiments were twofold. First, at 250C and 300C, the Group II product concentrations for the experiments with refiltered n-dodecane were lower than the six baseline experiment results, indicating that filtration apparently lowered product formation. However, if the Group II concentrations (in peak areas) are corrected by

subtracting their initial concentrations (at room temperatures), the reproducibility improves, as evidenced by the substantial decrease in the %RSD values. For example, the %RSD values at 250C and 300C using unsubtracted CIP II data is ± 54% and ± 29.6%, respectively. When the CIP concentrations were corrected to exclude initial CIP concentrations the corresponding %RSD values decreased to ± 36.5% and ± 14.2%, respectively, implying that small concentrations of Group II products present at ambient conditions do not affect baseline reproducibility. (The %RSD values for Group II data is very similar to the CIP II data). Secondly, cross-contamination effects are ruled out since the product profiles resulting from the latter two experiments are similar to the data obtained from the six baseline experiments, i.e., the peak areas are within the data scatter of the six baseline experiments.

Once the total Group II, III and IV peak area and the corresponding CIP area means were calculated at JFTOT temperatures of 250, 300, 350 and 400C, a matrix of 24 means (6 x 4 means) was created with corresponding 95% confidence interval values. Since a new baseline experiment generates 24 means, a baseline acceptance/rejection criteria based on the number of data points, which can lie outside the 95% confidence intervals of 24 calculated mean values, was necessary. Using independent probability theory, the 95% probability of all 24 means (considered as 24 independent events) to fall within the calculated 95% confidence

intervals (CI) is 29.2%. The event of one mean value falling within the calculated 95% CI constitutes a hit, whereas the possibility of the same mean value lying outside of the 95% CI is considered as a miss. If the independent and cumulative event probabilities for the sequence of events are calculated, the results are as follows:

COMBINATION OF EVENTS	PROBABILITY	
	Independent	Cumulative
All 24 hits $(0.95)^{24}$ X $(0.05)^{0}$X1	29.2%	29.2%
23 hits + 1 miss $(0.95)^{23}$X$(0.05)^{1}$X 24	36.9%	66.1%
22 hits + 2 misses $(0.95)^{22}$X$(0.05)^{2}$X24X23/2	22.3%	88.4%
21 hits + 3 misses $(0.95)^{21}$X$(0.05)^{3}$X24X23X22/6	8.9%	97.0%

Since the above events are not independent, the 95% (and greater) cumulative probability requiring a minimum of 21 hits (or a maximum of 3 misses) was chosen as the baseline acceptance criteria. When this criteria was applied to the eight experiments performed for the method development studies, the baseline data obtained from Run #1 were rejected since more than three data points were outside the 95% confidence intervals of the 24 mean values. Consequently, the statistics were corrected to include Runs #2 through #8 only, and are shown in Table 3.6. The results of baseline experiments (Runs #2 through 8) are also represented in Figs. 3.11 and 3.12 which plot CIP and total Group peak area response on the y-axis and JFTOT temperatures on the x-axis. Fig. 3.11 shows the CIP I-P, II, III and IV areas and their associated 95% confidence

TABLE 3.6

Reproducibility of the GC/OCI Analysis Technique for n-Dodecane Polar Fraction Samples Collected Between 200-400C

%RSD VALUES FOR STRESSED SAMPLE PRODUCT GROUPS II-IV USING TOTAL GROUP AND CIP REPRESENTATION

TEMPERATURE	CIP			GROUP		
	II	III	IV	II	III	IV
200C	00.00	00.00	00.00	00.00	00.00	00.00
250C	36.50	50.60	30.36	30.90	34.80	31.25
300C	14.2	10.20	4.93	17.18	16.10	5.62
350C	5.6	14.30	12.80	7.78	21.82	12.09
400C	9.4	6.93	32.26	14.82	7.71	34.48

Note: Calculations are based on Runs # 2 through # 8 only.

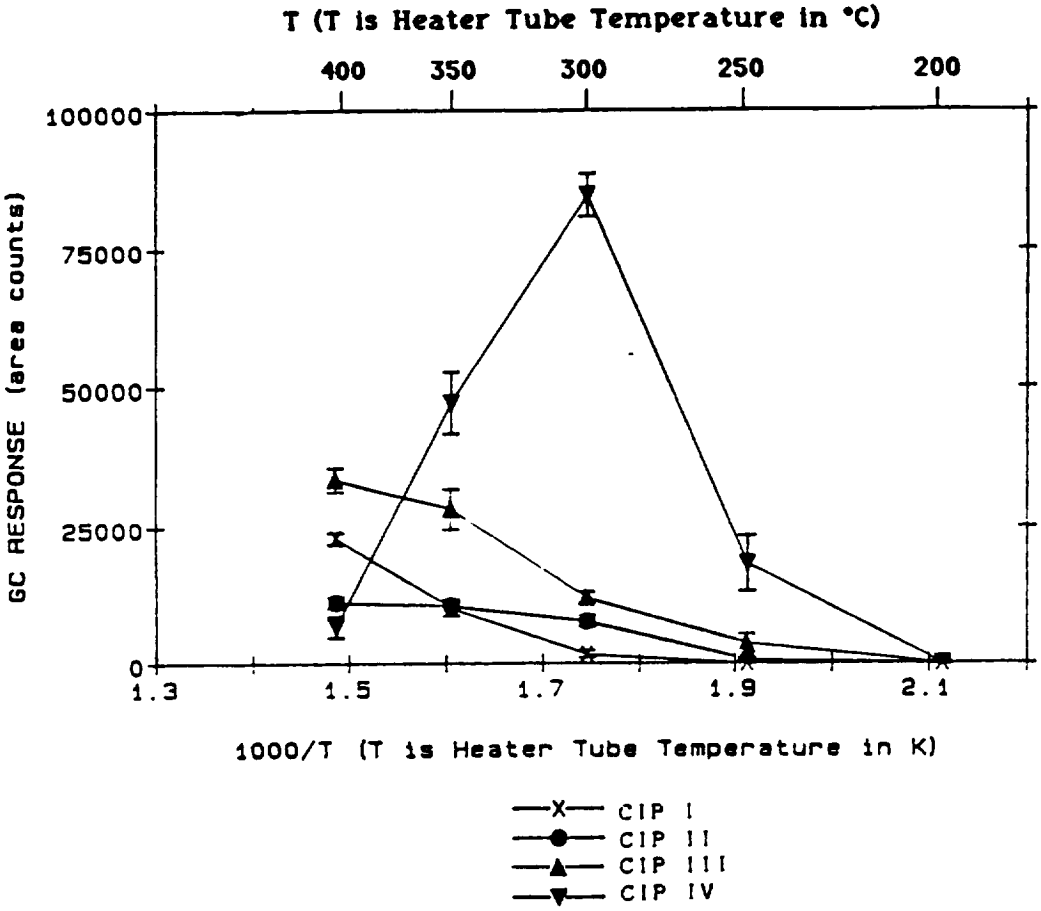

FIG. 3.11 Selected Group I, II, III and IV Impact Species From Testing of Aerated n-Dodecane

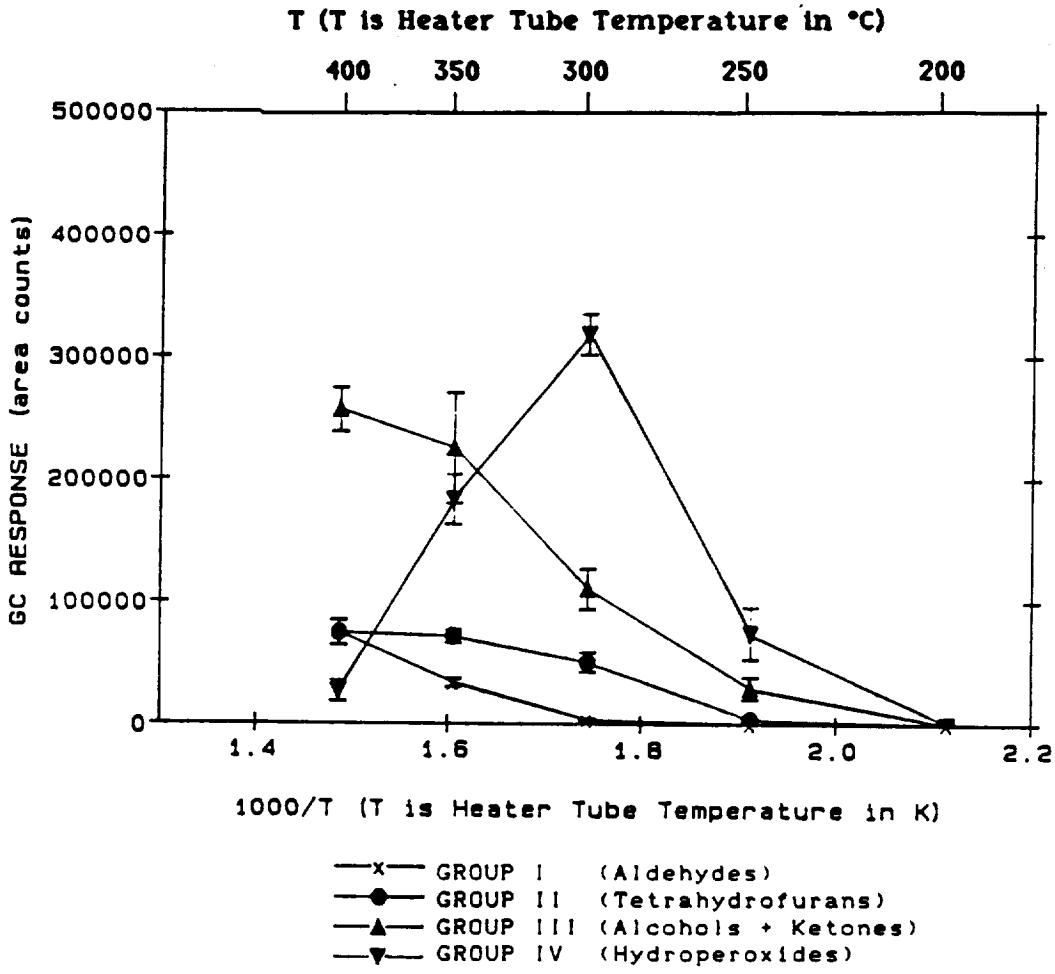

FIG. 3.12 Total Group I, II, III and IV Products From JFTOT Testing of Aerated n-Dodecane

intervals (as a function of JFTOT temperature). Fig. 3.12 shows that the total Group 1-P, II, III and IV area reproducibility between the 200-400C range of test temperatures is good with the exception of Group III peak areas (at 350C), which is poor due to the fused nature of the co-eluting dodecanol and dodecanone isomer peaks. The large total Group III area variability observed at 350C is minimized using the CIP representation, Fig. 3.11.

The baseline criteria, developed above, also was applied to the baseline data generated as part of the dopant experiments. Only the baseline data for the post-1000 ppm dibenzothiophene experiment was rejected, due either to improper JFTOT operation or to use of poor quality n-dodecane.

3.5.3 Long Term JFTOT System Reproducibility

Pure n-dodecane baseline runs performed after one year showed the same Group I-V products profiles and distributions as in the earlier work, Fig. 3.13. Although there were slightly different yields, these data verify the long term reproducibility of the modified JFTOT operation and the analytical protocols. The differences in the yields may be due to slight changes in FID detector sensitivity. Overall, the reproducibility in peak profiles of n-dodecane samples collected at a single temperature (within a JFTOT run), short term JFTOT operation, and long term JFTOT runs gave confidence in the modified JFTOT operation, sampling, and GC analysis procedures. Another good indicator of

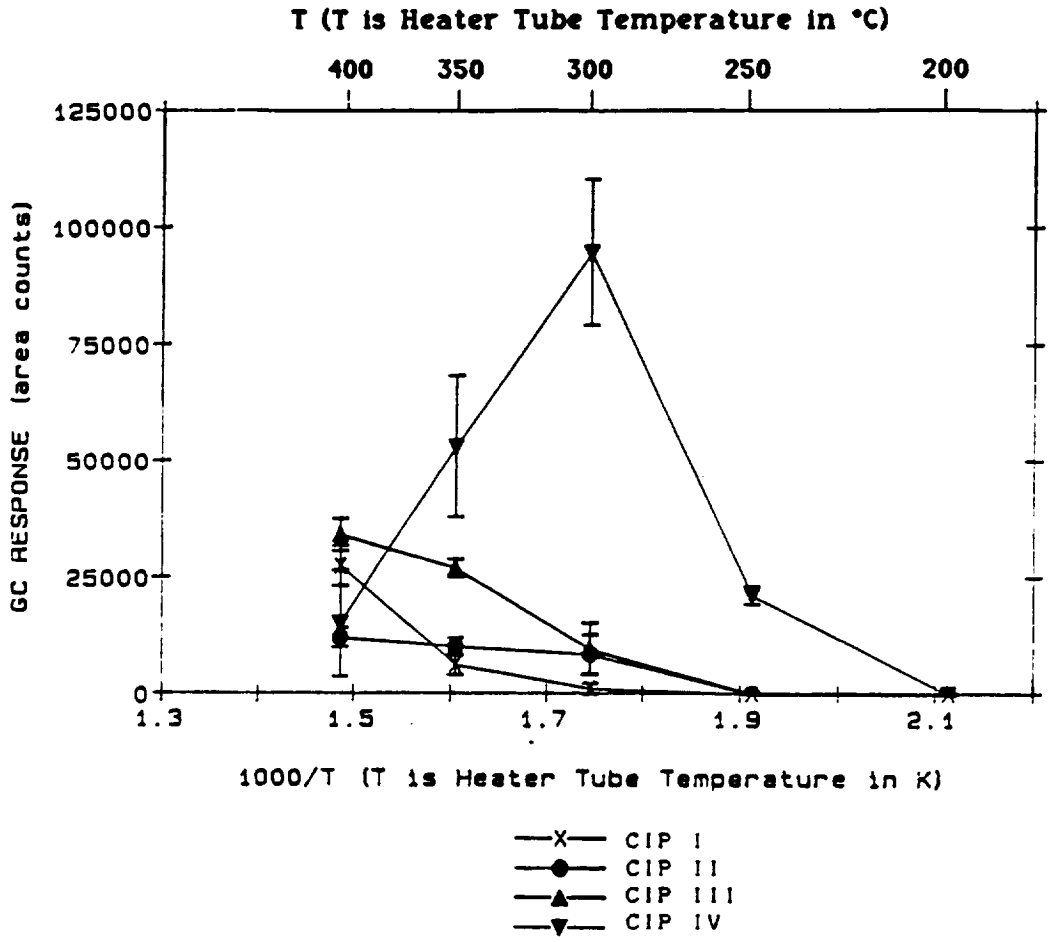

FIG. 3.13 Selected Group I, II, III and IV Impact Species From Testing of Aerated n-Dodecane After One Year

reproducibility is the ratio of Group I n-alkane to 1-alkene product yields. This measure factors out the variability in injection volume size and detector sensitivities. For the current work, typical values for the C7, C8, C9 n-alkane to 1-alkene ratios were 2.03 $\pm$ 0.21 ($\pm$ 10.3%) and 1.23 $\pm$ 0.10 ($\pm$ 8.1%) at 350 and 400C, respectively, while the n-decane to 1-decene yield ratios were 2.03 $\pm$ 0.21 ($\pm$ 10.3%) and 0.5 $\pm$ 0.09 ($\pm$ 18%) at 350 and 400C, respectively. The constancy of the n-alkane to 1-alkene ratios, for all the pure n-dodecane baseline runs, provided an additional indicator of long term system reproducibility.

CHAPTER 4

NEAT n-DODECANE RESULTS AND MECHANISM DISCUSSION

In this chapter experimental results and discussion of n-dodecane oxidation characteristics are presented. Pure dodecane experiments were undertaken primarily to establish a baseline neat n-dodecane data base, which provided the added benefit of comparing our results with previous n-dodecane work performed at the Naval Research Laboratory, NRL (Hazlett et al., 1977). The temperature dependence of the n-dodecane derived reaction products is examined in Section 4.1 and comparisons with past work are presented in Section 4.2. The effects of fuel aeration on the oxidation behavior is examined in Section 4.3 and the modified n-dodecane/oxygen reaction mechanism(s) in the autoxidative ($T \leq 300C$) and intermediate temperature regimes ($300 \leq T \leq 400C$) are presented in Section 4.4.

4.1 TEMPERATURE DEPENDENCE OF THE REACTION PRODUCTS

The polar product Groups I-P, II, III and IV and their reproducibility as a function of JFTOT temperature are presented in Figure 4.1. Group I-P aldehydes form at 300C, and increase in concentration as the JFTOT temperature increases. Group II product concentrations (corrected to exclude reactant contributions) increase up to 350C and stay constant thereafter. The Group III product build-up is faster than Group I-P and II products at all temperatures.

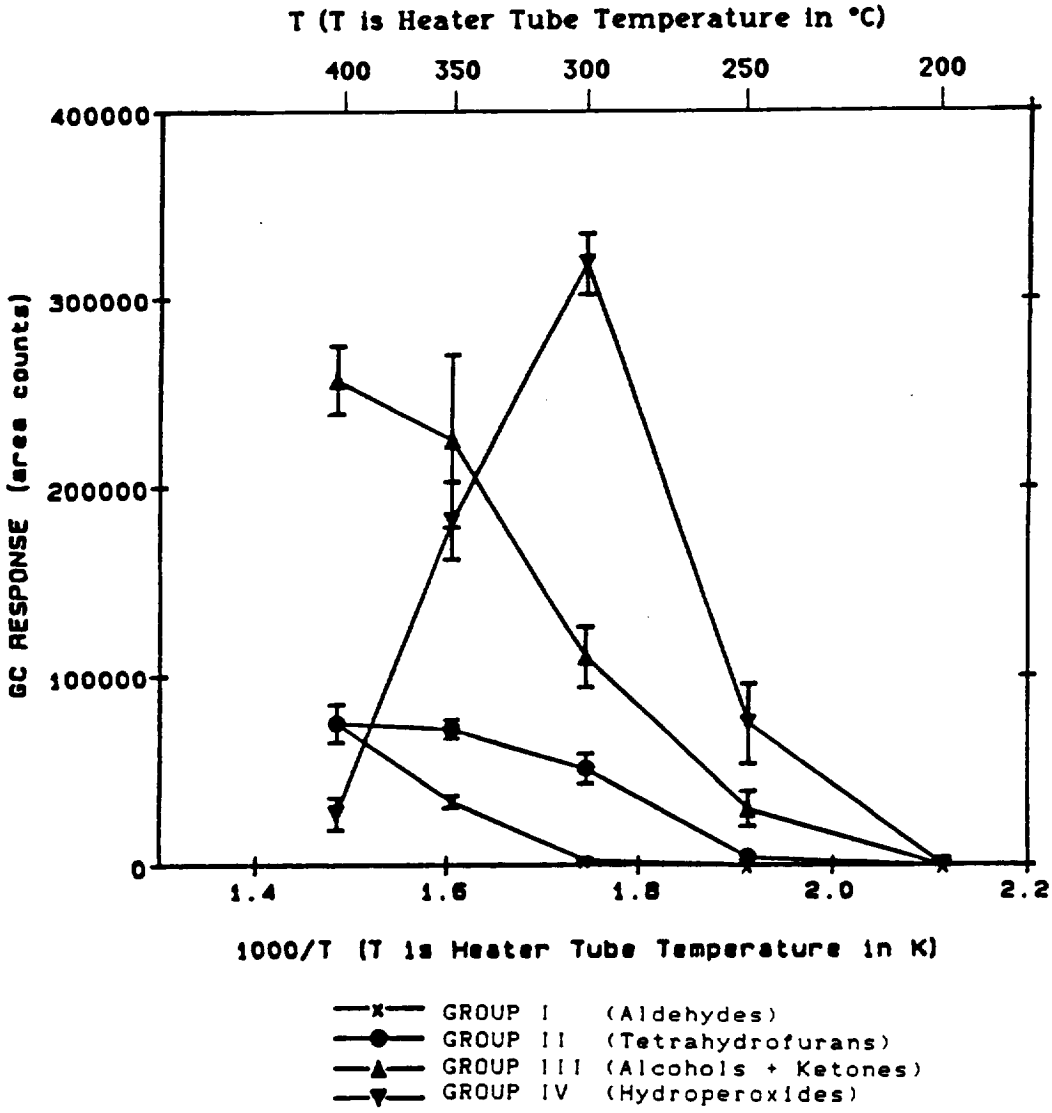

FIG. 4.1 Polar Reaction Products From JFTOT Testing of Aerated n-Dodecane Using GC/OCI Analysis

The variability in Group III data is high compared with Group I-P, II and IV data, due to the presence of C12 alcohol and ketone isomers which have nearly identical boiling points, and hence elute as fused peaks on the non-polar DB1 column. Group IV formation starts at 250C, reaches a maximum at 300C, and decays to very low concentrations at 400C.

The non-polar product Groups I-NP and V and their reproducibility are presented as a function of JFTOT temperature in Figure 4.2. The figure shows that Group I-NP alkanes and 1-alkenes (<C12) start forming at 300C and increase in concentration as the JFTOT temperature increases. Group V fuel dimers (C24) start appearing at 350C and increase in concentration thereafter. It is noted that the Group I-NP products form in much greater concentrations than the Group V products. In summary, Figs. 4.1 and 4.2 show the temperature dependence of the Group I-V reaction products resulting from JFTOT stressing of air saturated distilled n-dodecane.

4.2 SYSTEM VERIFICATION

The present studies provided an opportunity to identify and confirm the different regimes of the degradation mechanism proposed by Hazlett *et al*. (1977). Hazlett's group at NRL worked with aerated n-dodecane stressed on a similar JFTOT, but with modifications and conditions different from those used for the current work. For example,

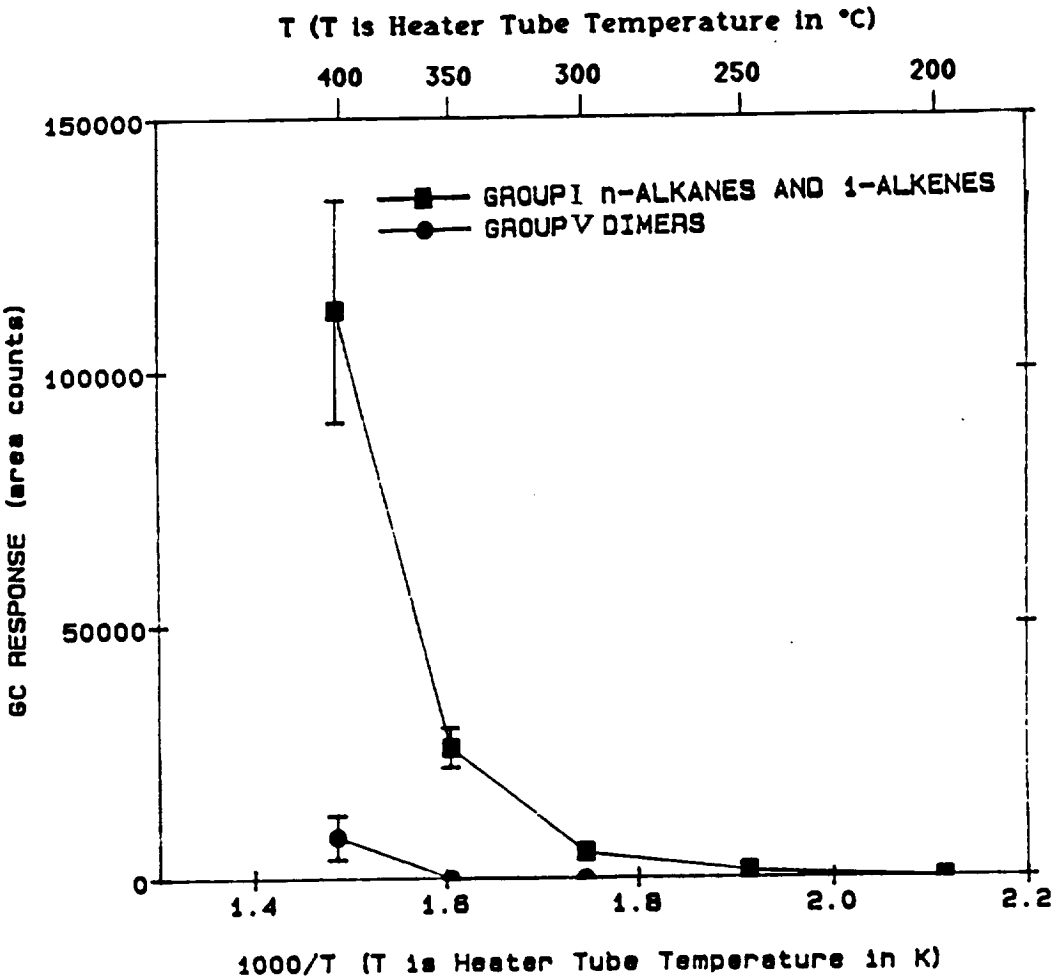

FIG. 4.2 Non-Polar Reaction Products From JFTOT Testing Aerated n-Dodecane Using GC/Split Injection Analysis

their study employed longer JFTOT heater tubes (5 inches versus 2 3/8 inches) and lower fuel flow rates (3.0 ml/min versus 3.75-4 ml/min), consequently increasing the fuel/heater contact times to 28 seconds relative to the 9 seconds experienced in the present work. Also, no tube deposit rating (the deposits are rated on a scale of 0-4 based on a light reflectance principle) correlations were done in the present work, since our procedure was to use one tube for several temperature conditions.

The two sets of data are displayed in Figure 4.3. The data could not be compared for temperatures greater than 400C (1000/T < 1.45) due to JFTOT operating limitations with the present setup. Further, since no absolute concentration measurements were attempted in the present study, the NRL data was scaled to match the present data by setting their ROOH curve maximum to be equal to the Group IV curve maximum. Subsequently, all of their data was normalized using this $ROOH_{max}$ as the normalizing factor. Comparing the two data sets shows that the temperature histories of Group III and IV data (present study) closely resemble the corresponding [ROH + Ketones] and [ROOH] curves (NRL data), although the Group IV maximum is shifted to a higher temperature. The NRL work has shown that metals have an effect on ROOH formation; aluminum tubes form ROOH the slowest while 304 stainless steel tubes (employed in their work) form ROOH the fastest; thus the shift may be due to the use of aluminum heater tubes in this study. The

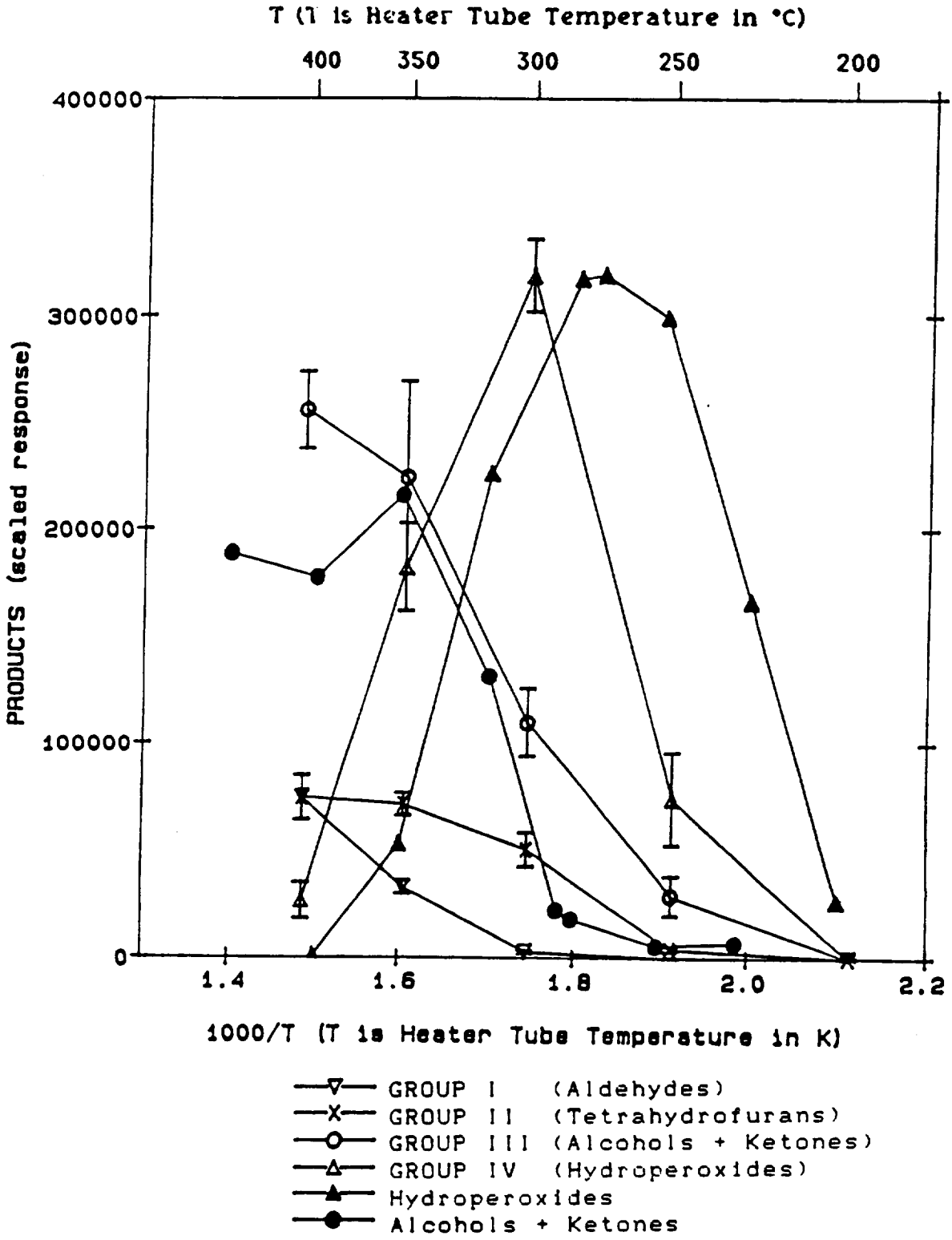

FIG. 4.3 Comparison of Aerated n-Dodecane Reaction Product Profiles
(Present - Open Symbols; NRL - Closed Symbols)
Note: See text for explanation of scaling

agreement in the Group III and IV product curves with the ROH + Ketones and ROOH curves verifies that the results obtained from the current work are consistent with the NRL results. It was deduced earlier that Group IV species were ROOH's or their decomposition products. The agreement in the Group IV and ROOH data provides additional evidence to support this deduction.

The presence of the Group II products is not explained by the existing n-dodecane degradation mechanism (Hazlett et al., 1977), which does not include tetrahydrofurans. Since they were detected and measured in the current work, tetrahydrofuran products should be included in the n-dodecane/oxygen degradation mechanism. Also, Group I-P aldehydes were measured in this work, but were not detected by Hazlett et al. However, they did postulate aldehyde formation via ROOH decomposition reactions based on the presence of carbon monoxide in their system, which is thought to originate from aldehydes. Obviously, the better analytical sensitivity of the current study is enabling some of the lower concentration intermediates to be detected and quantified. In particular, the aldehydes and tetrahydrofuran products were probably not observed previously due to the lower detection sensitivity of the GC/packed column/detector analytical configuration employed in their work compared to the current work. It is also possible that the longer residence times and higher bulk fuel temperatures involved in the JFTOT operation played a role in this difference.

As noted in Section 3.5.3, another good indicator of the system performance is the ratio of the individual Group I-NP n-alkane (paraffin) to 1-alkene (olefin) products (P/O ratio). This measure eliminates the variability in injection volume size and detector sensitivities. In the present work, typical values for the C7, C8 and C9 P/O ratios were 2.03 $\pm$ 0.21 ($\pm$ 10.3%) and 1.23 $\pm$ 0.1 ($\pm$ 8.1%) at 350 and 400C, respectively, which match quite closely with the NRL P/O ratios of 2.0 and 1.1 at 345 and 430C, respectively. Additionally, the present work shows a C10 P/O ratio of 0.5 $\pm$ 0.09 ($\pm$ 18%) at 400C, while the corresponding C10 P/O ratio at NRL was 0.5 at 430C. Thus, the agreement in the P/O product ratios provide an additional source of system verification.

4.3 EFFECT OF DISSOLVED OXYGEN

Experiments with deoxygenated fuels have been carried out by various researchers (e.g., Taylor, 1974). Results indicated a decrease in the deposit formation relative to air saturated fuel experiments for the majority of fuels investigated. In the present work, in addition to the aerated neat n-dodecane experiments, an oxygenated and a deoxygenated experiment were performed to examine the effect of oxygen concentration on the soluble product formation. These experiments also answered the question of what products form directly from alkylhydroperoxide (ROOH) decomposition.

Usually, the aerated n-C12 experiments are performed with 600 cc n-dodecane air saturated with 9 liters of air. The oxygenated experiment was performed by saturating n-C12 with 9 liters of oxygen and the deoxygenated experiment was performed by purging n-C12 with 22.5 liters of nitrogen. In all cases, no attempt was made to measure the dissolved oxygen content. The results are presented in Figs. 4.4-4.6.

Overall, soluble product formation is directly related to the amount of dissolved oxygen present in the fuel. Figs. 4.4 and 4.5 show the effect of deoxygenation and oxygenation, respectively, on polar product distributions relative to the aerated case. Fig. 4.4 shows that fuel deoxygenation decreases the concentration of the polar oxygenated products (Groups I-P, II, III and IV). This is not surprising since oxygen triggers the formation of the oxygenated products. The product concentration ratios for the aerated case relative to the deoxygenated case (A/D ratio), show that ROOH formation is greatly retarded compared to the other oxygenated products, i.e., aldehydes, tetrahydrofurans, and alcohols + ketone (A+K) products, indicating that they are most sensitive to oxygen concentration. This is to be expected because C12 ROOH's are the primary oxygenated products arising from n-C12 oxidation. The A/D A+K product ratio increases as temperature increases, beginning from a ratio of 2.21 $\pm$ 1.31 at 250C and attaining a ratio of 9.92 $\pm$ 1.25 at 400C, indicating that A+K product formation is sensitive to

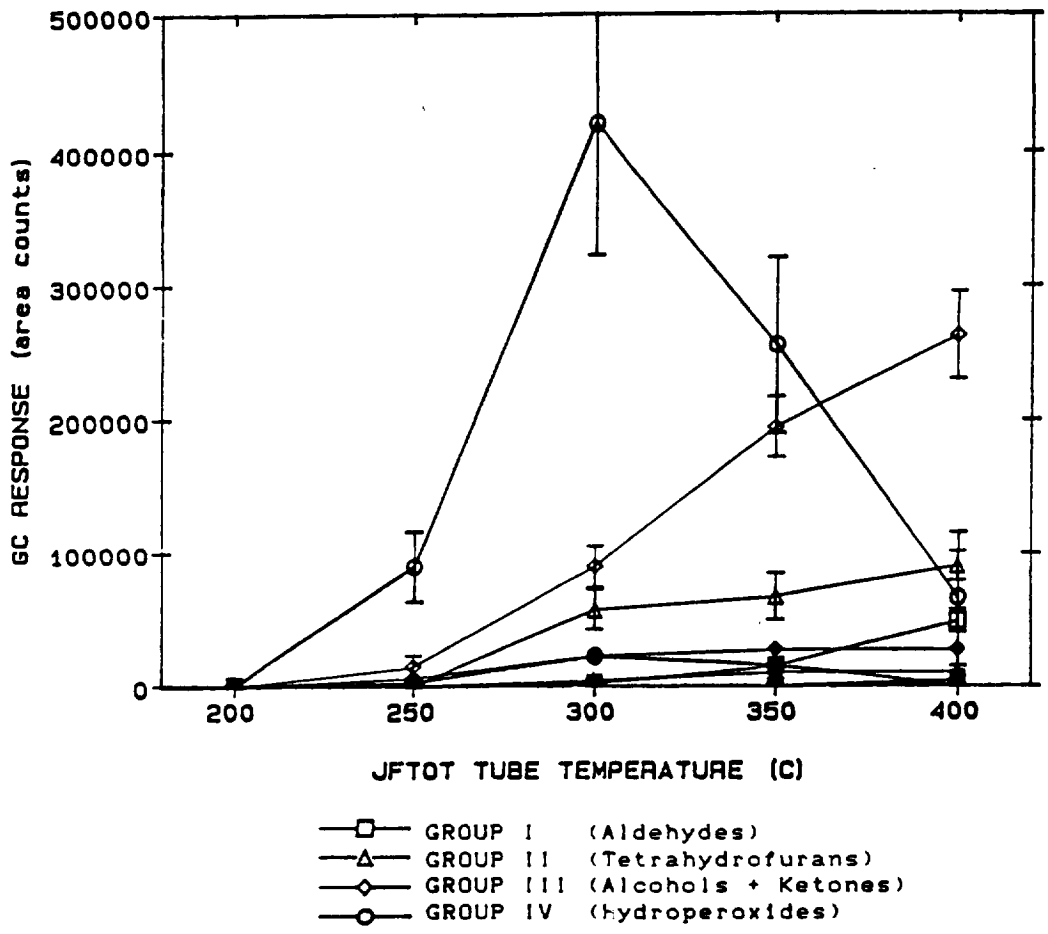

FIG. 4.4 Effect of Deoxygenation on Polar Reaction Products From JFTOT Testing of n-Dodecane Using GC/OCI Analysis of P1 Fractions (Air Saturated - Open Symbols; Nitrogen Purged - Closed Symbols)

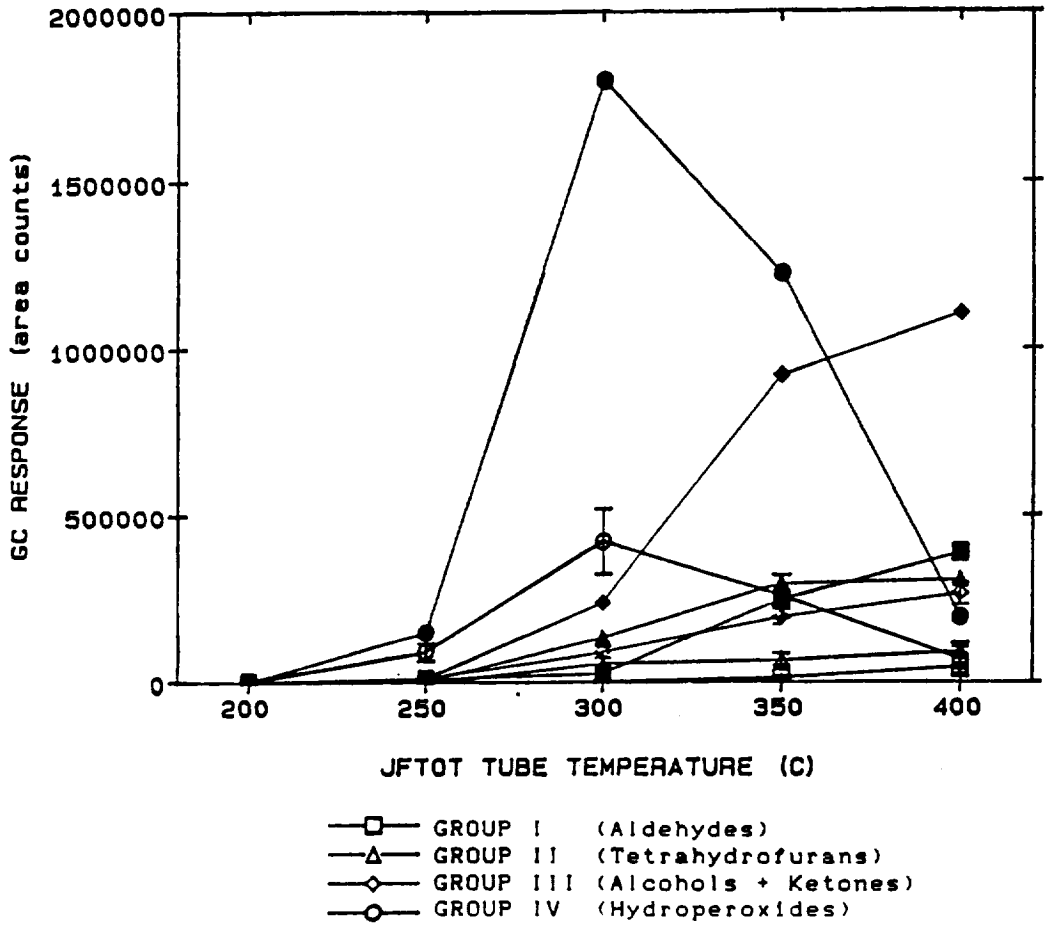

FIG. 4.5 Effect of Oxygenation on Polar Reaction Products From JFTOT Testing of n-Dodecane Using GC/OCI Analysis of Pi Fractions
(Air Saturated - Open Symbols;
Oxygen Saturated - Closed Symbols)

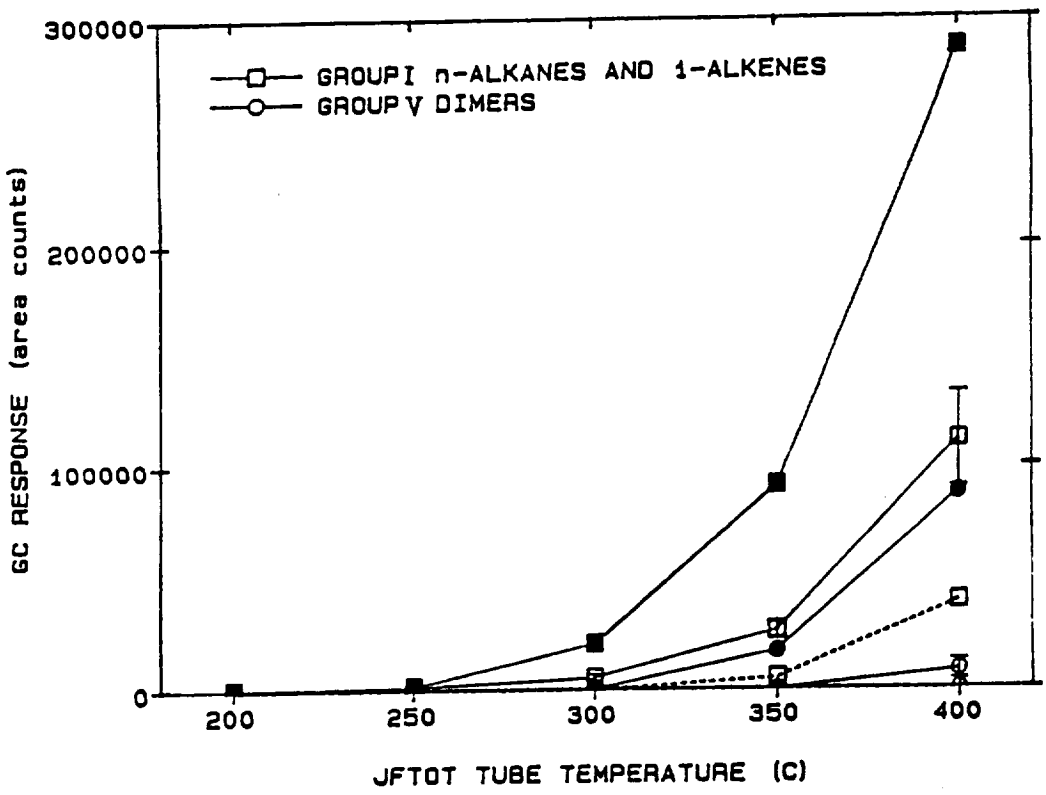

FIG. 4.6 Effect of Oxygen Concentration on Non-Polar Reaction Products From JFTOT Testing of n-Dodecane Using GC/Split Injection Analysis of Entire Samples (Air Saturated - Open Symbols; Oxygen Saturated - Closed Symbols; Nitrogen Purged - Dashed Lines)

temperature. At and beyond 300C, it is known that ROOH decomposes primarily to yield A+K products; consequently, aerated fuel with relatively high ROOH concentrations decompose primarily to A+K products (beyond 300C), while deoxygenated fuel with low ROOH concentrations keeps A+K concentration fairly constant. Also, deoxygenation greatly inhibits the formation of the primary oxidation product, ROOH, which is a precursor for A+K formation. Therefore, the A/D ratio increases with temperature.

Similarly, when the dissolved oxygen concentration increases relative to the aerated case, Fig. 4.5, the oxygenated product formation increases. As would be predicted from the deoxygenated case, the ROOH concentrations are increased, even higher than the other products, relative to the aerated case, indicating that they are the primary oxidation products most sensitive to oxygen concentration.

Fig. 4.6 shows the effect of oxygen concentration on non-polar reaction products (Group I and Group V) from JFTOT testing of n-dodecane. Even though these products do not contain any oxygen, a decrease in oxygen concentration inhibits their formation, indicating that oxygen plays a key role in their formation. Additionally, the Group I A/D ratios, and the corresponding product concentration ratios for the oxygenated case relative to the aerated case (O/A ratio), both decrease as temperature is raised from 350 to 400C (the A/D ratios are 5.01 + 0.62 at 350C, and 2.86 $\pm$

0.45 at 400C; and the O/A ratios are 3.53 ± 0.45 at 350C, and 2.56 ± 0.41 at 400C). With increasing temperature, the Group I A/D and O/A ratios decrease since fuel pyrolysis reactions start to dominate, consequently decreasing their dependence on oxygen concentration.

With deoxygenation (at 400C), the yield of Group I products, although smaller, exhibits patterns similar to the air saturated experiments, Fig. 4.7. This observation, along with the above results, leads to the conclusion that Group I-V products, which other workers have postulated as precursors of deposit formation, are all affected by oxygen concentration, in agreement with earlier work.

4.4 MODIFIED n-DODECANE/OXYGEN MECHANISM

As described in the last section, the present study confirmed the presence of the autoxidation and intermediate temperature regimes postulated by the NRL group. Thus, their mechanisms were used as a starting point in explaining the current results. Since no testing was done above 400C, the pyrolysis scheme of reactions cannot be addressed.

4.4.1 Autoxidation Regime (T ≤ 300C):

The autoxidation scheme of reactions, Reactions 1-3 and 6-8, have been well established as a result of many liquid phase oxidation studies (e.g., Emanuel et al., 1967; Brown and Fish, 1969; Benson and Shaw, 1972). The extent to which each of these steps, including additional Reactions 4, 5a and 5b, describe the oxidation of n-dodecane at temperatures

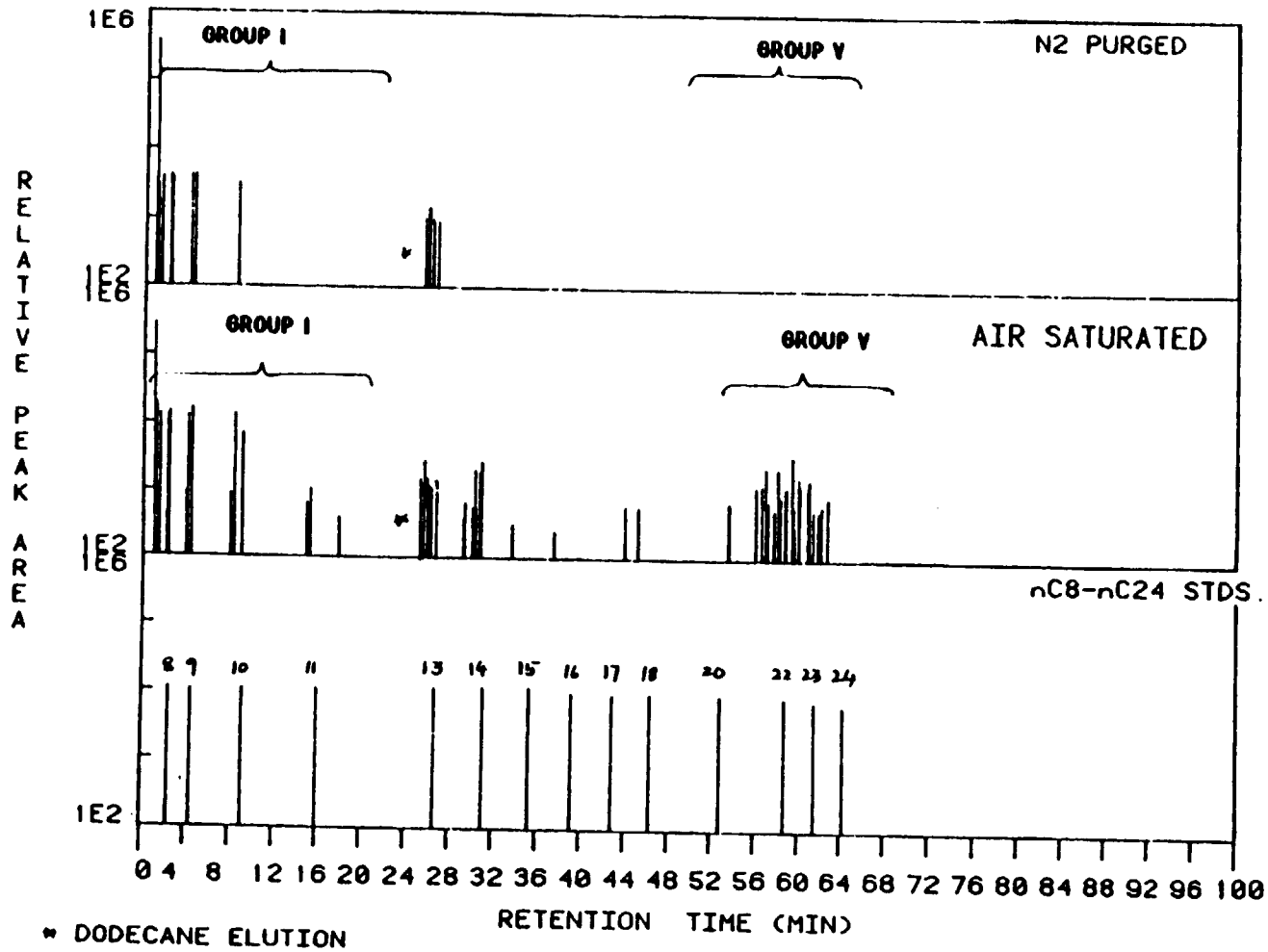

FIG. 4.7 GC Peak Profiles of JFTOT Stressed Air Saturated and Nitrogen Purged n-Dodecane Samples at 400C Using GC/Split Injection Analysis

between 200-300C will now be considered. This scheme is also illustrated in Fig. 4.8, in which the relative importance of various reaction steps is shown as lines of varying thickness.

Heterogenous Initiation

$$RH \text{ --- SURFACE ---> } R^* + (^*H) \quad (1)$$

Propagation

$$R^* + O_2 \text{ ---> } RO_2^* \quad (2)$$

$$RO_2^* + RH \text{ ---> } ROOH \text{ (Group IV)} + R^* \quad (3)$$

$$OH^* + RH \text{ ---> } R^* + HOH \quad (4)$$

Intramolecular H atom Abstraction and Decomposition

$$RO_2^* \text{ ---> } ^*QOOH \quad (5a)$$

$$^*QOOH \text{ ---> } QO \text{ (Group II)} + ^*OH \quad (5b)$$

Termination

$$RO_2^* + RO_2^* \text{ ---> } ROH + R''COR''' \text{ (Group III)} + O_2 \quad (6)$$

$$R^* + RO_2^* \text{ ---> } ROOR \quad (7)$$

$$R^* + R^* \text{ ---> } R\text{-}R \text{ (Group V)} \quad (8)$$

Initiation occurs in the present study on the hot aluminum metal surface by way of heterogenous catalysis giving alkyl radicals, Reaction 1 (Emanuel et al., 1967). The formation of secondary alkyl radicals is favored as the secondary C-H bond strength is about 3 kcal less than that for a primary C-H bond. The sec-alkyl radicals will react rapidly with molecular oxygen yielding secondary alkylperoxy radicals, RO_2^*, Reaction 2. Alkylperoxy radicals, on the other hand, react much more slowly with RH to form Group IV

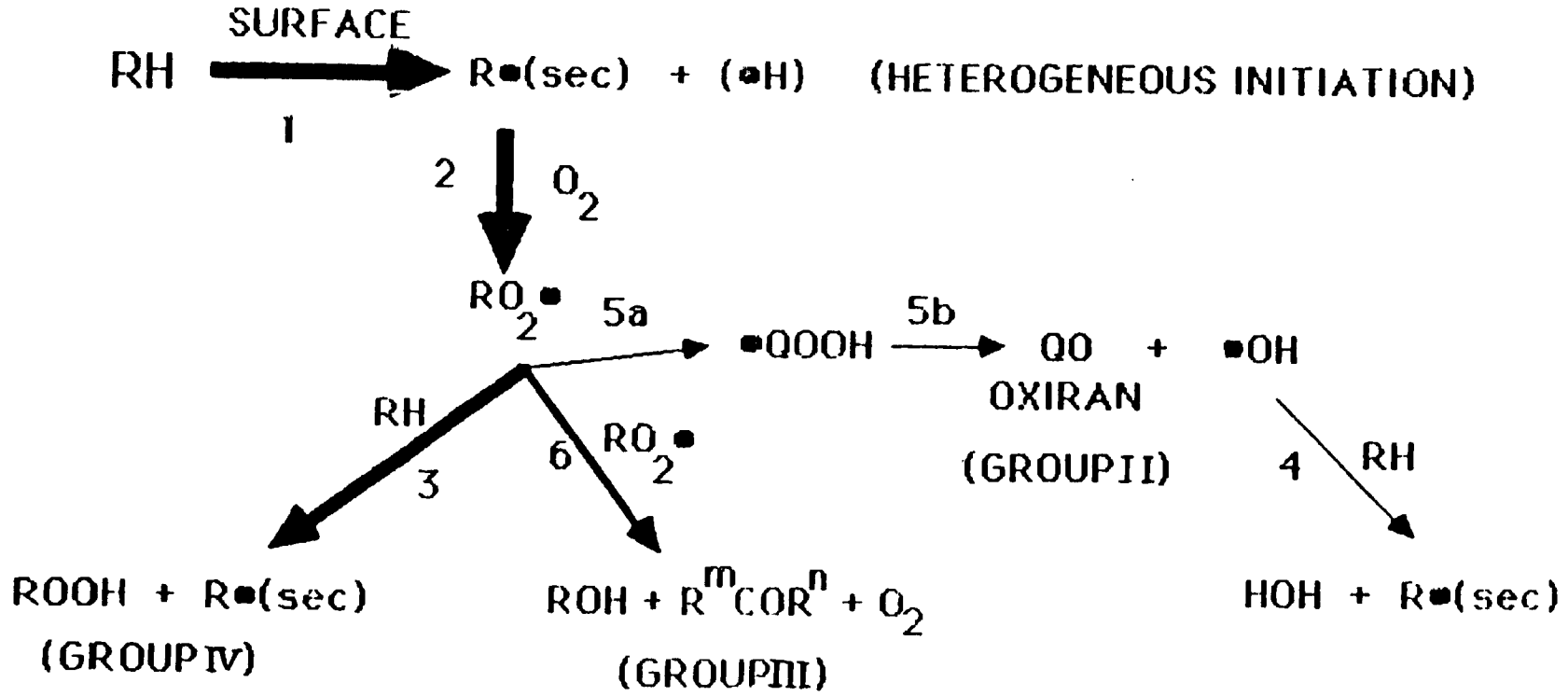

FIG. 4.8 n-Dodecane/Oxygen Reactions in the Autoxidation Temperature Regime (T $\leq$ 300C)

alkylhydroperoxides, ROOH's, Reaction 3. This step is slow and is usually the rate controlling propagation reaction.

The presence of Group II O-heterocyclic products, tetrahydrofurans (THF's), indicates the occurrence of RO_2* intramolecular H-atom abstraction reactions via Reactions 5a and 5b, which compete with the bimolecular RO_2* intermolecular H-atom abstraction, Reaction 3. The low Group II THF concentrations relative to the Group IV ROOH's implies that abstraction reactions are predominantly intermolecular, since the high RH concentrations (> 99.0%) favor bimolecular reactions. In liquid phase reactions, RO_2* intermolecular hydrogen abstraction reactions are possible if the high activation energy requirements are met (Fish, 1970; Mill and Hendry, 1980). Also, Benson (1965, 1972) has shown that with molecules consisting of six carbon atoms or greater, the intramolecular isomerization sequence becomes more feasible due to higher collision frequency factors and smaller activation energies. In the present case, THF formation starts at 250C with increasing concentration at higher temperatures, indicating that sufficient ROOH is present and that the activation energy barrier required for intramolecular reaction is overcome at least by 250C.

The formation of cyclic ethers such as THF is explained by the alkylperoxy isomerization and decomposition scheme (APRID scheme - Fish 1964, 1968), shown below.

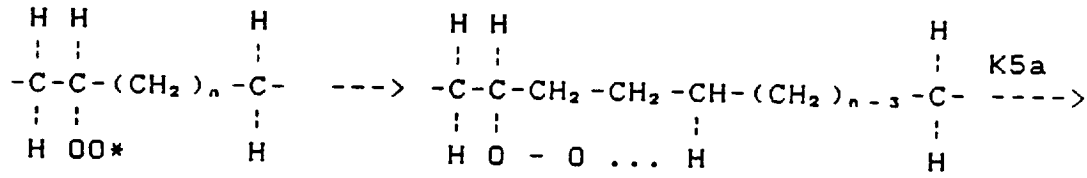

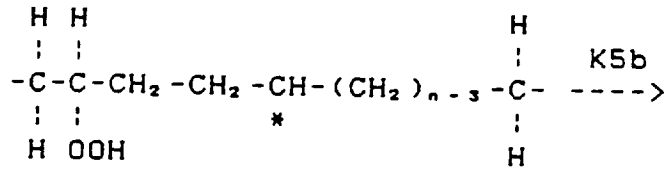

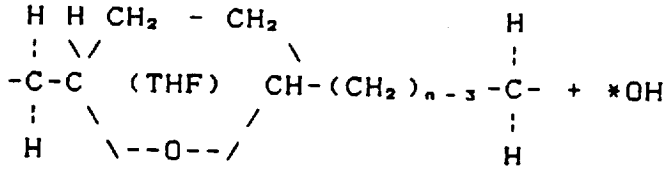

The sec-RO_2* radical intramolecular H-atom abstraction starts initially with the formation of a seven-centered transition ring involving the unpaired electron on the oxygen atom and the gamma hydrogen. In fact, previous experimental data on 5- and 7- center reactions using 2,3-dimethylbutane (Mill and Montorsi, 1973) and 2,5-dimethylhexane (Rust, 1957) show that the 7-centered transition states are favored over 5-centered states. The 7-centered state changes via internal H-atom transfer into the hydroperoxyalkyl radical, *QOOH, Reaction 5a, subsequently followed by C-O ring closure giving the five membered ether, THF, with alkyl substituents such as methyl, propyl, and pentyl groups attached at the 2- and 5- positions, and an hydroxyl radical, Reaction 5b.

Different classes of intramolecular products have been experimentally observed and confirmed in liquid phase n-alkane oxidation studies by Boss and Hazlett (1969)(n-C12

oxidation); Van Sickle et al. (1973) (n-C5 and n-C8 oxidation); and Jensen et al. (1979) (n-C16 oxidation). Van Sickle et al. found that the absolute rate of intramolecular abstraction by sec-pentylperoxy radicals (secondary C-H bonds) is one-eightieth of that of 2,4-dimethyl-2-pentyl-peroxy radicals (tertiary C-H bonds) and postulated reaction steps 5a and 5b to explain such products. In contrast, Cullis et al. (1981), working with liquid phase oxidation of decane between 172-192C, were unable to detect any O-heterocyclic compounds due to the lower test temperatures employed relative to the present case (200 - 400C). Apparently, the high activation energy required for RO_2* intramolecular isomerization involving secondary C-H bonds was not met at their test temperatures.

Further oxidation of the hydroperoxyalkyl radicals (*QOOH) giving bifunctional oxygenated products, such as dihydroperoxides and diols, will be slow due to the low oxygen and hydroperoxyalkyl concentrations present. Boss et al. (1973) employed similar low oxygen pressures as encountered in the JFTOT experiments, and showed that RO_2* intramolecular H-atom transfer results in small quantities of monofunctional oxygenated products (such as cyclic ethers and oxetanes) during n-dodecane oxidation experiments. However, they did not detect any bifunctional products. On the other hand, Brown and Fish (1969) and Jensen et al. (1979) detected the presence of mono- and bi- functional oxygenated products.

The hydroxyl radical arising from Reaction step 5b attacks the fuel, RH, to form water and alkyl radicals, Reaction 4. The activation energy for Reaction 4 is only 1 to 2 kcal/mol (Berces and Trotman-Dickenson, 1961). As a result, the attack of a hydroxyl radical on an alkane molecule is almost independent of the C-H bond broken and, consequently, far less selective than attack by an alkylperoxy radical (Brown and Fish, 1969). This reaction provides a small, additional route for alkyl radical formation.

Of the three termination steps, Reactions 6-8, Reactions 6 appears to be the dominant process since Group III alcohols and ketones were detected at 300C and below. Since no dimers (R-R) were detected, Reaction 8 is not important. Therefore, Group III alcohols and ketones detected in the present work can be accounted for by the RO_2* self termination Reaction 6 (Van Sickle et al., 1973; Mill et al., 1972). Reaction 8 is probably of small order as compared to Reaction 6 due to the very low R* concentrations.

In summary, the modified n-dodecane oxidation mechanism requires that alkylperoxyl radical reactions dominate in the autoxidation temperature regime ($T \leq 300C$). The dominant path is for the alkylperoxyl radical, RO_2*, to react bimolecularly with fuel to yield primarily alkylhydroperoxides. The RO_2* also undergoes self termination and unimolecular isomerization and decomposition reactions,

to yield smaller amounts of C12 alcohol plus ketone products and tetrahydrofuran derivatives, respectively. Thus, alcohol and ketone formation in this temperature regime implies that the main termination step is via RO_2* self termination reactions, which refutes an earlier hypothesis that R* radical termination reactions (giving C24 hydrocarbon isomers) are important (Hazlett et al., 1977).

4.4.2 Intermediate Temperature Regime ($300 \leq T \leq 400C$):

In the intermediate temperature range, between the autoxidation and the pyrolysis regimes, molecular oxygen does not play a dominant role. Hazlett et al. (1977), working with n-dodecane oxidation using stainless steel JFTOT tubes, showed that the fraction of oxygen reacted reaches 100% at 260C and beyond, implying that nearly all the available oxygen is used up. Since no direct oxygen measurements were attempted in the present study, the $[ROOH]_{max}$ temperature of 300C was taken as the 100% oxygen consumption temperature. Therefore, at 300C and beyond, nearly all available oxygen is reacted quickly, creating a reducing environment. The shift in the 100% oxygen consumption temperature from 260C to 300C is attributed to the aluminum tubes used in the present study, which, as noted earlier, form ROOH more slowly than 304 stainless steel tubes.

In addition to nearly all available oxygen being used up at higher temperatures ($T \geq 300C$), the relative rates of various reactions change. For example, at higher

temperatures, the rate of the (RO_2* --> *QOOH) reaction (Reaction 5a) increases relative to the rate at lower temperatures, as evidenced from the increase in Group II THF product yields at temperatures 300C and beyond. While Group II formation increases at higher temperatures, the Group IV ROOH concentrations decrease since the decomposition reactions dominate over formation reactions.

Thus, the oxygen-starved environment and higher temperatures cause the ROOH's to decompose to yield Group III alcohols and ketones, Group I-P aldehydes, and Group II THF's, while indirectly forming Group I-NP n-alkanes and 1-alkenes, and Group V dimer products. As before, the reaction scheme postulated in this regime is based on Hazlett et al's work, with additional reactions to account for Group II THF formation. Also the postulated Group V dimer product (R-R) formation is confirmed and included in this temperature regime.

Intramolecular H atom Abstraction

$$RO_2* \longrightarrow *QOOH \longrightarrow QO\ (\text{Group II}) + *OH \qquad (5a,5b)$$

ROOH Thermolysis

$$ROOH \longrightarrow RO* + *OH \qquad (9)$$

$$RO* + RH \longrightarrow ROH\ (\text{Group III}) + R* \qquad (10)$$

$$HO* + RH \longrightarrow HOH + R* \qquad (4)$$

$$R^{\alpha}\text{-}\underset{\displaystyle OOH}{\underset{|}{CH}}\text{-}R^{\eta} + X* \longrightarrow R^{\alpha}\text{-}\underset{\displaystyle OOH}{\underset{|}{C*}}\text{-}R^{\eta} + XH \longrightarrow R^{\alpha}\text{-}\underset{\displaystyle O}{\underset{||}{C}}\text{-}R^{\eta} + *OH \qquad (11)$$

(Group III)

B-Scission

(12)

Solvent Induced ROOH Decomposition

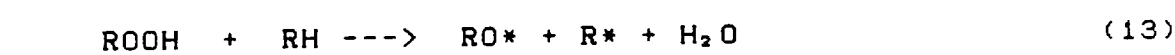

(13)

Heterogenous Initiation

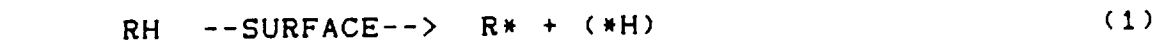

(1)

R* Radical Formation via ROOH Decomposition

(4,10,15)

(where Y* is ROOH derived RO*, OH* and R^n* radicals)

B-scission

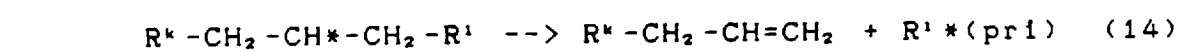

(14)

(Group I-NP)

Hydrogen Transfer

(15)

(Group I-NP)

Main Termination Step

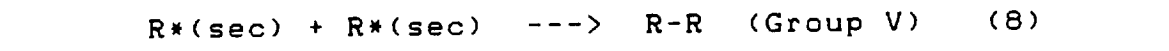

(8)

The RO_2* radicals, as noted above, isomerize and decompose into a THF and a hydroxyl radical via the APRID scheme, Reactions 5a and 5b. This scheme is energetically favored at intermediate temperatures relative to low temperatures, because the higher temperatures provide more ROOH and further overcome the activation energies associated with internal RO_2* rearrangement. This explains the increase in Group II THF concentrations at temperatures

greater than 300C. The hydroxyl radicals, produced from Reactions 5b (and Reactions 9 and 11), can also propagate the chain by abstracting a hydrogen from RH to form water plus an alkyl radical, Reaction 4 (Hazlett et al., 1977).

The thermal decomposition of a hydroperoxide is a complex process since different reactions can occur simultaneously and, in addition, the influence of the solvent may be important (Brown and Fish, 1969). The various ROOH decomposition paths and ensuing reaction steps are illustrated in Fig. 4.9. First, the simplest type of decomposition involves the unimolecular homolysis of the O-O link giving RO* and *OH radicals, Reaction 9 (Tobolsky and Mesrobian, 1954; Hiatt, 1972). Secondly, ROOH reacts with the solvent, RH, giving RO*, R* and H_2O, Reaction 13 (Emanuel, 1982). If the activation energies of the above reactions are considered, $\Delta H_9 = D_{(RO-OH)} \approx 35$ kcal/mol (Ingold, 1961), while $\Delta H_{13} = D_{(C-H)} + D_{(O-O)} - D_{(H-OH)} \approx 94 + 35 - 120 \approx 9$ kcal/mol for a secondary C-H bond. Brown and Fish (1969) experimentally determined an overall activation energy of ROOH decomposition. The occurrence of the bimolecular ROOH decomposition step cannot be confirmed experimentally because the R*(sec) and RO* radicals resulting from this decomposition form the same products as those resulting from unimolecular ROOH decomposition (i.e., ROH, RCHO and R"H). A third ROOH decomposition path involves ROOH collision with an X* radical yielding a C12 ketone and

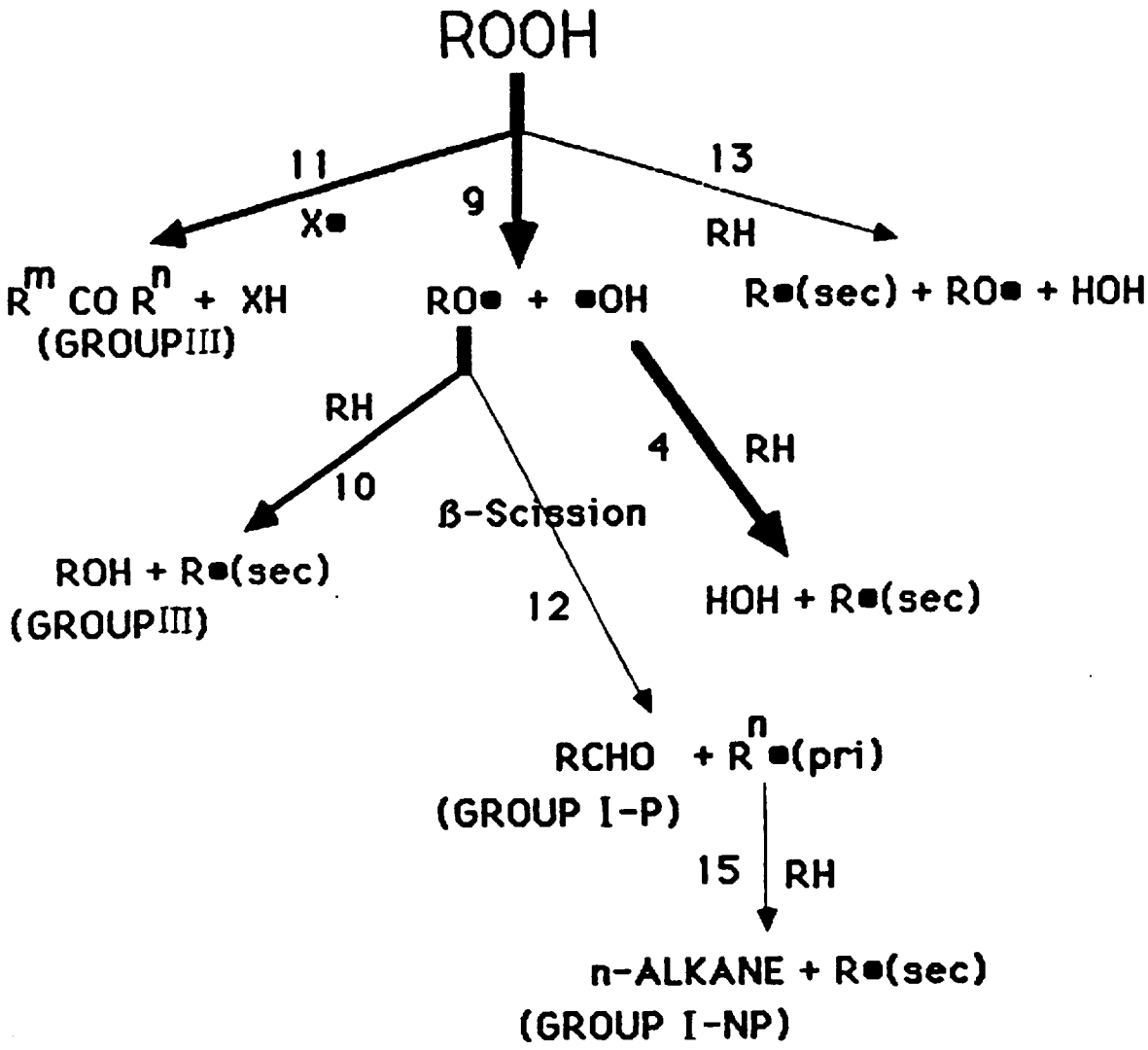

FIG. 4.9 Hydroperoxide Decomposition Reactions in the Intermediate Temperature Regime ($300 \leq T \leq 400C$)

a hydroxyl radical, Reaction 11 (Emanuel et al., 1967; Hazlett et al., 1977).

The sec-alkoxy radicals, RO*, produced from Reaction steps 9 and 13, primarily abstract a hydrogen to form Group III dodecanols, Reaction 10 (Brown and Fish, 1969). Secondly, at 300C and above, some of the alkoxy radicals decompose by B-scission forming a Group I-P aldehyde and a primary alkyl radical, Reaction 12 (Emanuel et al., 1967; Brown and Fish, 1969; Hazlett et al., 1977). The primary radicals formed in step 12 produce a Group I-NP n-alkane and a secondary alkyl radical via intermolecular H-atom abstraction from an RH molecule, Reaction 15. Alkoxy radical, RO*, reaction with ROOH to form ROH and a RO_2* radical (Brown and Fish, 1969) is unlikely in our case, since the energy required to break an ROO-H bond (forming an RO_2* radical) is far greater than that necessary to break the RO-OH bond, i.e., $D_{(O-H)} > D_{(O-O)}$. Another reason this reaction is not feasible is because of the relatively high RH concentrations compared to the ROOH concentrations, which makes RH reactions (RO* + RH ---> ROH + R*) more likely than ROOH reactions (ROOH + RO* ---> ROH + RO_2*).

The sec-alkyl radicals, R*, can form in two ways. The two R* radical formation paths and ensuing reaction steps are illustrated in Fig. 4.10. First, a pool of R* radicals is provided via RH heterogeneous metal initiation, Reaction 1. Secondly, at these elevated temperatures ($T \geq 300C$), ROOH decomposition results in RO*, OH* and R^n* radicals

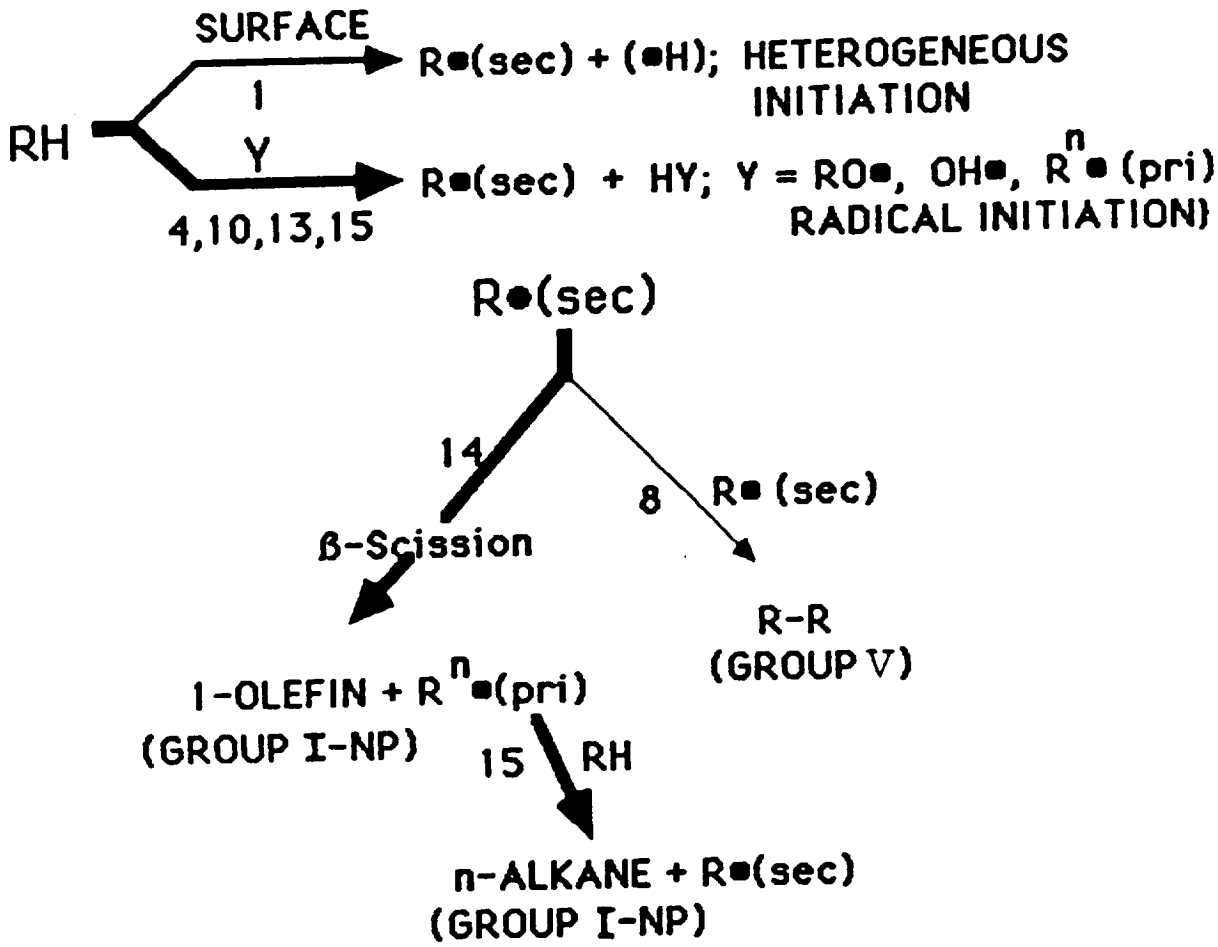

FIG. 4.10 Dodecyl Radical (R*) Reactions in the Intermediate Temperature Regime ($300 \leq T \leq 400C$)

which react, in turn, with the fuel, RH, giving R* radicals via Reactions 4, 10, and 15. The fraction of R* radicals formed due to ROOH decomposition versus heterogeneous metal initiation of the fuel can be inferred by comparing the n-dodecane derived Group I products from normal aeration experiments (9 liters of air passed through 600 cc of n-C12) with deoxygenation experiments (22.5 liters of nitrogen purged through 600 cc of n-C12), Fig. 4.6. As noted, the figure shows that deoxygenation greatly inhibits Group I n-alkane and 1-alkene product concentrations relative to the aeration case, indicating that oxygen plays an important role in Group I formation. Since Group I products form via R* radical reactions, this result implies that R* radical formation via oxygenated products, ROOH, dominates over heterogeneous metal initiation.

The R* radicals, formed by the radical and heterogeneous metal initiation steps, either decompose to form smaller 1-alkenes (< C12) and additional primary alkyl radicals via B-scission, Reaction 14, or self terminate to form dimers via Reaction 8. Subsequently, the primary alkyl radical formed via B-scission abstracts an H-atom from a fuel molecule to form a smaller n-alkane (< C12) and regenerates the R* radical, Reaction 15 (Hazlett et al., 1977). The sequence of reactions 1, 14 and 15 constitute a modified form of the single step Fabuss-Smith-Satterfield fuel pyrolysis scheme (Fabuss et al., 1964). Reactions 14 and 15 comprise propagating steps of a free radical chain

which afford more product than a 1:1 relationship to the ROOH decomposition step would indicate.

The higher concentrations of the Group I-NP, 1-alkenes and n-alkanes relative to the Group V n-C12 dimers indicates that Reaction 14 dominates over the termination step, Reaction 8, and becomes increasingly important as the temperature is raised from 350 to 400C. Dimer formation via alkyl radical recombination starts at 350C and increases as temperature is raised to 400C. Brown and Fish (1969) postulated that high temperatures favor alkyl radical formation relative to the RO_2* radicals. Therefore, it is not surprising that the R* radical derived products dominate at higher temperatures ($T \geq 300C$). Also, Hazlett et al. (1977) postulated that the main termination reaction at these elevated temperatures is via R* radical self termination, yielding R-R dimer products. In the present work, dimer product detection confirms the R* radical self termination hypothesis.

In summary, in the intermediate temperature regime ($300 \leq T \leq 400C$), the R* alkyl radical reactions dominate the RO_2* reactions, since the R* radical products such as n-alkanes and 1-alkenes form in greater concentrations than the RO_2* products such as ROOH's, C12 alcohols, C12 ketones and tetrahydrofurans. The R* radicals form mainly via two sources: (i) ROOH decomposition reactions, which yield stable reaction products such as C12 alcohols, C12 ketones, <C12 aldehydes and a pool of R* radicals; and (ii)

direct fuel pyrolysis. The R* radicals thus formed have two major reaction pathways. B-scission forming n-alkanes and 1-alkenes constitutes the dominant path, while R* radical dimerization reactions forming C24 alkane isomers makes up the minor reaction path. Small amounts of tetrahydrofuran products can be explained by RO_2* isomerization and decomposition reactions.

4.5 CONCLUSIONS

In summary, the system verification studies showed that the < C12 n-alkanes and 1-alkenes, C12 alcohols and ketones and ROOH (hypothesized) product profiles agree with the NRL data. However, additional < C12 aldehydes, tetrahydrofurans and C24 isomers were detected due to the better sensitivity of the analytical instrumentation and protocols employed in this work. Consequently, the existing n-dodecane degradation mechanisms were modified to include these products.

The modified n-dodecane oxidation mechanism requires that alkylperoxyl radical reactions dominate in the autoxidation temperature regime ($T \leq 300C$). The dominant path is for the alkylperoxyl radical, RO_2*, to react bimolecularly with fuel to yield primarily alkylhydroperoxides. The RO_2* also undergoes self termination and unimolecular isomerization and decomposition reactions, to yield smaller amounts of C12 alcohol and ketone products and tetrahydrofuran derivatives, respectively. Thus, alcohol and ketone formation in this temperature regime implies that the

main termination step is via RO_2* self termination reactions, which refutes an earlier hypothesis that R* radical reactions (giving C24 isomers) are important (Hazlett et al., 1977).

In the intermediate temperature regime ($300 \leq T \leq 400C$), the R* radical reactions dominate the RO_2* reactions. The main supply of R* radicals comes from ROOH decomposition reactions, while heterogeneous metal initiation constitutes the secondary source. The R* radicals, in turn, decompose to form n-alkanes and 1-alkenes (< C12) and trace amounts of C24 isomers.

CHAPTER 5

n-DODECANE PLUS DOPANT RESULTS AND MECHANISM DISCUSSION

Polar heterocyclic compounds containing sulfur, nitrogen and oxygen atoms, unavoidably present in the fuel, are involved in many of the chemical processes affecting fuel thermal instability. In order to study dopant effects, a few compounds were selected based on their reported deposition tendency, and added to the n-dodecane model fuel; the resulting mixtures were tested on the modified JFTOT apparatus. The sulfur compounds selected were: 3,4-dimercaptotoluene (high deposition tendency), dibutylsulfide (low deposition tendency) and dibenzothiophene (no effect on deposition), while the nitrogen compounds chosen were pyrrole (high deposition tendency), 2,5-dimethylpyrrole (high deposition tendency) and pyridine (low deposition tendency). A typical dopant test sequence involved: baseline, 10 ppm, 100 ppm, 1000 ppm (molar ratios) JFTOT experiments; a 150 cc distilled n-dodecane flush; followed by a second baseline JFTOT experiment. Also, prior to the second baseline experiment, the last portion of the flush was analyzed on the GC and checked for dopant carry over. If any trace of dopant was detected, additional flushes were carried out until no dopant was detected.

Following these experiments, the control and stressed samples were analyzed for the soluble oxidation products

using GC and GCMS techniques. The soluble products detected were the same as for neat n-dodecane oxidation (Groups I-V), however changes in their distributions were noticed. The dopant derived product distributions relative to the baseline could be classified into three categories: no significant differences, differences with no discernable trends, and differences with definite trends. The first case indicates that dopant addition introduces virtually no changes in the neat n-dodecane reaction mechanism. The second case implies that the reaction rates for some of the product Groups change relative to the baseline, due to dopant addition. The third case indicates that definitive mechanism inferences relative to the baseline can be made due to the product trends observed with changes either in temperature and/or dopant concentration.

No dopant related products were detected, however, due either to very low concentrations (ppb levels) or to a polarity mismatch between solvent and dopant oxygenates during Sep-pak fractionation. Hence, all dopant mechanism inferences are based on changes in n-dodecane derived Group I-V product distributions alone. As noted, since all changes in product distributions with dopant addition are relative to the baseline results, the modified n-dodecane mechanism discussed in Section 4.4 serves as the starting point for explaining the n-dodecane plus dopant results, with new reactions involving dopants and n-dodecane having reaction numbers starting with 16.

5.1 NITROGEN DOPANT EXPERIMENTS

Nitrogen heterocyclic compounds commonly occurring in distillate fuels include alkylated pyridines, quinolines, tetrahydroquinolines, indoles, pyrroles and carbazoles. In this study, pyrrole and pyridine were chosen to study the effect of a five- and six- membered N containing heteroatom, respectively. An alkylated pyrrole (2,5-dimethylpyrrole, DMP) was also examined for the following reasons: (a) alkyl-pyrroles have been detected in high-nitrogen middle distillate fractions, (b) highly pure DMP is commercially available, (c) alkylation adjacent to the nitrogen atom in an active heterocyclic nucleus is very influential in fuel instability, and (d) DMP promotes the formation of significant amounts of insoluble material during storage stability testing of diesel and jet fuels (Cooney et al., 1986; Frankenfeld et al., 1981 and 1982).

n-Dodecane was individually doped with pyrrole, pyridine and DMP and tested using the protocols described above. As noted, the major soluble degradation products were the n-dodecane derived Group I-V products, but with shifts in their distributions. Major differences were observed with DMP, but the addition of pyrrole and pyridine changed the degradation product distributions only slightly. Therefore, a detailed analysis was performed only for the DMP data, while a more qualitative analysis was made for the latter two dopant species.

5.1.1 Pyrrole

With pyrrole addition, the Group II-IV product distributions change as seen in Fig. 5.1. The Group II product curves follow a 10, 1000 ppm > baseline > 100 ppm trend at all temperatures tested, indicating that a decrease in product formation occurs at the intermediate pyrrole concentration of 100 ppm, Fig. 5.1a. In the 200-300C autoxidation temperature range, Group III products follow a 1000 ppm > 100 ppm > 10 ppm > baseline trend, implying that pyrrole addition accelerates the RO_2* self termination reactions, enhancing Group III formation. At 350C this trend changes, since the Group III products follow a 1000 ppm > baseline > 10 ppm > 100ppm trend, indicating that pyrrole addition at 10 and 100 ppm levels appears to inhibit Group III formation, while the 1000 ppm dopant level still promotes their formation, Fig. 5.1b. The 10 ppm Group IV curve shows higher levels in comparison with the baseline curve at all temperaures tested indicating that addition of 10 ppm pyrrole enhances Group IV product formation, but higher dopant levels decrease Group IV formation below baseline results, Fig. 5.1c. (The Group IV 300C, 1000 ppm data is not valid due to improper sample collection).

5.1.2 Pyridine

Pyridine experiments were carried out only at 10 and 1000 ppm levels, with Group II and IV product distributions changing as seen in Fig. 5.2. The Group II formation appears to be delayed to 250C (relative to 200C for the baseline

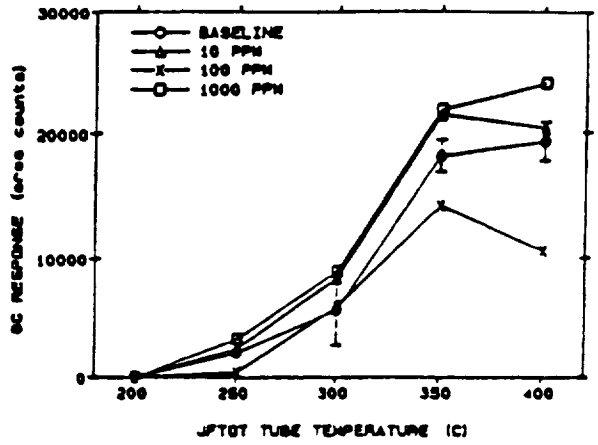

(a) GROUP II

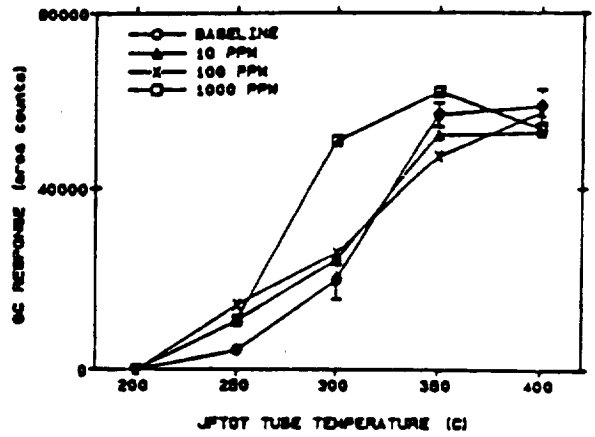

(b) GROUP III

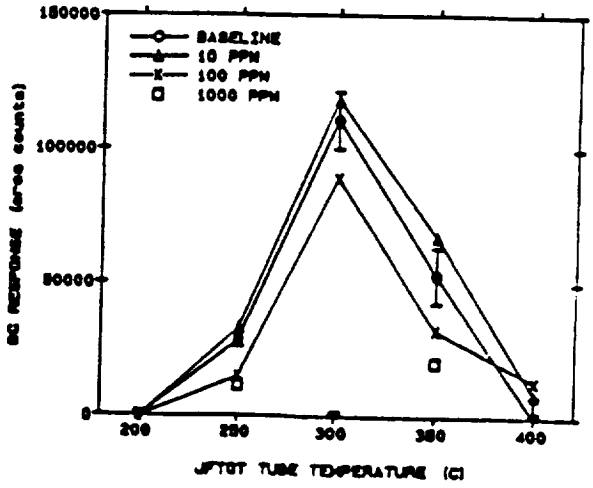

(c) GROUP IV

FIG. 5.1 Effect of Pyrrole on Group II-IV Species in the P1 Fractions Using GC/OCI Analysis

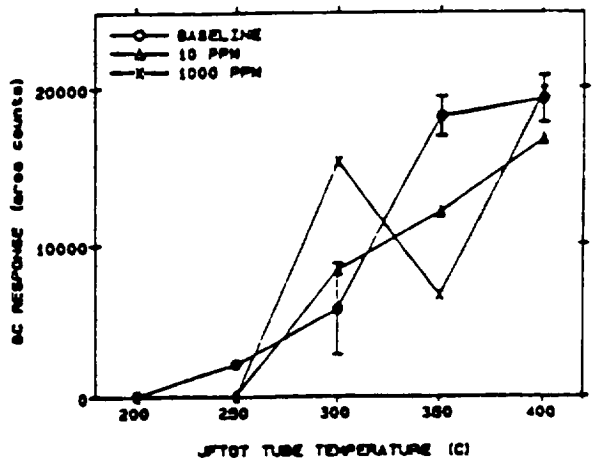

(a) GROUP II

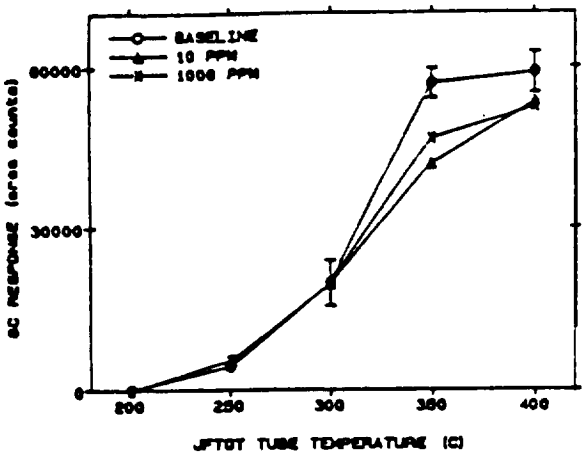

(b) GROUP III

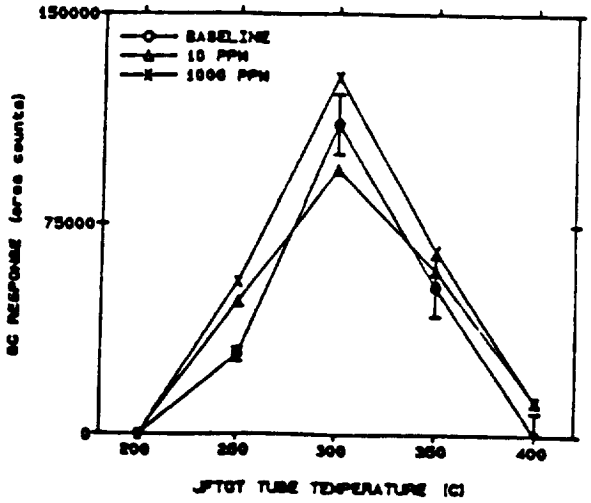

(c) GROUP IV

FIG. 5.2 Effect of Pyridine on Group II-IV Species in the P1 Fractions Using GC/OCI Analysis

case) in the presence of pyridine, indicating possible inhibition of RO_2* isomerization and decomposition rates. However, as the temperature is raised to 250C and then to 300C, the pyridine causes Group II formation to increase relative to the baseline case, while the opposite occurs in the 300-350C region, Fig. 5.2a. A slight inhibition of Group III products is observed in the 300-400C range, Fig. 5.2b. The addition of 1000 ppm pyridine appears to consistently show Group IV concentrations higher than the baseline and 10 ppm runs, indicating that pyridine promotes ROOH formation, Fig. 5.2c.

5.1.3 2,5-Dimethylpyrrole (DMP)

With DMP dopant addition, the Group II-IV product distributions change as seen in Fig. 5.3. In the 200-300C autoxidation temperature regime, high DMP concentrations (added at the 100 and 1000 ppm levels) appear to inhibit Group IV (ROOH) formation, relative to the baseline and 10 ppm DMP cases, implying that DMP molecules successfully compete with n-dodecane for the available oxygen through cooxidation reactions, Fig. 5.3c. This is explained by the fact that at low temperatures the energy required to break a $(C_4NH_3)(CH_2-H)$ bond is about 85 kcal/mol, which is 10 kcal/mol less than that of the secondary C-H bond in the n-dodecane molecule (95 kcal/mol). The decrease in ROOH formation (with addition of the more reactive DMP to n-dodecane) agrees with the work done by Mayo et al. (1983), who showed that small amounts of fast-oxidizing indene (a

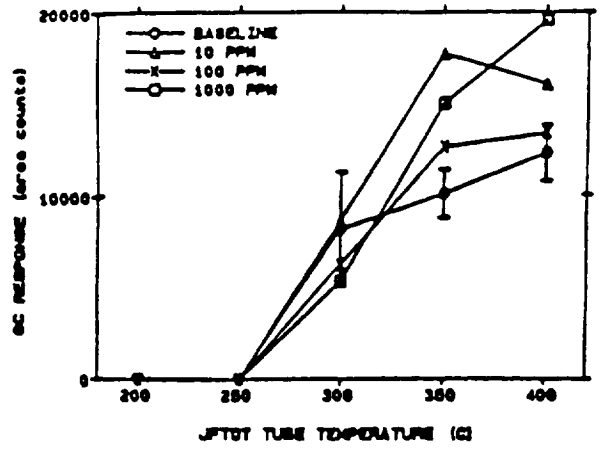

(a) GROUP II

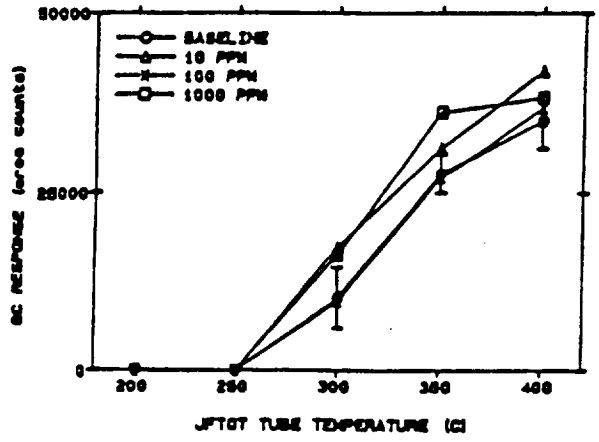

(b) GROUP III

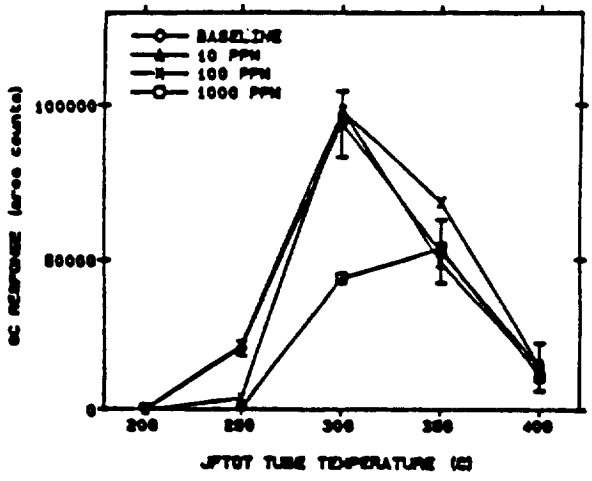

(c) GROUP IV

FIG. 5.3 Effect of 2,5-Dimethylpyrrole on Group II-IV Species in the P1 Fractions Using GC/OCI Analysis

compound with a similar five sided ring as DMP) added to slow-oxidizing n-dodecane fuel retarded, rather than accelerated, the amount of oxygen reacted by the n-dodecane. In contrast, Cooney et al. (1986) working with storage stability experiments involving DMP and shale-derived diesel fuels concluded that oxygen addition to DMP was the primary step (thereby suppressing hydroperoxide formation) followed by charge transfer.

However, as temperature is increased beyond 300C, all Group IV curves (with and without added DMP) have the same concentration levels, indicating that the energy requirement for H-atom abstraction from n-dodecane and DMP molecules is met, making the H-atom abstraction non-selective and consequently rendering the cooxidation reactions involving DMP and oxygen (related to Group IV inhibition) unimportant. Alternatively, the DMP-O_2 reaction may be inhibited due to a less favorable equilibrium at higher temperatures for the molecular association complex or charge transfer (Cooney et al., 1986).

With DMP addition, Group II THF formation increases relative to the baseline in the 300-400C range due to an increase in the alkylperoxy radical (RO_2*) isomerization and decomposition reaction rates, Fig. 5.3a.

Physical examination of the Sep-pak matrices showed that the 100 and 1000 ppm DMP stressed sample Sep-pak matrices collected between 200-400C were brown in color (normally the Sep-pak matrices are white in color after the

fractionation procedure), indicating that highly polar, chromophoric products are formed which do not coelute with the n-dodecane derived Group II-IV products in the P1 fractions. The highly polar products are yet to be identified.

5.2 SULFUR DOPANT EXPERIMENTS

Daniel et al. (1983) carried out storage stability experiments involving Jet 'A' fuel doped with sulfur compounds. They found that thiols and thiophenes increased deposit formation relative to a pure jet fuel, and that the rate of deposition was a function of the concentration of the added sulfur compound. In contrast, alkyl sulfides and disulfides decreased the deposit formation rate. Frankenfeld et al. (1982) evaluated a variety of organic sulfur compounds for their tendency to promote sediment formation in hydrocarbon fuels under accelerated storage conditions. They found that, with the exception of sulfonic acids and aromatic thiols, none of the sulfur compounds produced sediments during storage at ambient or near ambient conditions when tested by themselves. These findings are in sharp contrast with the results of thermal stability studies (Taylor and Wallace, 1968) in which many sulfur compounds were quite deleterious to jet fuels tested between 93-232C. In particular, thiols, sulfides, disulfides and condensed thiophenes (at 1000 ppm S levels) increased the rate of deposit formation, while diphenylsulfide and

dibenzothiophene did not affect the rate of deposit formation. The formation of deposits under high temperature conditions apparently proceeds by different pathways than in the case of ambient or near ambient storage.

In order to clarify the effects of sulfur compounds during high temperature testing, three dopant test sequences involving a sulfide (dibutylsulfide), a thiol (3,4-dimercaptotoluene or 3,4-toluenedithiol) and a thiophene (dibenzothiophene) were performed using the protocols described above. The major soluble degradation products were n-dodecane derived Group I-V products, but with shifts in their distributions with 3,4-dimercaptotoluene and dibutylsulfide addition.

5.2.1 3,4-Dimercaptotoluene (DMT)

With DMT addition, the soluble oxidation product distributions (Groups I-V) change relative to the baseline case as illustrated in Fig. 5.4. Also, Fig. 5.5 gives the peak profiles of the chromatograms from the baseline and dopant samples at 400C and shows that Group I and V products are selectively inhibited with dopant addition, with the 1-alkene species being inhibited to a greater extent than the other Group I species.

In order to explain this behavior, the neat n-dodecane reaction scheme was modified to include DMT dopant (DH) reactions, Figs 5.6 and 5.7. In the autoxidation regime, the modified scheme is (Fig. 5.6):

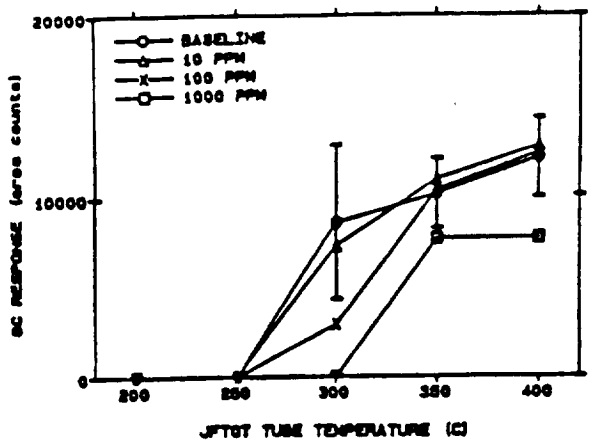

(a) GROUP II

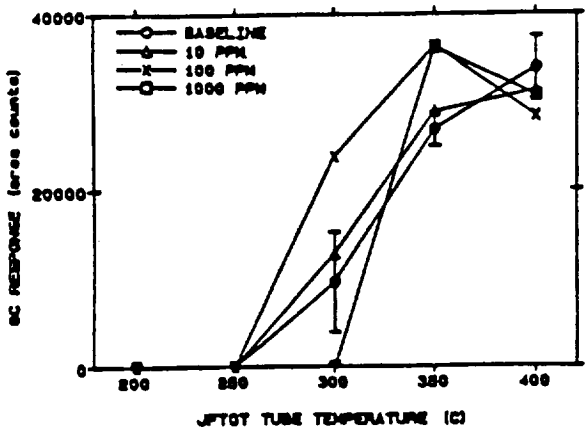

(b) GROUP III

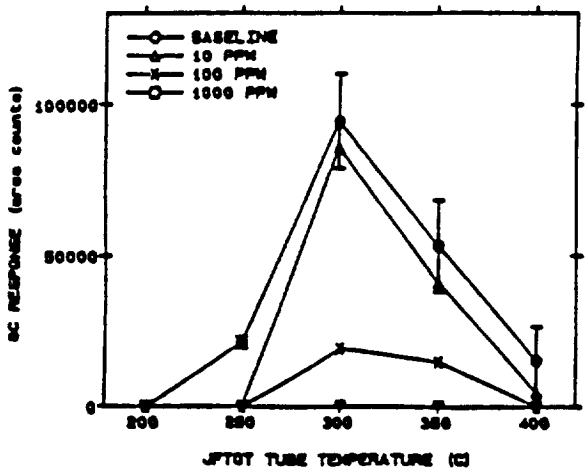

(c) GROUP IV

FIG. 5.4 Effect of 3,4-Dimercaptotoluene on Group II-IV Species in the P1 Fractions Using GC/OCI Analysis

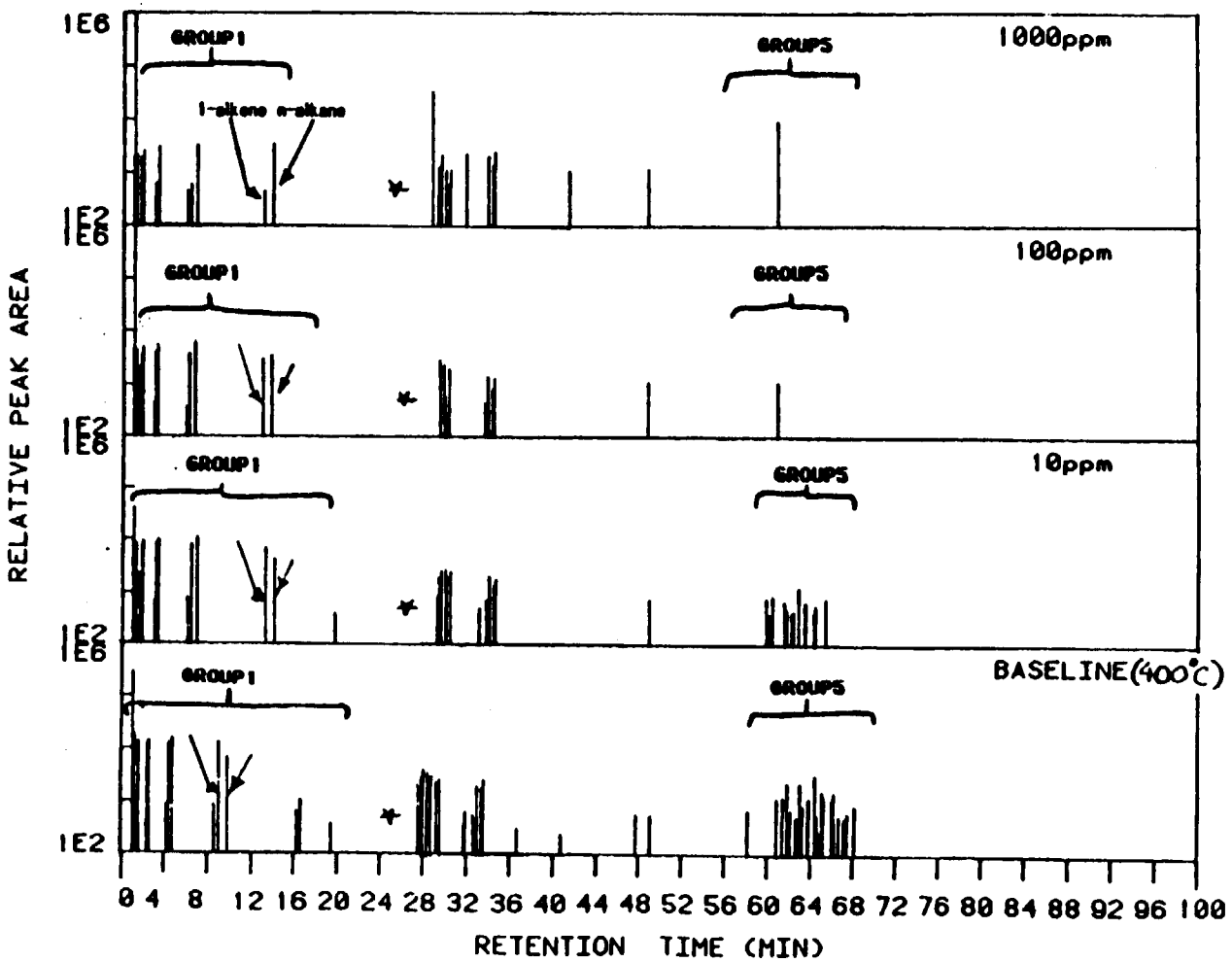

FIG. 5.5 Effect of 3,4-Dimercaptotoluene on Group I and V Species in the Entire Samples Using GC/Split Injection Analysis (400C samples)

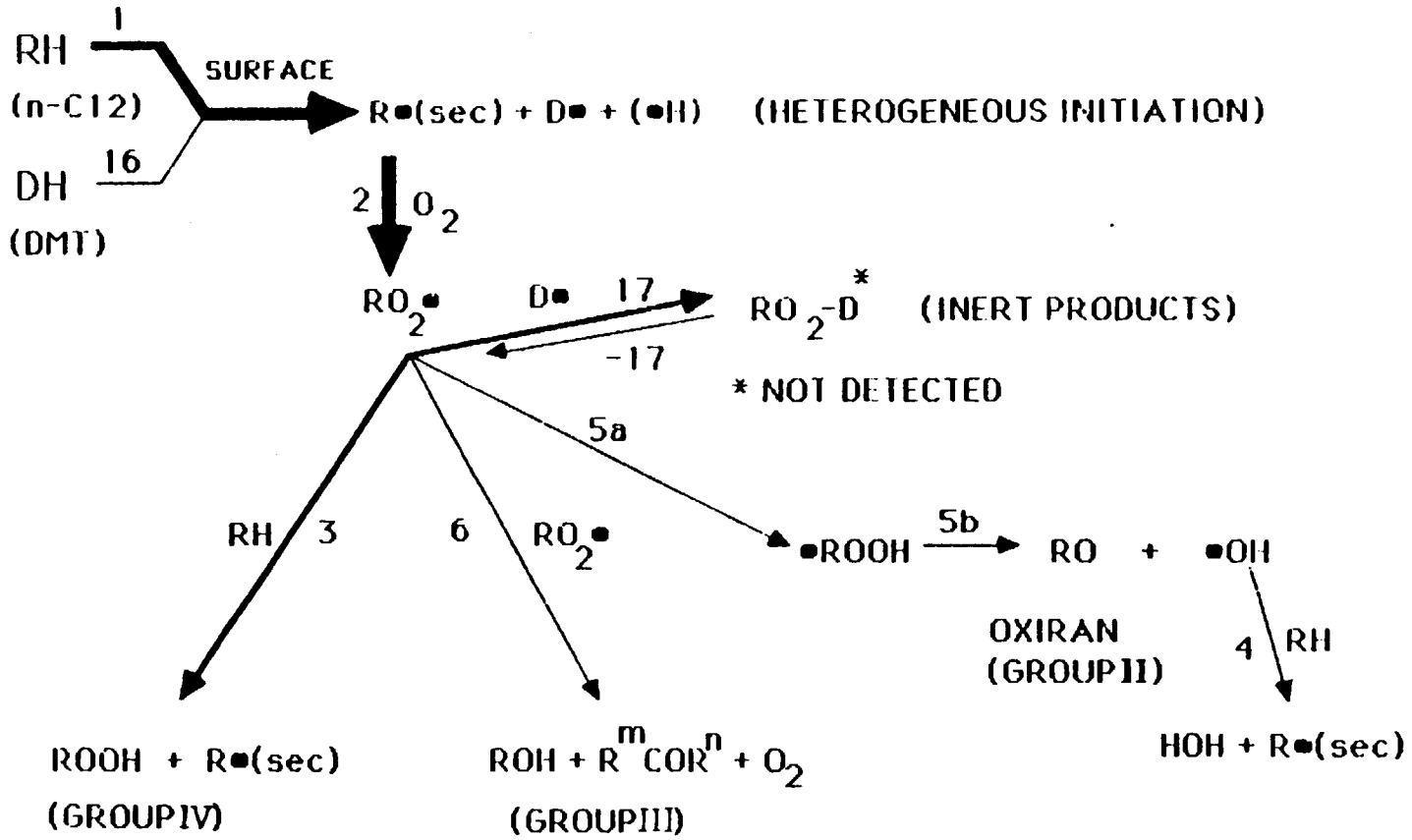

FIG. 5.6 (n-Dodecane + DMT)/Oxygen Reactions in the Autoxidation Temperature Regime (T $\leq$ 300C)

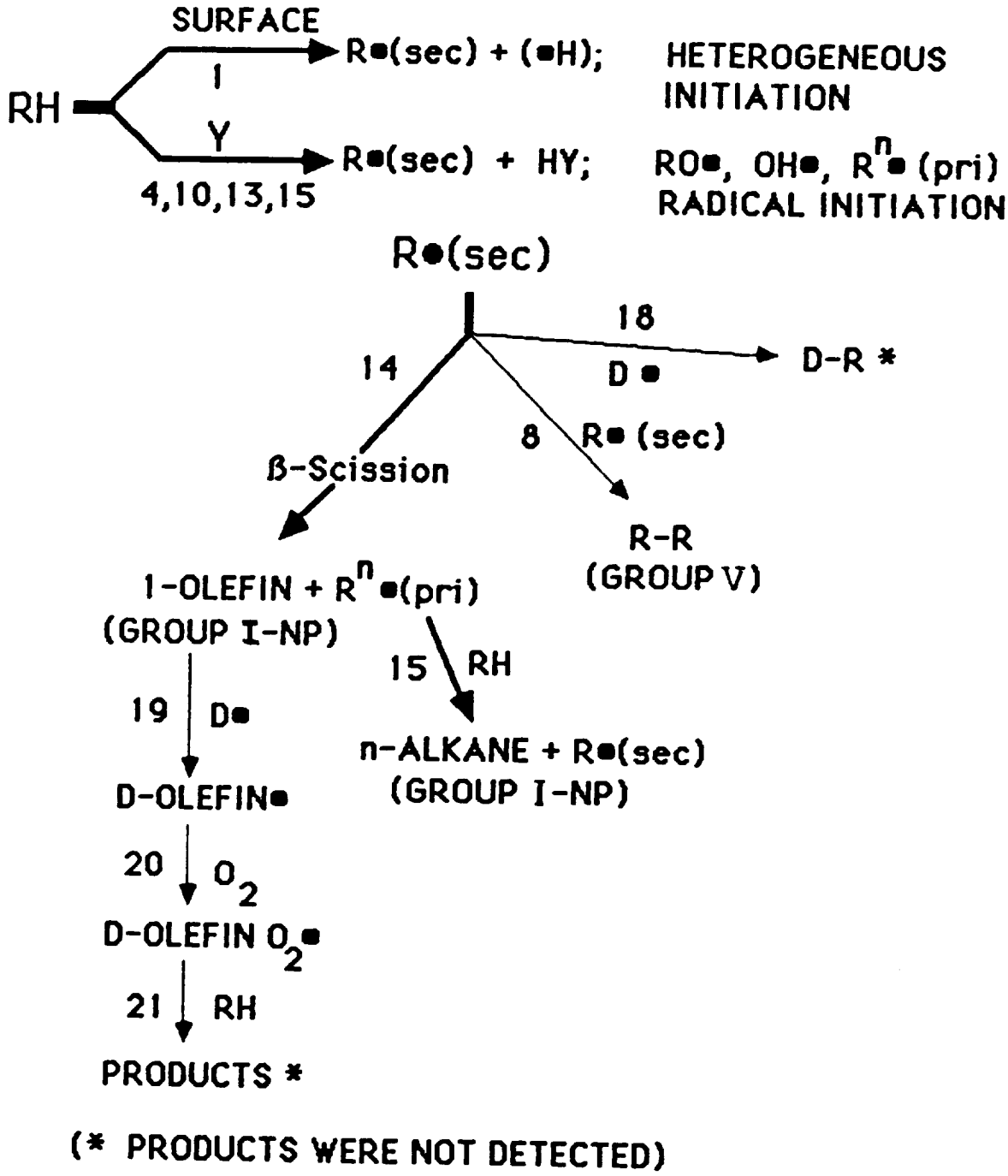

FIG. 5.7 Dodecyl (R*) and DMT Radical (D*) Reactions in the Intermediate Temperature Regime ($300 \leq T \leq 400C$)

Heterogenous Initiation

$$RH \text{ --SURFACE--> } R^* + (^*H) \quad (1)$$

$$DH \text{ --SURFACE--> } D^* + (^*H) \quad (16)$$

Propagation

$$R^* + O_2 \text{ --> } RO_2^* \quad (2)$$

Termination

$$RO_2^* + D^* \text{ --> } ROOD^{\wedge} \quad (17)$$

(^ Products were not detected)

At low temperatures, surface catalyzed radical initiation is possible for DMT molecules, since the S-H bond energy (in DMT) is lower than the C-H bond energy (RH - primary and secondary) in n-dodecane. This implies that the DMT radical (D*) formation competes with dodecyl radical (R*) formation, even though DMT concentrations are much lower than RH concentrations, Reaction 16. The D* radicals do not react with oxygen to form the corresponding peroxy radical, DO_2^* (Taylor and Frankenfeld, 1986), but react with the alkylperoxy radical (RO_2^*) forming the inert product, ROOD, Reaction 17 (Denisov, 1973). The ROOD product formation decreases the available supply of RO_2^* radicals, consequently decreasing Group II and IV concentrations in the autoxidation temperature regime with increasing DMT concentrations, Figs. 5.4a and 5.4c. The Group III data, however, is not consistent with this decreasing trend with increasing DMT addition, Fig. 5.4b. This effect is yet to be understood.

In the intermediate temperature regime, the RO_2* and D* radical reactions dominate. The sequence of reactions is (Fig. 5.7):

ROOD Thermolysis

ROOD ---> RO_2* + D* (17r)

RO_2* Radical Reactions

RO_2* ---> *ROOH (5a)

*ROOH ---> RO(THF) + *OH (Group II) (5b)

$2RO_2*$ ---> R"COR" + ROH + O_2 (Group III) (6)

D* Radical Reactions

D* + R* ---> R-D^ (18)

D* + 1-olefin ---> D-1-olefin* (19)

D-1-olefin* + O_2 ---> D-1-olefinO_2* (20)

D-1-olefinO_2* + RH ---> Products^ (21)

(^ Products were not detected)

At the higher temperatures, the ROOD molecule breaks down giving back the RO_2* and D* radicals, Reaction 17r (reverse of Reaction 17). The RO_2* radicals react further to form Group II products via reactions 5a and 5b and Group III products via reaction steps 6 or 9-11. This explains the increase in DMT derived Group II and III curves, which attain concentration levels similar to the baseline case as temperature increases beyond 300C. The D* radicals, on the other hand, can react with an R* radical forming the dimerized product, R-D, Reaction 18 (Denisov, 1973). D*

radical dimerization reactions involving two D* radicals (and giving D-D product) are not likely since the D* radical concentrations are considerably lower than the R* radical concentrations. Alternatively, the D* radicals can react with reactive Group I 1-alkenes forming D-Olefin* radicals which subsequently oxidize to form other products, Reactions 19-21. This route is preferred, since this sequence of reactions constitutes the well known "sweetening" process employed commercially for decreasing mercaptan odor (Oswald et al., 1963). Further evidence for the presence of these reactions is an observed decrease in 1-alkene concentrations relative to the other Group I constituents (e.g., n-alkanes), Fig. 5.5, indicating selective reactions of 1-alkenes.

Group I and V products also are selectively inhibited with increasing DMT concentration, indicating that the available dodecyl radical supply (responsible for Group I and V product formation) is decreased. This results either from a decrease in alkyl radical (R*) formation as a byproduct of decreased RO_2* radical concentrations (which, in turn, produce R* radicals) or from reactions involving dodecyl radicals (R*) and D* radicals. The dominant cause cannot be determined at this time.

5.2.2 Dibutylsulfide (DBS)

With DBS addition, the Group II-IV product distributions change, as seen in Fig. 5.8. In the autoxidation temperature regime, the sulfide interferes with

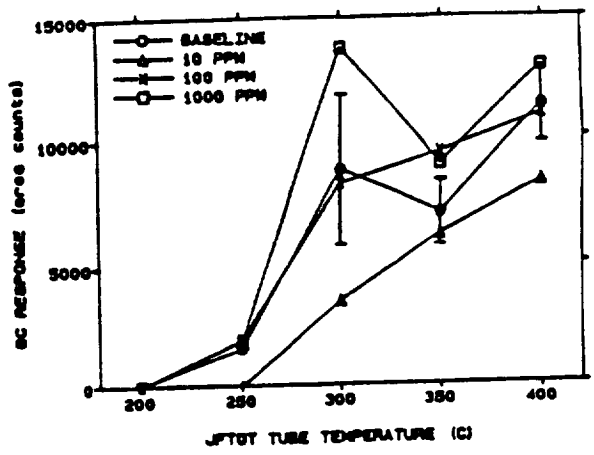

(a) GROUP II

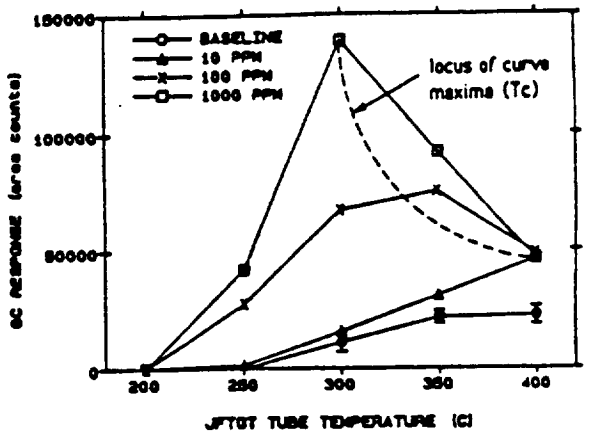

(b) GROUP III

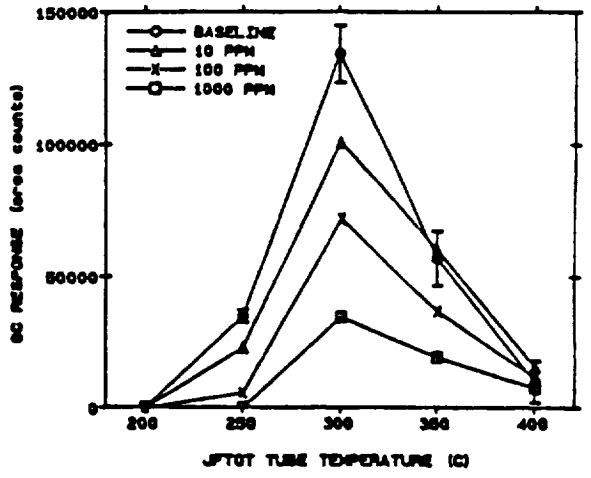

(c) GROUP IV

FIG. 5.8 Effect of Dibutylsulfide on Group II-IV Species in the P1 Fractions Using GC/OCI Analysis

the hydrocarbon oxidation chain at the hydroperoxide step (Bateman and Hargrave, 1954), viz.

ROOH Interference Reactions

$$R'SR'' + ROOH \longrightarrow R'SOR''^{\wedge} + ROH \quad (22)$$

$$R'SR'' + ROOH \longrightarrow R'SOR''^{\wedge} + R^{\bullet}\text{-}CO\text{-}R'' \quad (23)$$

(^ Products were not detected)

This decreases Group IV (ROOH) concentrations and, consequently, increases Group III alcohol and ketone formation, Figs. 5.8b and 5.8c.

As temperature increases ($T \geq 300C$), the dopant derived Group III product curves show curve maxima occurring at a critical temperature (Tc), with the locus of the curve maxima (Tc) shifting to lower temperatures as dopant concentrations are increased, Fig. 5.8b. For example, at 1000 ppm DBS, Tc occurs at 300C and shifts to about 325C for the 100 ppm DBS curve. No Tc is observed for the Group III 10 ppm DBS curve, with the Group III product concentrations increasing monotonically between 300C and 400C. The shift in Tc to lower temperatures with increasing DBS concentrations may be explained by the reaction

$$DBSO^{\wedge} + ROH(R^{\bullet}COR'') \longrightarrow Products^{\wedge} \quad (24)$$

$$(T > Tc)$$

(^ Products were not detected)

This reaction occurs only when the temperature is greater than Tc. Thus, Tc depends on DBSO concentration, which in turn depends on the initial DBS concentration.

5.2.3 Dibenzothiophene (DBT)

With DBT addition, the Group II-IV product distributions change only slightly, as seen in Fig. 5.9. The Group II product curves are inhibited relative to the baseline curve in the 250-350C range, indicating that DBT addition inhibits tetrahydrofuran formation, Fig. 5.9a. At 250C, DBT addition promotes Group IV relative to the baseline case, but at 300C and beyond, the 100 and 1000 ppm curves are inhibited to concentrations slightly lower than the baseline and 10 ppm curves, Fig. 5.9c. This indicates that DBT promotes Group IV formation up to 250C, but starts acting as an inhibitor at the 1000 ppm concentrations as temperature increases to 300C and beyond. Additionally, Group II and IV product distributions appear to be related somewhat at 250C. With DBT addition, the Group IV products appear to increase with a corresponding decrease in Group II products relative to the baseline data at 250C, indicating that DBT promotes the (RO_2* + RH ---> ROOH + R*) reaction (Reaction 3) while inhibiting the (RO_2* --> *ROOH --> RO + OH*) reactions (Reactions 5a and 5b) at this temperature. At 250C, the Group III product curves follow a 1000, 100 ppm > baseline > 10 ppm trend, implying that high DBT concentrations promote Group III formation, while low concentrations tend to inhibit their formation, Fig. 5.9b.

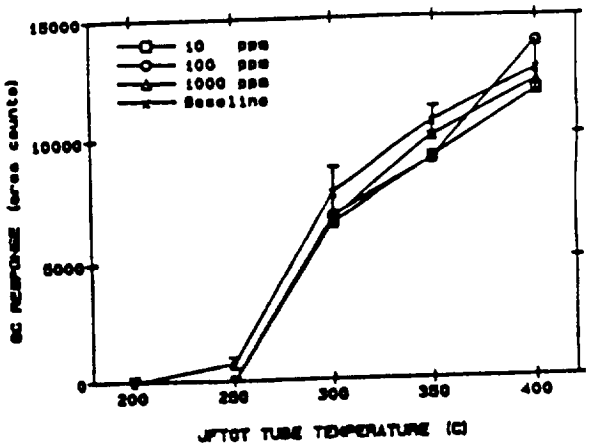

(a) GROUP II

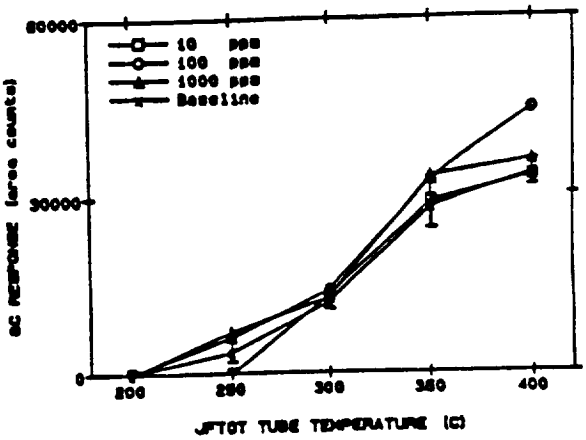

(b) GROUP III

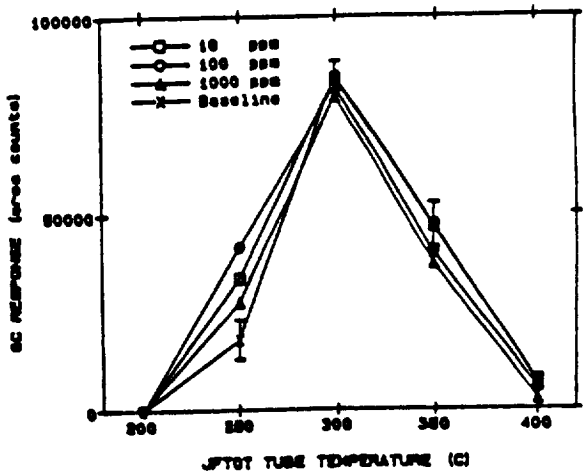

(c) GROUP IV

FIG. 5.9 Effect of Dibenzothiophene on Group II-IV Species in the P1 Fractions Using GC/OCI Analysis

5.3 CONCLUSIONS

Dopant addition showed that the major soluble products were always the same, with and without dopants, but that their distributions varied considerably. No dopant derived products were detected, however, due to low product concentrations and analytical difficulties. 3,4-dimercapto-toluene and dibutylsulfide dopants individually added to n-dodecane interfere with the hydrocarbon oxidation chain at the alkylperoxy radical and the alkylhydroperoxide link, respectively, and alter the n-dodecane derived product distributions (Group I-V). 2,5-dimethylpyrrole dopant, on the other hand, introduces cooxidation reactions involving dopant and oxygen and, consequently, inhibits ROOH formation. Pyridine, pyrrole and dibenzothiophene individually added to n-dodecane showed few significant mechanistic effects.

CHAPTER 6

DISCUSSION, CONCLUSIONS AND RECOMMENDATIONS FOR FUTURE WORK

A comparison between previous in-use fuel deposit and gum formation studies and the fuel degradation mechanism postulated from this study is discussed in Section 6.1. The summary and conclusions are presented in Section 6.2, while recommendations for future work are presented in Section 6.3.

6.1 FUEL DEGRADATION MECHANISM: CORRELATION WITH ACTUAL DEPOSIT AND GUM FORMATION STUDIES

The standard JFTOT was modified to collect various control and stressed fuel samples exposed to temperatures over the range from ambient to 400C with a single filling of the JFTOT reservoir. With this modification, surface deposition on the heater tubes (tube deposit rating, TDR) and gum formation (measured as Δp across test filter) could not be quantified. However, because of the low stress conditions utilized in this study, the model fuel and dopant combination experiments did not show any surface deposition.

Previous studies of fuel thermal stability were performed at the Naval Research Laboratory (Hazlett, 1979). Their data consists of TDR, [ROOH], [CO], and [n-alkanes] versus JFTOT tube temperature for a model fuel (n-dodecane) and an actual fuel (RAF-177). The NRL conclusions were: (i) in n-dodecane systems, deposits correlated with ROOH

decomposition, Fig. 6.1, while (ii) in the RAF-177 actual fuel system, deposits correlated with ROOH formation, Fig. 6.2.

System verification studies using n-dodecane data has shown good agreement in the soluble degradation product distributions (and concentrations) obtained by the NRL group and the present work. Hence, it is assumed that correlations and comparisons between the modified fuel degradation mechanism hypothesis and NRL deposit data (TDR data) is valid.

In the intermediate temperature regime ($300 \leq T \leq 400C$), the fuel degradation mechanism hypothesizes that R* radical reactions dominate the RO_2* reactions. The NRL n-dodecane derived n-alkane versus TDR data, Fig 6.3, shows that all of the R* radical derived product profiles, i.e., n-C1, n-C3, n-C9 and n-C10 curves, parallel the TDR build-up. The strong correlation between n-alkane and TDR indicates that R* radical reactions are probably important in the deposit formation process. Furthermore, the n-alkane product profiles correlate very well with TDR in the pyrolysis temperature regime ($T \geq 500C$), indicating that R* radical reactions are probably important in deposit formation in this temperature regime also. This is not surprising since at pyrolysis temperatures the fuel cracks to form R* radicals, which decompose further forming n-alkanes and 1-alkenes (Fabuss et al., 1964). Hence, R*

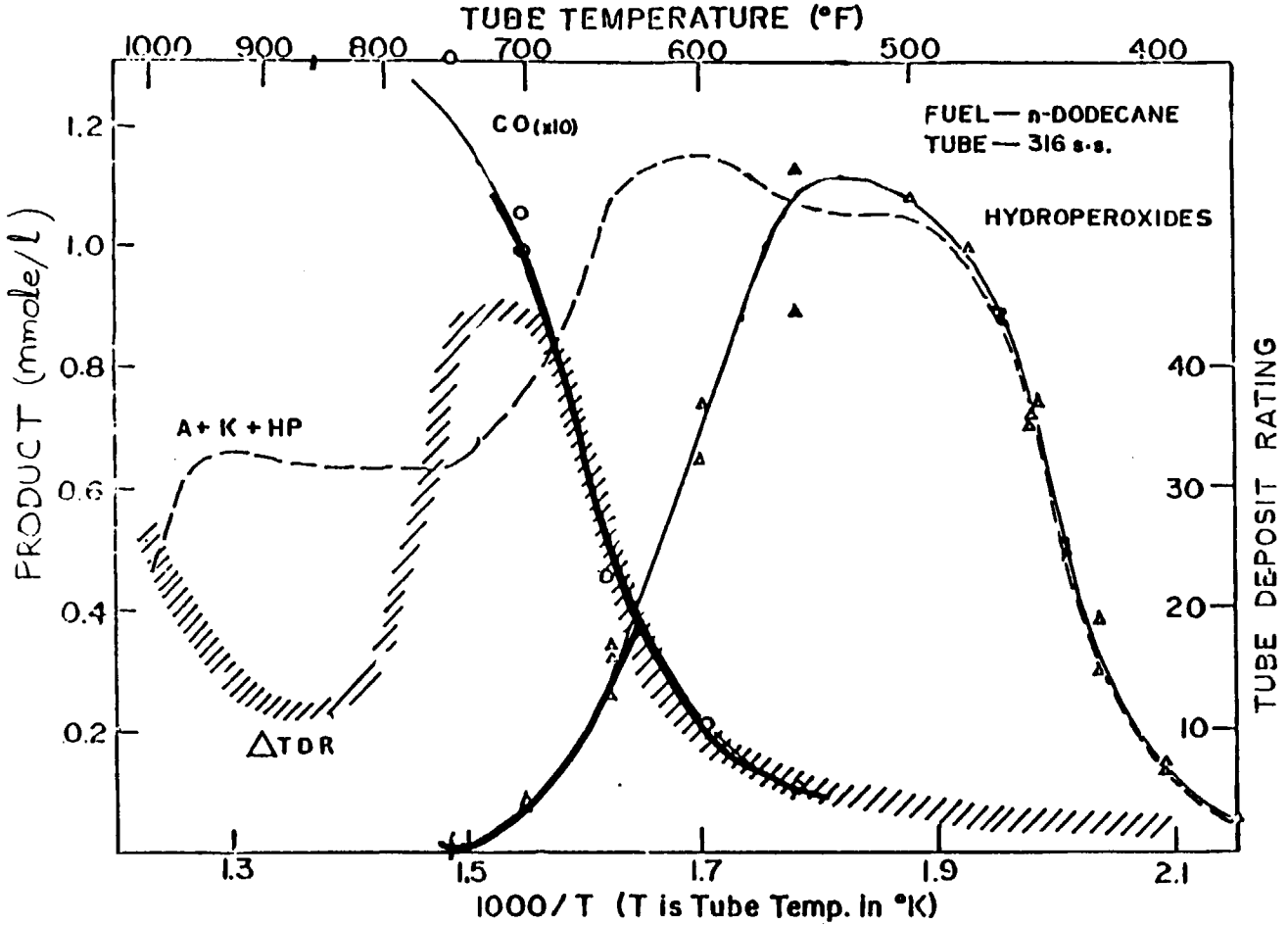

FIG. 6.1 Model Fuel, n-Dodecane Derived ROOH versus TDR Data (Hazlett, 1979)

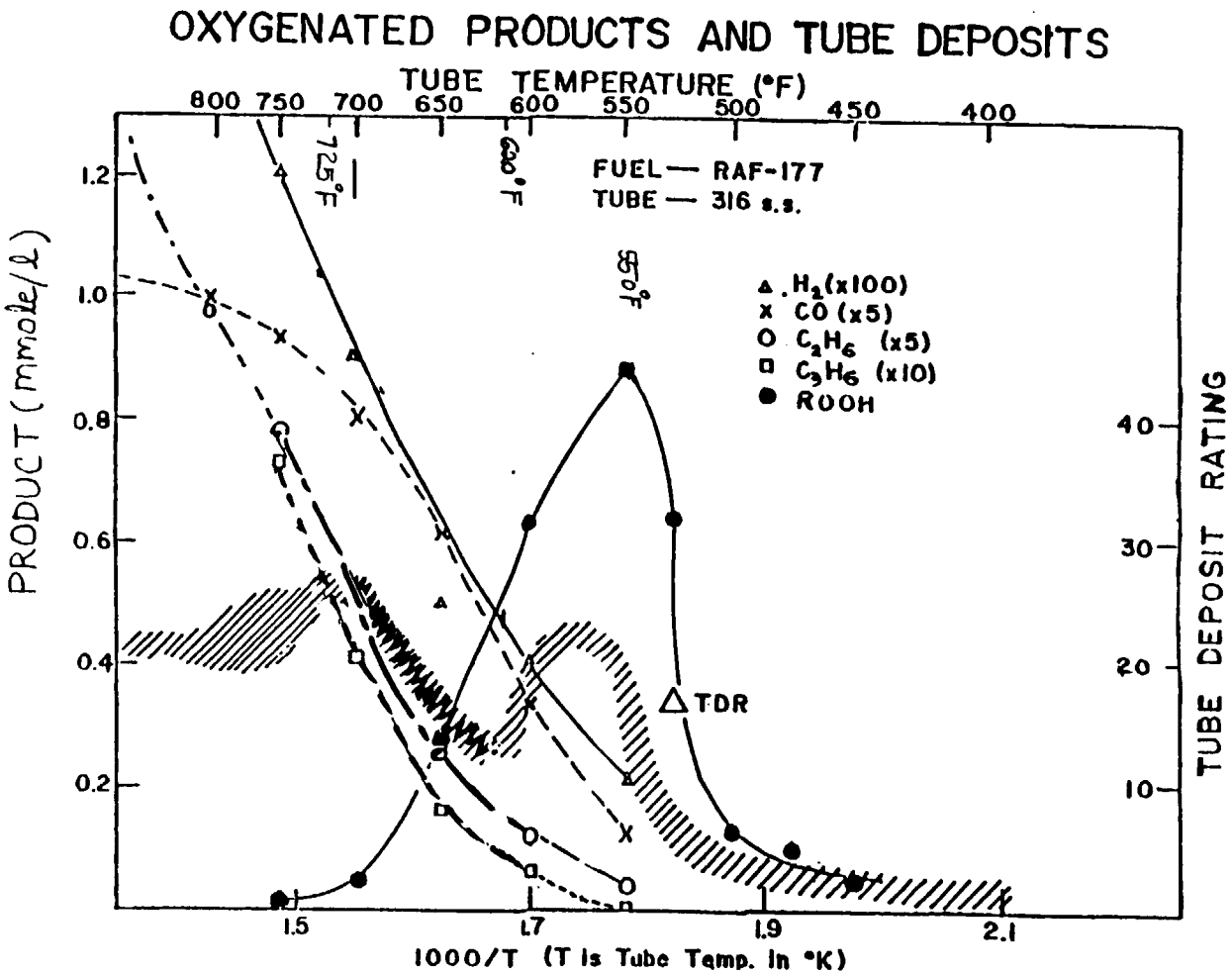

FIG. 6.2 Actual Fuel, RAF-177 Derived Oxygenated Product versus TDR Data (Hazlett, 1979)

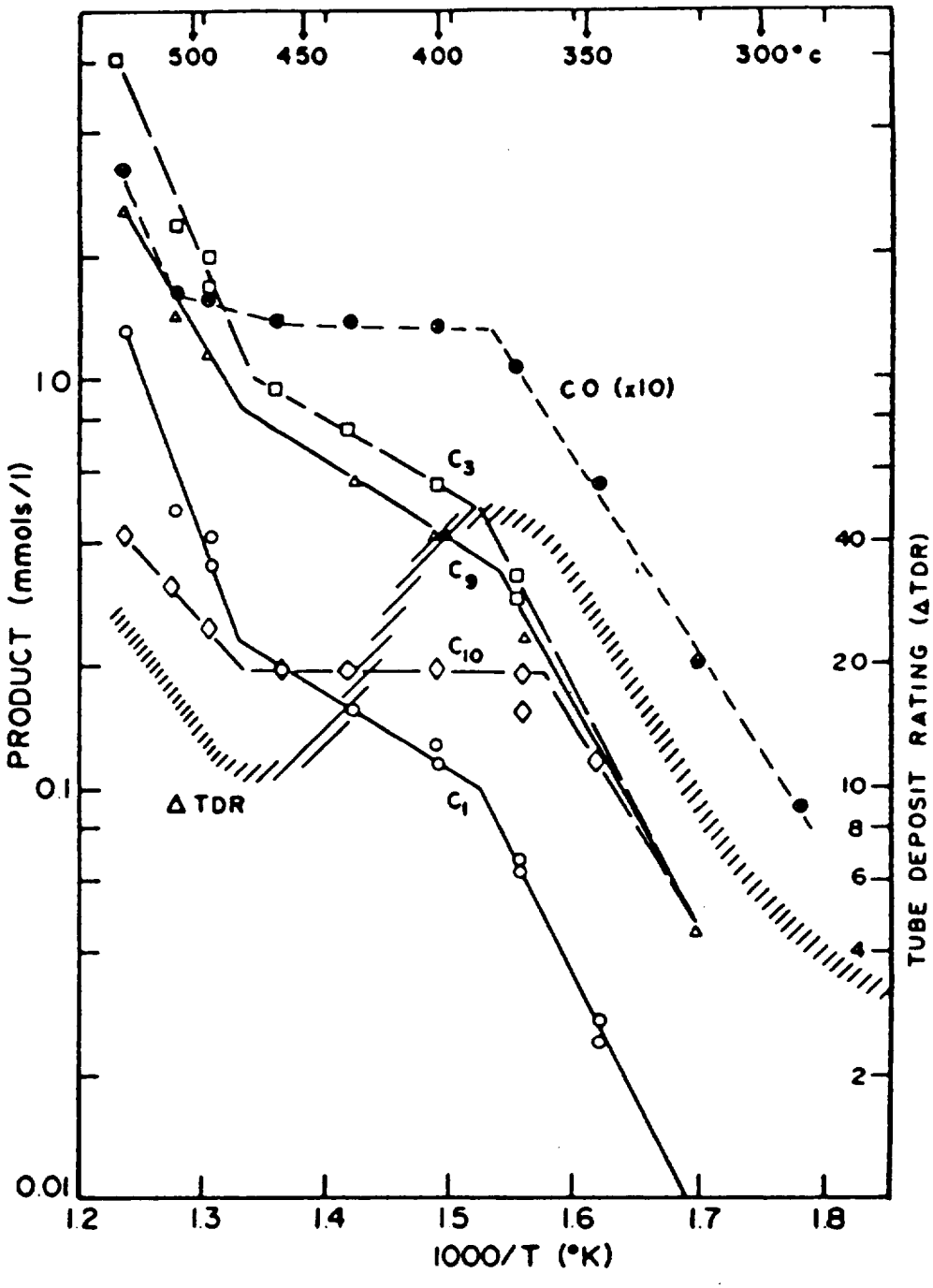

FIG. 6.3 Model Fuel, n-Dodecane Derived n-Alkane Product versus TDR Data (Hazlett, 1979)

radicals are probably responsible for deposit formation in the pyrolysis range of temperatures.

In the zone of minimum reactivity situated between the intermediate and pyrolysis range of temperatures ($400 \leq T \leq 500C$), the TDR curve dips down, while all of the n-alkane curves show a slight increase (or stay the same). This indicates a poor correlation between TDR and n-alkane concentration. A possible explanation for this behavior is that ROOH is depleted to near zero concentrations, Fig.6.1. This causes a sharp decrease in the available R* radical pool, since RH pyrolysis becomes the sole source of R* radicals.

The relative R* radical contributions via ROOH decomposition (R%) and RH pyrolysis (P%) reactions in the intermediate range of temperatures can be inferred from the Group I-NP (n-alkane and 1-alkene) profiles using the air saturated and nitrogen purged n-dodecane data, Fig.6.4. The air saturated Group I-NP data is a summation of the (R+P) data, while the nitrogen purged data includes contributions from P alone. It is observed that both R and P (absolute) increase from 300C to 400C. If the same data is replotted with R% and P% on the y-axis and temperature depicted on the x-axis, it is noted that R% decreases from 100% to 65% while P% increases from 0% to 35% between 300 and 400C, Fig. 6.5. In the zone of minimum reactivity, it is known that ROOH concentrations are near zero, Fig. 6.1, implying that R% is also close to 0%. This implies that P% should attain 100%

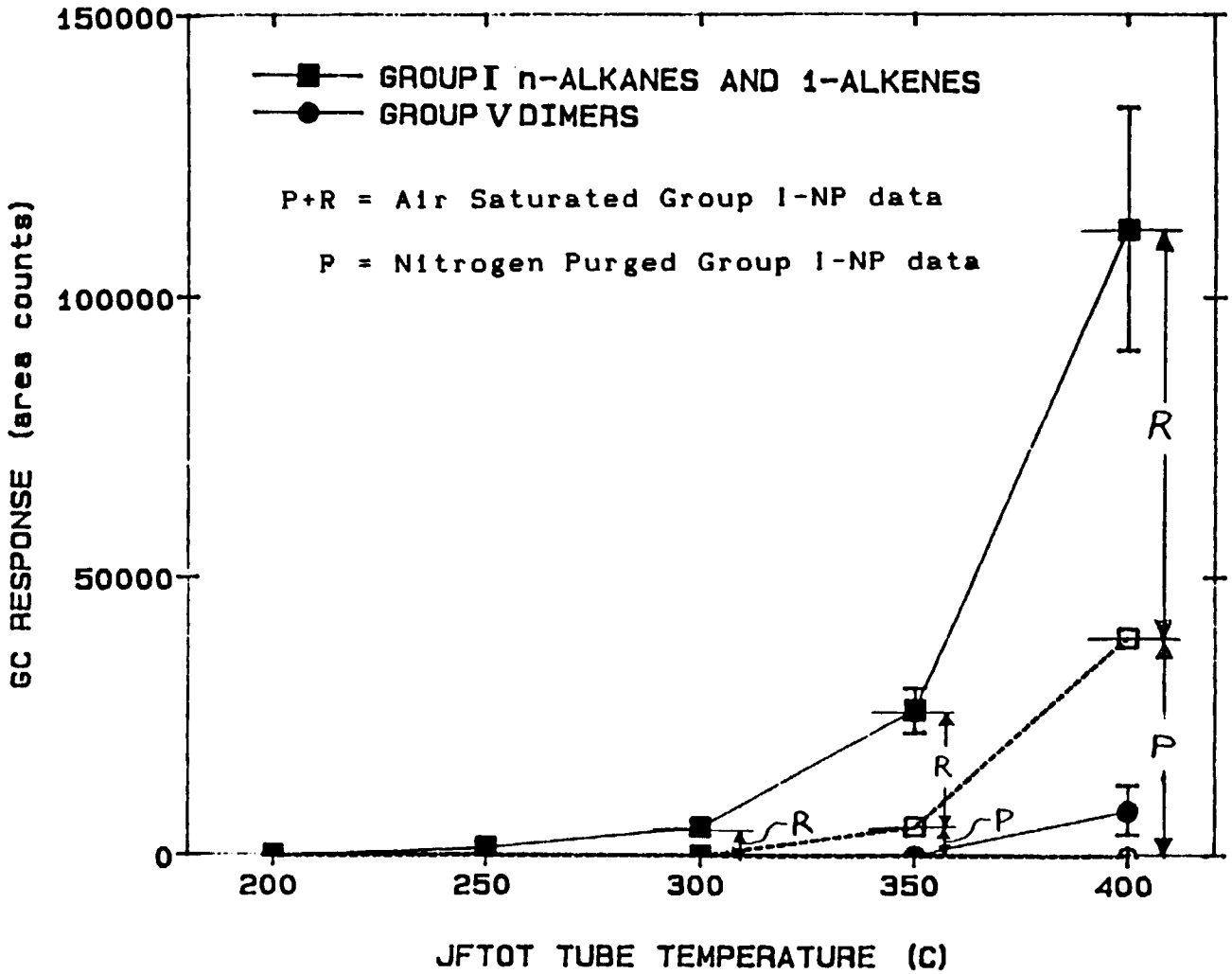

FIG. 6.4 Effect of Oxygen Concentration on R* Radical Derived Non-Polar Products Using GC/Split Injection Analysis of Entire Samples

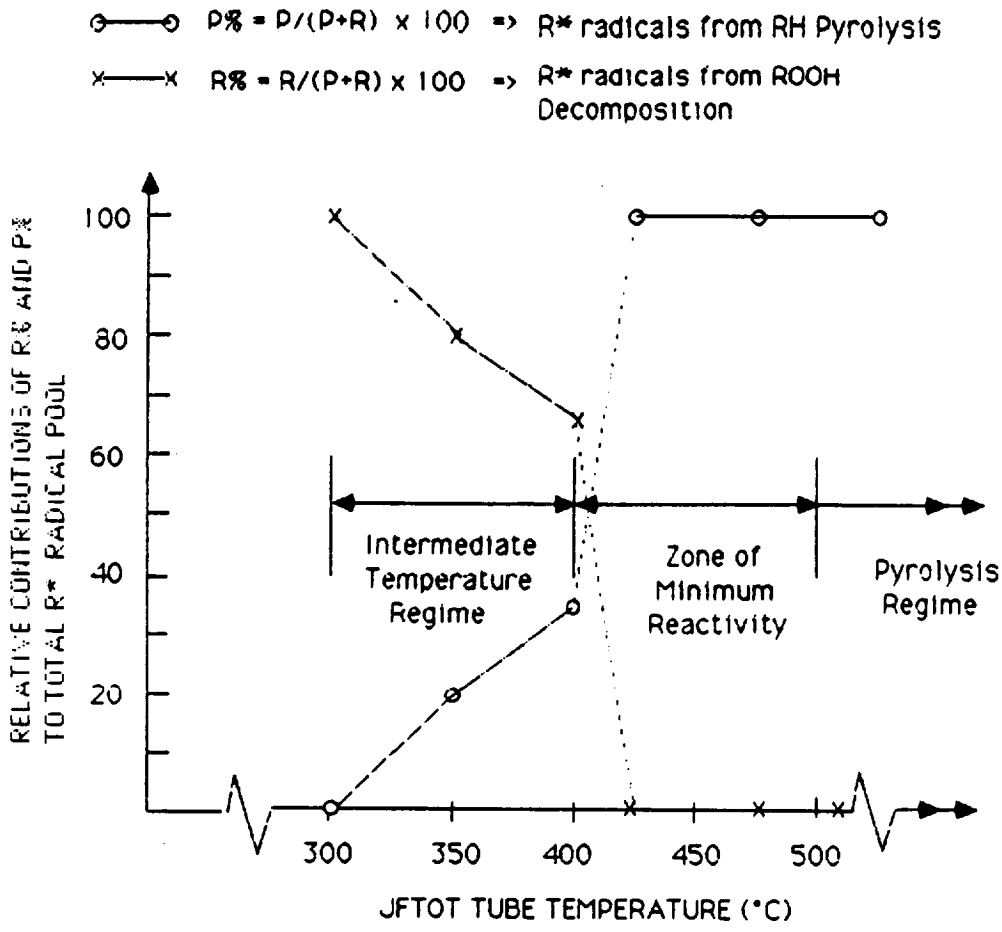

FIG. 6.5 R* Radical Contributions from ROOH Decomposition and RH Pyrolysis Reactions

just when ROOH's are completely depleted. Additionally, from available fuel pyrolysis mechanisms, it is known that P% is 100% and R% is zero at temperatures greater than 500C. Therefore, with the additional information regarding the pyrolysis and the minimum reactivity range of temperatures, Fig. 6.5 can be extended to include all temperatures greater than 300C.

In the zone of minimum reactivity, it is noted that R% decreases sharply from 65% at 400C to 0% when ROOH concentrations reach zero. On the other hand, P% increases from 35% to 100% when the R% contribution goes to zero. The dip in the TDR data observed in Fig. 6.2 is probably due to the sharp decrease in the available R* radical pool caused by the elimination of the major R* supplier (R% --> 0) and the absolute P contribution being of a small order relative to the absolute R contribution. Thus, R* radical concentrations appear to correlate with surface deposition (TDR data) in the intermediate, minimum reactivity and pyrolysis range of temperatures ($T \geq 300C$). Additionally, R* radical derived products such as n-alkanes (Group I-NP) are better correlated with TDR profiles than ROOH decomposition as cited in the NRL work. Therefore, n-alkanes appear to be better correlators of surface deposition than ROOH's, with the added advantage of easier detection and quantification. The postulated fuel degradation mechanism developed from the n-dodecane work at $T \geq 300C$ appears to work reasonably well for the RAF-177 actual fuel data, since n-alkanes again

correlate with TDR between 620 - 720F (327 - 382C). However, beyond 720F (382C), the TDR does not correlate with the n-alkane profiles, possibly due to the presence of several other hydrocarbons, heteroatomic species, metals, natural and artificial inhibitors, etc. These species may react with the n-alkanes or possibly inhibit fuel pyrolysis reactions, thereby skewing the TDR versus n-alkane correlation.

At temperatures less than 300C where autoxidation predominates, the modified fuel degradation mechanism hypothesizes that RO_2* radical reactions are more important than R* reactions. To verify if RO_2* radical reactions are important in fuel deposition processes (at $T \leq 300C$), the NRL data for [ROOH] plotted with respect to TDR for n-dodecane and RAF-177, Figs. 6.1 and 6.2, were examined. Figs. 6.1 and 6.2 show that the model fuel ROOH data does not correlate with TDR, but the actual fuel ROOH formation curve parallels the TDR curve, suggesting that the RO_2* radicals probably contribute to deposits at autoxidation controlled temperatures. The anomalous TDR versus ROOH behavior in the case of the model fuel is attributed to the absence of other fuel constituents (major and minor species) which are probably important and significant in the overall deposit formation process.

In addition to JFTOT apparatuses, static reactors were used by Mayo and Lan (1986) to study the gum and deposit formation using model and actual fuels. They measured the rates of oxygen absorption (Ro) and soluble gum formation

(Rg) at 130C for both model and actual fuels, and found that the actual fuels generated more gum for the oxygen absorbed than pure hydrocarbon fuels (high Rg/Ro values). It was concluded that the low Rg/Ro values observed for model fuels is due to the absence of minor constituents in these fuels which are important in the gum and deposit formation processes. Since soluble gums are precursors of insoluble gums and deposits, the relatively lower amounts of gums observed in the case of model fuels (Mayo and Lan, 1986) agrees with the low TDR observed for n-dodecane at autoxidation temperatures (Hazlett, 1979). This implies that the fuel degradation hypothesis developed using a flow reactor (modified JFTOT) is applicable to static reactor systems. Admittedly, Mayo and Lan's experiments were performed at 130C while the temperatures cited in the JFTOT studies are much higher. However, the actual bulk fuel temperatures in the JFTOT may be 50-100C lower as discussed in Chapter 3.

In summary, the RO_2* radical reactions appear to be important in the deposit formation processes at the autoxidation range of temperatures ($T \leq 300C$), while the R* radicals appear to be responsible in the intermediate, minimum reactivity and pyrolysis range of temperatures ($T \geq 300C$). Therefore, if the RO_2* and R* radicals can be suitably scavenged in the appropriate temperature regimes using anti-oxidants, inhibitors, radical scavengers, etc., the fuel degradation process probably can be inhibited/

modified or arrested. If the the fuel degradation problem cannot be solved due to pre-existing deposits, the fuel can be analyzed for the RO_2* derived product (ROOH) and/or the R* derived product n-alkane) to get a rough estimate of the surface deposition (TDR).

6.2 SUMMARY AND CONCLUSIONS

The thermal stability characteristics of hydrocarbon fuels have been studied. The fuels, n-dodecane and n-dodecane plus dopants, were aerated by bubbling air through the fuels and stressed on a modified JFTOT facility between 200-400C. The resulting samples were fractionated to concentrate the soluble products and then analyzed using gas chromatography and mass spectrometry techniques to quantify and identify the stable reaction intermediate and product species.

The modified JFTOT operation and analytical protocols employed in the present work are reproducible and capable of monitoring the changes in soluble product distributions with temperature and fuel compositional changes. Data analysis using product Groups and character impact peaks from each of these Groups produced more accurate, reproducible and simplified analysis without losing any fundamental information.

System verification results using neat n-dodecane oxidation showed that the <C12 n-alkane and 1-alkenes, alkylhydroperoxides and C12 alcohol plus ketone data trends

agree with the NRL data, thereby verifying both sets of data. However, additional products, i.e., tetrahydrofurans and C24 alkane isomers (fuel dimers), were detected in this work as a result of better analytical sensitivity. Consequently the existing n-dodecane degradation mechanisms were suitably modified to include these new products.

The experimental results for n-dodecane show a clear transition in the oxidation chemistry from autoxidation temperature ($T \leq 300C$) to intermediate temperature ($300 \leq T \leq 400C$) regimes. The main features of the oxidation mechanisms were discussed. The autoxidation temperature regime is dominated by alkylperoxyl radical reactions. The dominant path is for the alkylperoxyl radical, RO_2*, to react bimolecularly with fuel to yield primarily alkylhydroperoxides. The RO_2* also undergoes self termination and unimolecular isomerization and decomposition reactions to yield smaller amounts of C12 alcohol plus ketone products and tetrahydrofuran derivatives, respectively. Thus, alcohol and ketone formation in this temperature regime implies that the main termination step is via RO_2* self termination reactions. This observation refutes an earlier hypothesis that R* radical termination reactions (giving C24 alkane isomers) are important at low temperatures.

In the intermediate temperature regime ($300 \leq T \leq 400C$), the R* radical reactions dominate the RO_2* reactions. The major supply of R* radicals is via ROOH decomposition reactions while heterogeneous metal initiation constitutes

the secondary source. The R* radicals, in turn, decompose to form smaller n-alkanes and 1-alkenes (<C12), and small amounts of C24 isomers.

Dopant addition to n-dodecane showed that the major soluble products were always the same, with and without the dopants, but that their distributions varied considerably. The relative amounts and shifts in the distribution of these species with dopant addition led to inferences about the reaction mechanisms. No dopant derived products were detected, however, due to low product concentrations. 3,4-dimercaptotoluene and dibutylsulfide interfere with the hydrocarbon oxidation chain at the alkylperoxy radical and the alkylhydroperoxide link, respectively, and alter the n-dodecane derived product distributions (Groups I-V). 2,5-dimethylpyrrole dopant, on the other hand, introduces co-oxidation reactions involving dopant and oxygen, and consequently inhibits ROOH formation. Pyridine, pyrrole and dibenzothiophene individually added to n-dodecane showed no significant mechanistic effects.

In relating the findings of this work to the fuel degradation problem, the RO_2* radical reactions appear to be important in the deposit formation processes at the autoxidation range of temperatures ($T \leq 300C$), while the R* radicals appear to be responsible in the intermediate, minimum reactivity and pyrolysis range of temperatures ($T \geq 300C$). Therefore, if the RO_2* and R* radicals can be suitably scavenged in the appropriate temperature regimes

using anti-oxidants, inhibitors, radical scavengers, etc., the fuel degradation process can probably be arrested. If the fuel degradation problem cannot be solved due to pre-existing deposits, the fuel can be analyzed for the RO_2* derived product (ROOH) and/or the R* derived product (n-alkane) to get a rough estimate of the surface deposition (TDR). If the ROOH's and/or the n-alkanes are found in high concentrations, the fuel should be downgraded and mixed with a lower (and heavier) distillation cut.

It is concluded that this research has led to a better understanding of the reaction mechanisms associated with fuel degradation. The mechanisms derived appear to explain the work of other investigators. It has also formed the basis for future research to address other aspects of the fuel degradation problem.

6.3 RECOMMENDATIONS FOR FUTURE WORK

The current line of research should be pursued, since a start has been made in understanding the decomposition of model fuels singly and in combination with deleterious sulfur and nitrogen heteroatomic compounds, which are known precursors of fuel deposits. Based on the identification of stable and intermediate reaction species, fuel degradation mechanism information has been obtained. Additional testing can lead to a more comprehensive fuel degradation mechanism. Two or more dopants added to the model fuel simultaneously will be of interest, since the possible synergistic/

antagonistic effects and resulting changes in reaction mechanism(s) relative to the single dopant cases can be studied. Attention can be turned, next, to the testing of binary and ternary model fuel mixture combinations doped with deleterious sulfur, nitrogen, and oxygen heteroatom species. In this way, the testing of fuel and dopant combinations will yield a more general fuel degradation mechanism(s) than is currently available. The flow of information starting with basic research followed by bench scale studies can move on to simulative studies, eventually leading to the use of thermally stable fuels in actual aircraft and diesel engines.

In view of the research work conducted in this thesis, some specific recommendations for improving the experiments, enhancing the data to be collected, and some interesting experiments are as follows:

1. Currently the amount of degradation products being formed is very small, making sample handling, chromatographic analysis, and data interpretation difficult. Higher oxygen pressures and addition of radical initiators such as tertiarybutylhydroperoxides to the model fuels should be tried out to alleviate this problem.

2. With dopant addition, co-oxidation and radical forming/scavenging reactions become important, making identification of dopant derived products (ppb to ppm concentration range) necessary to follow changes occurring in the fuel degradation mechanism. Therefore, it would

be desirable to use improved sample enrichment techniques such as Kuderna-Danish techniques, Sep-pak materials (i.e., amine-, hydroxy- bonded Sep-paks, etc.) and other non-polar and polar solvent combinations to handle the low product concentrations in a variety of sample matrices.

3. A byproduct resulting from the current research is the study of thermally stressed samples under storage. The sample product concentrations can be followed by employing GC techniques to observe differences (if any) in the product profiles and distributions relative to the time of original storage. The above analysis can yield information about the long term effects of intermediates formed during thermal stressing.

4. More recent chemical techniques that exploit the high solvating power and mass transport properties of supercritical fluids should be investigated for chemically characterizing the deposits and sediments resulting from fuel degradation.

The ultimate goal of this work is to relate the fuel degradation mechanisms with the insoluble product formation. This will identify the precursors (soluble oxidation products) responsible for insoluble product formation.

LIST OF REFERENCES

LIST OF REFERENCES

Bateman, L., and Hargrave, K. R. (1954), "Oxidation of Organic Sulfides II. Interaction of Cyclohexylsulfide with Hydroperoxides in Hydrocarbons, " Proc. Roy. Soc. (London), Ser. A. 224, p. 399.

Benson, S. W. (1965), "Effects of Resonance and Structure on the Thermochemistry of Organic Peroxy Radicals and the Kinetics of Combustion Reactions," J. Am. Chem. Soc. 87, p. 972.

Benson, S. W., and Shaw, R. (1972), "Thermochemistry of Organic Peroxides, Hydroperoxides, Polyoxides, and Their Radicals," Organic Peroxides, Vol. 1, Chapter 2, (editor Swern, D.), Wiley-Interscience, New York, p. 105.

Benson, S. W. (1972), "The Mechanisms of Pyrolysis, Oxidation, and Burning of Organic Materials," Nat'l. Bur. Stand. (U.S.), Spec. Publ., No. 357, p. 121.

Benson, S. W. (1981), "Some Researches into Problems of Molecular Structure and Chemical Reactivity," J. Phy. Chem. 85, p. 3375.

Berces, T., and Trotman-Dickenson, A. F. (1961), "The Reactions of Hydroxyl Radicals with Hydrocarbons in Aqueous Solutions," J. Chem. Soc., p. 4281.

Bolland, J. L., and ten Haave, P. (1947), "Liquid Phase Oxidation of Hydrocarbons," Trans. Faraday Soc. 43, p. 201.

Boss, B. D., and Hazlett, R. N. (1969), "Oxidations of Hydrocarbons in the Liquid Phase: n-Dodecane in a Borosilicate Glass Chamber at 200C," Can. J. Chem. 47, p. 4175.

Boss, B. D., Hazlett, R. N., and Shepard, R. L. (1973), "Analysis of n-Paraffin Oxidation Products in the Presence of Hydroperoxides," Anal. Chem. 45, p. 2388.

Bridgewater, A. J., and Sexton, M. D. (1978), "Mechanism of Antioxidant Action: Reactions of Alkyl and Aryl Sulphides with Hydroperoxides," J. Chem. Soc., Perkins Trans. 2, p. 530.

Brinkman, D. W., Whisman, M. L., and Bowden, J. N. (1979), "Stability Characteristics of Hydrocarbon Fuels from Alternative Sources," Bartlesville Energy Technology Center, Report No. BETC/RI-78/23.

Brinkman, D. W., Bowden, J. N., and Giles, H. N. (1980), "Lube Oil and Finished Fuel Storage Stability: An Annotated Review," DOE/BETC/RI-79-13.

Brown, D. M., and Fish, A. (1969), "The Extension to Long-Chain Alkanes and to High Temperatures of the Hydroperoxide Chain Mechanism of Autoxidation," Proc. Roy. Soc. (London) Ser. A. 308, p. 547.

Cooney, J. V., Hazlett, R. N., and Beal, E. N. (1986), "Mechanisms of Syncrude/Synfuel Degradation," Naval Research Laboratory, Report No. DOE/BC/10525-15, Third Annual Report.

Coordinating Research Council (1979), "Literature Survey on the Thermal Oxidative Stability of Jet Fuel," CRC Report No. 509.

Cullis, C. F., Hirschler, M. M., and Rogers, R. L. (1981), "The Oxidation of Decane in the Liquid and Gaseous Phases," Proc. Roy. Soc. (London), Ser. A. 375, p. 543.

Daniel, S. R. (1983), "Studies of the Mechanisms of Synfuel Degradation," NASA Report. NSG 3122.

Denisov, E. T. (1973), "Elementary Reactions of Oxidation Inhibitors," Russian Chemical Reviews 42, (3), p. 157.

Emanuel, N. M., Denison, E. T., and Maizus, Z. K. (1967), Liquid-Phase Oxidations of Hydrocarbons, English Translation, Plenum Press, New York.

Emanuel, N. M. (1981), "Chemical and Biological Kinetics," Russian Chemical Reviews 50, 10, p. 901.

Emanuel, N. M. (1982), "80's in the Field of Liquid Phase Oxidation of Organic Compounds," Oxidation Communications 2, No. 3-4, p. 221.

Fabuss, B. M., Smith, J. O., and Satterfield, C. N. (1964), "Thermal Cracking of Pure Saturated Hydrocarbons," Adv. Pet. Chem. Refin. 9, p. 157.

Faith, L. E., Ackerman, G. H., and Henderson, H. T. (1971), "Heat Sink Capability of Jet A Fuel: Heat Transfer and Coking Studies," NASA-CR-72951.

Fish, A. (1964), "Radical Rearrangement in Gas-Phase Oxidation and Related Processes," Quart. Rev., Chem. Soc. London 18, p. 243.

Fish, A. (1968), "The Cool Flames of Hydrocarbons," Adv. Chem. Ser. 96, p. 69.

Fish, A. (1970), "Rearrangement and Cyclization Reactions of Organic Peroxy Radicals," Organic Peroxides, Vol. 1, Chapter 3, (Editor Swern, D.), Wiley-Interscience, New York, p. 141.

Frankenfeld, J. W., Taylor, W. F., and Brinkman, D. W. (1981), "Fundamental Synthetic Fuel Stability Study," Exxon Research and Engineering Co. Report No. DOE/BC/10045-12.

Frankenfeld, J. W., Taylor, W. F., and Brinkman, D. W. (1982), "Fundamental Synthetic Fuel Stability Study," Exxon Research and Engineering Co. Report No. DOE/BC/10045-23.

Giammaria, J. J., and Norris, H. D. (1962), "High-Temperature Inhibition of Normal Paraffin Oxidation by Alkylaromatics," Ind. Eng. Chem., Prod. Res. Dev. 1, p. 16.

Goetzinger, J. W., Thompson, C. J., and Brinkman, D. W. (1983), "A Review of Storage Stability Characteristics of Hydrocarbon Fuels, 1952-1982," DOE/BETC/IC-83-3.

Hazlett, R. N., Hall, J. M., and Matson, M. (1977), "Reactions of Aerated n-Dodecane Liquid Flowing Over Heated Metal Tubes," Ind. Eng. Chem., Prod. Res. Dev. 16, 2, p. 171.

Hazlett, R. N. (1979), "Some Chemical Aspects of Deposit Formation," NASA Technical Memorandum 79231.

Hazlett, R. N., and Hall, J. N. (1981), "Jet Aircraft Fuel System Deposits," Div. Pet. Chem., Preprints, ACS Meeting, Vol. 26, Atlanta, Georgia.

Hendry, D. G., Mill, T., Piskiewicz, L., Howard, J. A., and Eigenmann, H. K. (1974), "A Critical Review of H-atom Transfer in the Liquid Phase: Chlorine Atom, Alkyl, Trichloromethyl, Alkoxy and Alkylperoxy Radicals," J. Phy. Chem. Ref. Data 3, p. 937.

Hiatt, R. (1972), "Alkyl Peroxides," Organic Peroxides, Vol. 3, Chapter 1, (Editor Swern, D.), Wiley-Interscience, New York, p. 1.

Ingold, K. U. (1961), "Inhibition of the Autoxidation of Organic Substances in the Liquid Phase," Chem. Rev. 61, p. 563.

Jensen, R. K., Korcek, S., Mahoney, L. R., and Zinbo, M. (1979), "Liquid-Phase Autoxidation of Organic Compounds at Elevated Temperatures. 1. The Stirred Flow Reactor Technique and Analysis of Primary Products from n-Hexadecane at 120-180C," J. Am. Chem. Soc. 101, p. 7574.

Kharach, M. S., Nudenberg, W., and Mantell, G. J.(1951), "Reactions of Atoms and Free Radicals in Solution. XXV. The Reactions of Olefins with Mercaptans in the Presence of Oxygen," J. Org. Chem. 16, p. 524.

Knight, H. B., and Swern, D. (1954), "Tetralin Hydroperoxide," Org. Syntheses 34, p. 90.

Koelewijn, P., and Berger, H. (1972), "Mechanism of the Antioxidant Action of Dialkyl Sulfoxides," Rec. Trav. Chim. 91, p. 1275.

Koelewijn, P., and Berger, H. (1974), "Mechanism of the Antioxidant Action of Dialkyl Sulfoxides," Rec. Trav. Chim. 93, p. 63.

Kossiakoff, A., and Rice, F. O. (1943), "Thermal Decomposition of Hydrocarbons, Resonance Stabilization and Isomerization of Free Radicals, " J. Amer. Chem. Soc. 65, p. 590.

Li, J., and Li, C. N. (1985), "Storage Stability of Jet Fuels," Fuel 64, p. 1041.

Loeffler, M. C., and Li, N. C. (1985), "Role of Nitrogen- and Sulfur- Containing Compounds in the Ageing of Liquid Fuels," Fuel 64, p. 1047.

Lundberg, W. O. (1962), Autoxidation and Antioxidants, John Wiley, New York.

Maillard, B., Ingold, K. U., and Sciano, J. C. (1983), "Rate Constants for the Reactions of Free Radicals with Oxygen in Solution," J. Amer. Chem. Soc. 105, p. 5095.

Marteney, P. J., Colket, M. B., and Vranos, A. (1982), "Experimental Study of the Thermal Stability of Hydrocarbon Fuels," NASA-CR-168027.

Mayo, F. R., Miller, A. A., and Russell, G. A. (1958), "The Oxidation of Unsaturated Compounds. IX. The Effect of Structure on the Rates and Products of Oxidation of Unsaturated Compounds," J. Amer. Chem. Soc. 80, p. 2500.

Mayo, F. R. (1968), "Free-Radical Autoxidations of Hydrocarbons," Accounts of Chem. Res. 1, p. 193.

Mayo, F. R., Richardson, H., and Mayorga, G. D. (1975), "The Chemistry of Jet Turbine Fuel Deposits and their Precursors," Div. Pet. Chem., Preprints, ACS Meeting, Vol. 20, Philadelphia, p. 38.

Mayo, F. R., Lan, B., Cotts, D. B., Buttrill, S. E. Jr., and St. John, G. A. (1983), "Oxidation and Formation of Deposit Precursors in Hydrocarbon Fuels," SRI-2115, SRI International, NASA CR-168121.

Mayo, F. R., and Lan, B. (1986), "Gum and Deposit Formation from Jet Turbine and Diesel Fuels at 130C," Ind. Eng. Chem., Prod. Res. Dev. 25, p. 333.

Mill, T., and Hendry, D. G. (1980), "Kinetics and Mechanisms of Free Radical Oxidation of Alkanes and Olefins in the Liquid Phase," Comprehensive Chemical Kinetics, Vol. 16, Chapter 1, (Eds. Bamford, C. M., and Tipper, C. F. H.), Elsevier Scientific Publishing Co., Amsterdam.

Mill, T., and Montorsi, G. (1973), "The Liquid Phase Oxidation of 2,4-Dimethylpentane, " Intl. J. Chem. Kinetics 5, p. 119.

Mill, T., Mayo, F. R., Richardson, H., Irwin, K., and Allara, D. C. (1972), "Gas and Liquid-Phase Oxidation of n-Butane," J. Am. Chem. Soc. 94, p. 6802.

Mushrush, G. W., Hazlett, R. N., Hardy, D. R., and Watkins, J. M., (1986), "Liquid Phase Oxidation of Sulfur Compounds," Proceedings of the Second International Conference on Long-Term Storage Stabilities of Liquid Fuels, San Antonio, Texas, p. 512.

Nassan, K. (1983), The Physics and Chemistry of Color, John Wiley and Sons, New York.

Nixon, A, C. (1962), "Autoxidation and Antioxidants of Petroleum," Autoxidation and Antioxidants, Vol. 2, Chapter 17, (Editor- Lundberg, W. O.), John Wiley, New York.

Nixon, A. C., and Thorpe, R. E. (1956), "The Effect of Composition on the Stability and Inhibitor Response of Jet Fuels," Amer. Chem. Soc., Div. Pet. Chem., Preprints, 1, No. 3, p. 265.

Oswald, A. A., and Noel, F. (1961), "Role of Pyrroles in Fuel Instability," J. Chem. and Eng. Data 6, No. 2, p. 294.

Oswald, A. A., and Ruper, C. B. (1959), "Co-oxidation of Mercaptans and Olefins," Am. Chem. Soc., Div. Petrol. Chem., Preprints, 4, 1, p. 27.

Oswald, A. A., Hudson, B. E. Jr., Rodgers, G., and Noel, F. (1962), "Organic Sulfur Compound. VII. Some Addition and Co-oxidation Reactions of Thiols with 2,5-Dimethyl-2, 4-hexadiene," J. Org. Chem. 27, p. 2439.

Oswald, A. A., Griesbaum, K., and Hudson, B. E. Jr. (1963), "Organic Sulfur Compound, XII. Factors Determining a 1,2- vs. 1,4-Mechanism of Radical Reactions of Conjugated Diolefins. Co-oxidation with Thiols by Oxygen," J. Org. Chem. 28, p. 2355.

Peat, A. E. (1982), "Fuel Thermal Stability. Propulsion and Energetics Panel, Working Group 13 on Alternative Jet Engine Fuels," Vol. 2, R. B. Whyte, Ed., Report No. AGARD-AR-181-Vol. II.

Rafikova, V. S., Maizus, Z. K., Skibida, I. P., and Emanuel, N. M. (1971), "Role of the R1* + R2H Chain Transfer Reaction in the Degenerate-Branched Chain Oxidation of Hydrocarbons," Dokl. Akad. Nauk, SSSR, 198, No. 5, p. 1131.

Reich, L., and Stivala, S. S. (1969), Autoxidation of Hydrocarbons and Polyolefins, Marcel Dekker Inc., New York.

Reynolds, T. W. (1977), "Thermal Stability of Some Aircraft Turbine Fuels Derived from Oil Shale and Coal," NASA TM-X-3551.

Russel, G. A. (1955), "The Competitive Oxidation of Cumene and Tetralin," J. Amer. Chem. Soc. 77, p. 4583.

Rust, F. F. (1957), "Intramolecular Oxidation. The Autoxidation of Some Dimethylalkanes," J. Am. Chem. Soc. 79, p. 4000.

Sauer, R. W., Weed, A. F., and Headington, C. E. (1958), "A Mechanism of Organic Sediment Formation in Heating Oils," Pet. Chem. Div. Preprints, Vol. 3, No. 3, Chicago.

Schirmer, R. M. (1970), "Morphology of Deposits in Aircraft and Engine Fuel Systems," SAE paper 700258.

Scott, G. (1965), Autoxidation, Atmospheric Oxidation and Antioxidants, Elsevier, Amsterdam.

Shala, F. J. (1983), "Characterization and Analysis of Diesel Exhaust Odor," Ph. D. Thesis, Department of Chemistry, Drexel University, Philadelphia, PA.

Smith, J. D. (1967), "The Effect of Metals and Alloys on the Thermal Stability of Avtur 50," Aircraft Eng., p. 19.

Taylor, W. F., (1968), "Kinetics of Deposit Formation from Hydrocarbons. III. Heterogeneous and Homogeneous Metal Effects," J. Appl. Chem. 18, p. 251.

Taylor, W. F., and Wallace, T. J. (1968), "Kinetics of Deposit From Hydrocarbons: Effect of Trace Sulfur Compounds," Ind. Eng. Chem., Prod. Res. Dev. 7, p. 198.

Taylor, W. F. (1969), "Kinetics of Deposit Formation From Hydrocarbons: Fuel Composition Studies," Ind. Eng. Chem., Prod. Res. Dev. 8, p. 375.

Taylor, W. F. (1974), "Deposit Formation from Deoxygenated Hydrocarbons - I: General Features," Ind. Eng. Chem., Prod. Res. Dev. 13, p. 133.

Taylor, W. F. (1976a), "Deposit Formation from Deoxygenated Hydrocarbons - II. Effects of Trace Sulfur Compounds," Ind. Eng. Chem., Prod. Res. Dev. 15, p. 64.

Taylor, W. F. (1976b), "Deposit Formation from Deoxygenated Hydrocarbons - III. Effects of Trace Nitrogen and Oxygen Compounds," Ind. Eng. Chem., Prod. Res. Dev. 15, p. 68.

Taylor, W. F. (1979), "Jet Fuel Thermal Stability," NASA TM-79231.

Taylor, W. F., and Frankenfeld, J. W. (1986), "Chemistry and Mechanism of Distillate Fuel Stability," Proceedings of the Second International Conference on Long-term Storage Stabilities of Liquid Fuels, San Antonio, Texas, p. 496.

Thompson, R. B., Bruge, L. W., and Chenicek, J. A. (1979), Ind. Eng. Chem. 41, p. 2415.

Tobolsky, A. V., and Mesrobian, R. B. (1954), Organic Peroxides; their Chemistry, Decomposition and Role in Polymerisation, Interscience, New York, N. Y.

Trimm, D. L. (1980), "The Liquid Phase Oxidation of Sulfur, Nitrogen, and Chlorine Compounds" Comprehensive Chemical Kinetics, Vol. 16, Chapter 4, (Eds. Bamford, C. M., and Tipper, C. F. H.), Elsevier Scientific Publishing Co., Amsterdam.

Van Sickle, D. E., Mill, T., Mayo, F. R., Richardson, H., and Gould, C. W. (1973), "Intramolecular Propagation in the Oxidation of n-Alkanes. Autoxidation of n-Pentane and n-Octane," J. Org. Chem. 38, p. 4435.

Vranos, A., and Marteney, P. J. (1980), "Experimental Study of the Stability of Aircraft Fuels at Elevated Temperatures," NASA CR-165165.

Walling, C. (1968), "The Role of Heteroatoms in Oxidation," The Oxidation of Organic Compounds, ACS Advances in Chemistry, 75, Chapter 13, p. 166.

Watt, J. J., Evans, A. Jr., and Hibbard, R. R. (1968), "Fouling Characteristics of ASTM Jet A Fuel When Heated to 700F in a Simulated Heat Exchanger Tube," NASA-TN-D4958.

Wong, E. L., and Bittker, D. A. (1983), "Effect of Hydrocarbon Fuel Type on Fuel Stability," NASA-TM-82916.

APPENDICES

APPENDIX A

MODIFIED JFTOT OPERATING PROCEDURE

The following procedure has been adopted to run a JFTOT experiment using the modified JFTOT apparatus described in Section 3.1 and illustrated in Fig. 3.1. The heater tube temperature controller is calibrated prior to each experiment by melting pure tin and utilizing the freezing point of tin (232C) as a standard. Suitable corrections are applied to the heater tube temperature if the indicated temperature differs from 232C. The electrical insulation components for the heater tube and the fuel reservoir piston lip seal are inspected for scratches and abrasions and replaced suitably prior to cleaning. The heater tube, prefilter, test filter and fuel reservoir components are thoroughly rinsed employing pentane solvent, with the heater tube assembly rinsed further with trisolvent (equal parts of toluene, isoproponal and acetone, 99% grade) to ensure removal of all fuel derived soluble products and deposits. 600 cc of test fuel (n-dodecane or n-dodecane plus dopants) is poured into the assembled fuel reservoir. The fuel is aerated with 9 liters of air to provide an oxygen saturated fuel with a fixed concentraton of dissolved oxygen which is constant for all JFTOT fuel experiments. The reservoir piston lip seal is placed on top of the aerated fuel and the reservoir top is sealed, assembled and

connected to the fuel pressurization circuit. The whole JFTOT system is pressurized to 500 psig, employing nitrogen, ensuring that the system is leak proof. The JFTOT elapsed time indicator is reset to read zero time and the timer for the run time is set to 2 1/2 hours. The coolant water flow employed to cool the heater tube bars is adjusted to be within 38 $\pm$ 8 liters/min. The heater tube temperature controller is set to ambient temperature and the heater and fuel pump are switched on.

To start a test sequence, the sampling tap is cracked open to provide a steady flow and ensure constant flushing of the fuel lines up to the sample tee (maintain system pressure at 500 psig). This modification increases the total instrument flow from 3 ml/min to approximately 3.75-4.0 ml/min. Once the temperature deviation meter indicates a zero deviation from the controller setting, the spent fuel flow is diverted across the manometer (only main fuel flow lines are shown in Fig. 3.1) and the differential pressure is adjusted to read zero (mercury column in mm) on the manometer scale. The fuel pump flow is determined with a stop watch by measuring the time for 20 fuel drops passing through the reservoir top equipped with a sight window (9 $\pm$ 1.0 seconds). The differential pressure recorder is started, at this point, to record differential pressure. 15 minutes is allowed for system equilibration and stabilization (making sure that the heater tube temperature and system pressure is constant at the preset conditions) and adequate

flushing of the sample lines including the sample tee and tap to ensure impurity free representative sample collection (sample vials are flushed with fuel flowing through the tap before actual sampling). The heater tube controller temperature is increased to 200C, and 15 minutes allowed for system equilibration and stabilization (which is similar to the ambient temperature case). Representative 200C samples are collected and the procedure is repeated for 250C, 300C, 350C, and 400C samples.

Finally, to shut the system down, the heater tube temperature is decreased to ambient temperature to allow flushing of the fuel lines including the tee and sampling tap with room temperature fuel. This procedure flushes the soluble thermal decomposition products from the fuel lines. The fuel pump and heater are switched off and the nitrogen pressurization valve is closed. The manometer bypass valve is opened and nitrogen is bled from the system. The fuel reservoir assembly, the heater tube assembly, and the pre and test filter assemblies are disassembled and set aside for cleaning and reuse.

APPENDIX B

OPERATION OF VACUUM DISTILLATION APPARATUS

The following procedure has been adopted to start a distillation using the vacuum distillation apparatus described in Section 3.3 and shown in Fig. 3.3. Initially, fill the traps with ice and water and charge the pot no more than half full with the material to be distilled, including boiling chips to prevent bumping and overheating of the glass pot. Connect the pot to the bottom of the column, place the heater under it, and adjust the supports as appropriate. Turn on the cooling water and turn on the heat using the rheostat. Adjust the heat such that an acceptable amount of vapor starts rising in the column (too low a heat will cause insufficient vapor production and too high a heat will cause excessive vapor production, which will prevent the liquid from coming back into the pot and cause flooding of the column). Turn on the vacuum by starting the vacuum pump. If the manostat has been preset, no adjustment is necessary; otherwise, see the separate manostat instructions and set the mercury level to obtain an absolute pressure of 3 mm of mercury column. Once the system has come to equilibrium, check for leaks by shutting off the vacuum at the distillation head; fix any leaks as appropriate and restore vacuum. Set the system for total reflux with no condensed vapors being bled off as distilled product. Open the valve allowing vacuum to the column and product

receiver. Let the column equilibrate for 20-30 minutes. Open the receiver valve and collect product for about 10 minutes; following this, close the receiver valve. Continue this process until about 10 percent of the original charge is collected or until the boiling characteristics of the product reach the desired value. The sample collected up to this point is waste.

The desired boiling characteristics are determined by comparison with published data for the material being distilled. The temperature at the distillation head is read using a thermometer and the absolute pressure is obtained from the manometer and manostat readings [Pabs = Pbar - Pman]. Generally, sufficient front end wastage has been collected when the experimental boiling temperature (at the system pressure) is within $\pm$ 0.1% of the published boiling curve. Once the initial 10% is collected (or the boiling curve is matched), the product receivers are changed and distilled product is collected. Roughly 70-80 percent of the initial charge is collected as usable products. The system is shut down by turning off the heat, vacuum and water, and slowly repressurizing the system.

VITA

VITA

Kishenkumar Tadisina Reddy was born [redacted] in [redacted] He attended Osmania University, Hyderabad, graduating with a Bachelor of Engineering degree in Mechanical Engineering in June 1978. He pursued graduate studies at the Indian Institute of Technology, Madras, India, and obtained the Master of Technology degree in Mechanical Engineering in June 1980. After working for a year at National Thermal Power Corporation, New Delhi, India, he came to Drexel University to further his education. He received a Master of Science degree in Mechanical Engineering in June 1983 and a Doctor of Philosophy degree in Mechanical Engineering in October 1987. During his stay at Drexel, he served as a graduate research and teaching assistant in the Mechanical Engineering and Mechanics Department.

Mr. Reddy has co-authored two journal papers, two conference papers, and a NASA final report in the area of thermal stability of distillate hydrocarbon fuels while studying at Drexel. He is an honorary member of the International Association for Stabilities and Handling of Liquid Fuel Forms. He is also a member of the American Society of Mechanical Engineers, Society of Automotive Engineers, Combustion Institute, and the American Institute of Aeronautics and Astronautics.